Optimal Control Strategies for Operation of Hybrid Multi-Prime-Mover Ship Propulsion Powertrains in Transient Conditions

by

Sotirios K. Topaloglou

Submitted to the School of Naval Architecture and Marine Engineering
in fulfillment of the requirements for the degree of

Doctor of Philosophy

at the

NATIONAL TECHNICAL UNIVERSITY OF ATHENS

October 2016

Thesis Supervisor:
Professor Nikolaos P. Kyrtatos

Optimal Control Strategies for Operation of Hybrid Multi-Prime-Mover Ship Propulsion Powertrains in Transient Conditions

by

Sotirios K. Topaloglou

Abstract

The prime movers used for ships today have certain limitations in their load response. As a ship accelerates, the diesel engine due to the temporary inability of the turbocharger to supply a sufficient amount of air to burn completely the fuel quantity required to meet the increasing load, emits smoke. One way of addressing this issue is the use of a hybrid diesel-electric configuration. Examples of ships with where a hybrid system could be useful, are vessels with fast maneuvering requirements with rapidly changing propeller demand. This Thesis investigates the improvement in performance of a combustion engine with the assistance of an electric motor, with appropriate control systems, for transient load uptake, smoke emission reduction, reduced pollutant emissions and lower fuel consumption. The Hybrid Integrated Propulsion POwertrain (HIPPO-1) test bed at NTUA/LME consists of a medium-duty 448 kW, turbocharged marine diesel engine, a water brake and an AC electric motor with frequency inverter rated at 110 kW, coupled to a water brake on the same shaft in a parallel hybrid configuration. The main purpose of the electric motor in the HIPPO-1 powertrain is to assist the diesel engine at lower speed bands, where the engine produces low torque, to meet faster the increasing torque demand. For the hybrid diesel electric powertrain, two energy control management strategies are proposed, that dictate the required torque from the electric motor so as to track a reference air-to-fuel ratio/stoichiometric (λ-value) in the diesel engine. The reference λ-values are stored in lookup tables which consider engine parameters, such as produced torque, speed and intake manifold pressure, derived from experimental data during steady-state operation. The feasibility and validity of the proposed control strategy was tested experimentally, using rapid prototyping development tools. The tested loading time series is based on performance data from ship-board measurements with a multitude of engine loading conditions. A comparison between the hybrid powertrain and the standard engine setup (without the assistance from the electric motor), shows the benefits of a hybrid setup during transient loading conditions.

Thesis Supervisor: Prof. N. Kyrtatos

Acknowledgments

Firstly, I would like to express my sincere gratitude to my advisor, Professor N. Kyrtatos for the continuous support of my Ph.D study and related research, providing instructive comments and suggestions. He entrusted me and guided me with his immense knowledge through the stages of building and using the entire test-bed for all the required experimental results.

My special thanks go to Assistant Professor G. Papalambrou, member of my Thesis Committee. His guidance helped me in all the time of research with his knowledge on control theory and applications, as well as with endless optimism despite the difficulties.

I would like also to thank Prof. Frangopoulos, member of my Thesis Committee, for his insightful comments and encouragement.

My sincere thanks also goes to Dr.-Ing. N. Alexandrakis for his most valuable comments and fruitful conversations.

I would also like to thank the technicians of the Laboratory, C. Sarris and G. Ntaliapes, for helping through all the phases in the build-up of the hybrid test-bed.

I would also like to thank DNV/GL for the partial financial support of my doctoral studies. The HIPPO-1 test-bed was built with support from the Greek state funds via NTUA/LME, the Lloyds Register Foundation, within the LRF/NTUA Centre of Excellence in Ship Total Energy-Emissions-Economy and the EC/DG RTD H2020/HERCULES-2 project. Their financial support is gratefully acknowledged.

Last but not the least, I would like to thank my family: my parents, Konstantinos and Athanasia, my wife Hara and daughter Anthi, for supporting me spiritually throughout my studies and my life in general.

THIS PAGE INTENTIONALLY LEFT BLANK

Contents

THIS PAGE INTENTIONALLY LEFT BLANK

List of Figures

Nomenclature

λ AFR/AFR$_{stoich}$

AFR Air-to-Fuel Ratio

AFR_{stoich} stoichiometric Air-to-Fuel Ratio

ARX AutoRegressive models with eXogenous input

C_r Crest factor

CV Controlled Variables

DE Diesel Engine

DV Measured Disturbances

E EnergyJ

$ECAs$ MARPOL Emission Control Areas

ECU Engine Control Unit

EM Electric Motor

$EMcmd$ Electric Motor Frequency Inverter Command

EMS Energy Management Strategy

$FDPD$ Frequency-Domain Power Distribution

H_∞ H-infinity control methods

H_p MPC Prediction Horizon

H_u MPC Control Horizon

$HIPPO-1$ Hybrid Integrated Propulsion POwertrain mark-1

ICE Internal Combustion Engine

IMO International Maritime Organization

KS control sensitivity function

L The open loop transfer function

LQ linear quadratic

MAP Diesel engine inlet manifold absolute pressure

$MARPOL$ International Convention for the Prevention of Pollution from Ships

$MIMO$ Multi-Input Multi-Output

$MISO$ Multi Input Single Output

$MPC401$ Un-constrained MPC design

$MPC900$ Constrained MPC design

MV Manipulated Variables

$N4SID$ Subspace Algorithm

N_E Diesel Engine rotational speed

NO_x nitrogen oxides

PEM Prediction Error Minimization Method

$PRBS$ Pseudo-Random Binary Signal

$PWMsignal$ Pulse-Width Modulation signal

S The sensitivity transfer function

$SISO$ Single-Input Single-Output

SO_x sulfur oxides

SVF State Variable Filters

T The complementary sensitivity function

$TorqueWB$ Torque Load imposed by the water brake dynamometer

WB Water Brake

THIS PAGE INTENTIONALLY LEFT BLANK

Preface

Objectives of this Thesis

The objective of the present work is the optimal operation of hybrid powertrains for ships, under a multitude of conditions, including transient operation. The impact of the hybridized ship propulsion powertrain (under closed loop control) on fuel consumption and exhaust gas emissions, compared to a conventional one, is investigated.

Contributions of this Thesis

The main contribution of this Thesis is the development and analysis of two model-based controller concepts, which track the air ratio of an Internal Combustion Engine, while engaging an electric motor in a hybrid propulsion arrangement. These controllers do not interfere with the fueling of the ICE, which allows their application also as a retro-fit solution.

At lower speeds, where the diesel engine produces low torque, the electric motor assists the powertrain to meet up with the torque demand faster. At higher speeds, where the diesel engine can produce more power than needed and operates at better efficiency points, the extra available power can be converted into electricity charging the batteries, in a typical hybrid scheme (although not investigated in this Thesis, as this work focuses on the transient phenomena).

The full scale multi-prime-mover experimental facility development HIPPO-1 (Hybrid Integrated Propulsion POwertrain) was built at LME/NTUA during this Thesis and was used for detailed experimental investigations to validate the developed models and test the controllers. The HIPPO-1 testbed setup consists of a high speed

marine diesel engine, an electric motor and a water dynamometer, capable of providing detailed experimental data, under finely regulated and repeatable operating conditions. The water brake can emulate the load of a propeller or waterjet, with realistic loading scenarios, obtained from full scale ship-board measurements.

The research performed within the framework of this Thesis has yielded the following scientific publications:

- S. Topaloglou, K. Bardis, G. Papalambrou, N. Kyrtatos, "Transient Load Share Management of a Diesel Electric Hybrid Powertrain for Ship Propulsion", International Journal of Powertrains, accepted (September 2016) for publication.

- S. Topaloglou, G. Papalambrou, N. Kyrtatos, "Robust Control of Diesel-Electric Hybrid Power Split for Marine Propulsion", submitted (July 2016) to IEEE Transactions on Control Systems Technology.

- S. Samokhin, S. Topaloglou, G. Papalambrou, K. Zenger, N. Kyrtatos, "Adaptive power-split control design for marine hybrid diesel powertrain", ASME Journal of Dynamic Systems, Measurement and Control, February 2017, Volume 139.

- S. Topaloglou, G. Papalambrou, N. Kyrtatos, "Energy management controller design for hybrid ship propulsion during transient operation", The 28^{th} CIMAC Congress, June 2016, Helsinki, Finland.

- S. Topaloglou, G. Papalambrou, N. Kyrtatos, "Controller Design for Hybrid Diesel Electric Ship Propulsion During Transient Operation", The 26^{th} International Ocean and Polar Engineering Conference, June 2016, Rhodes, Greece.

- G. Papalambrou, S. Samokhin, S. Topaloglou, N. Planakis, N. Kyrtatos, K. Zenger, "Model predictive Control for Hybrid Diesel-Electric Marine Propulsion", submitted (November 2016) to IFAC 2017 World Congress, Toulouse, France.

- N. Kyrtatos, G. Papalambrou, S. Topaloglou, A. Stamatellos, O. Zogou, "Design and Experimental Verification of a Variable Path Exhaust Gas Prototype After-treatment System for Marine Engines", International Marine Design Conference 2015 (IMDC 2015), Tokyo, Japan, May 2015.

- G. Papalambrou, S. Glaros, S. Topaloglou, and N. Kyrtatos "Model Reference Adaptive Control of a Marine Diesel Engine Combined with Electric PTI/PTO Motor", in Proceedings of Powertrain Modelling and Control (PMC) Conference, September 2012, Bradford, UK.

Structure of this Thesis

The Thesis is divided into the following chapters:

Introduction. The introductory chapter provides a survey on the current state of research and applications on the control of hybrid powertrains, as well as the description of the problem and the principles of operation of the hybrid testbed used for this Thesis.

Experimental facility. In this chapter, the experimental setup of the hybrid testbed, including the main sensors, used for this Thesis is described.

System Modeling. This chapter introduces the plant models which were derived experimentally, includes the design of a λ virtual sensor, and the experimentally derived engine parameters' maps.

Robust controller design. In this chapter a robust H_∞ controller is synthesized. The method is investigated in simulation and tested experimentally.

Model predictive controller design. This chapter introduces a model predictive controller. Simulation results and experiments on the hybrid test bed are presented.

Conclusions. The Thesis closes with a summary of the main results and suggestions for future work.

THIS PAGE INTENTIONALLY LEFT BLANK

Chapter 1

Introduction

The International Convention of Prevention of Pollution from Ships (MARPOL) has imposed stricter emission requirements for many special areas, called Emission Control Areas (ECAs) [59]. MARPOL defines certain sea areas as "special areas" in which, for technical reasons related to their oceanographical and ecological condition and to their sea traffic, the adoption of special mandatory methods for the prevention of sea pollution is required. Under the Convention, these special areas are provided with a higher level of protection than other areas of the sea. The adoption of Annex VI limits the main air pollutants contained in ships exhaust gas. Annex VI Regulations for the Prevention of Air Pollution from Ships establishes certain ECAs with more stringent controls on sulfur oxides (SO_x) and nitrogen oxides (NO_x) emissions.

Moreover, the International Maritime Organization (IMO) is in the process of tightening the emission limits in the future. The majority of the emissions of marine diesel engines are regulated with standards already in force (Tier I, II, III), except for the PM emissions, for which no emission standard has been adopted yet. In view of these requirements, emission reduction is a key driven factor for the development of novel technologies in the field of marine propulsion. One promising technology for emission and fuel consumption reduction is the hybrid diesel-electric propulsion.

Typically in the existing marine technology framework, ships are equipped with direct-driven propulsion machinery occasionally combined with a shaft generator system, known as Power Take Out (PTO), generating power for some of the electrical

demands of ship. Current trends consider the usage of auxiliary power to assist the main engine in some load situations, such as high bollard pull, sailing in icy conditions, harbor maneuvering or "take-home" power, thus using Power Take In (PTI) operation through powertrain *hybridization*. In this way, the size of main engine could be optimized to the propulsion power needed under normal conditions while additional power boost can be taken from auxiliary generators as required. For relevant information see [10].

Depending on their architecture, Hybrid Electric Powertrains (HEP) fall into one of several categories: 1) parallel; 2) series; or 3) power split. In the parallel scheme, both the engine and the motor are connected to the transmission, and thus, they can power the vehicle either separately or in combination. In series hybrids, the prime mover acts only as an electricity generator and the transmission is only connected to electric motor. In that case an energy storage system of high turnaround efficiency is required [40]. Finally, the power split scheme can operate either as a parallel or a series HEP, combining the advantages of both but with increased complexity.

The performance of a hybrid powertrain in terms of reducing both fuel consumption and exhaust emissions critically depends on the energy management strategy (EMS). An EMS is the supervising control algorithm that determines how the total power demand is shared between the power sources [30]. One main category of EMSs with limited however potential for marine power plants due to the requirement of the exact knowledge of the loading cycle, includes the optimization techniques found in [58], [49], [31] and [51]. Moreover, heuristic methods such as fuzzy logic and neural networks have been adopted in [55], [57] and [7] but they achieve neither an optimal solution, nor robustness with respect to performance.

Of the many advanced control design methodologies, MPC seems to be the most capable to handle multivariable processes, satisfy constraints, deal with long time delays and utilize plant response to measured and unmeasured disturbances knowledge [60]. MPC has been used in a broad range of applications, such as diesel engine control [43] and [2], catalyst control [38], etc.

The above control strategies have dealt mainly with fuel economy without a par-

ticular emphasis in emissions reduction. The subject of emissions reduction in a quasi-static framework is discussed in [61], [30], [29] and [25]. However the incorporated quasi-static models for emission formation disregard the substantial rise of pollutant emissions during transient operation of diesel engines (DE) due to the presence of thermodynamic delays mainly associated with turbocharger.

The formulation of transient emission reduction is presented in [42], where the optimal EMS for a diesel hybrid electric powertrain is calculated, considering the transient pollutant particulate matter emissions. In the same direction an EMS is considered in [26], using a frequency-domain power distribution (FDPD) strategy, which requires a priori knowledge of the loading profile.

The reduction of NOx emission in both steady state and transient operating conditions has been examined in [19]. The optimal power split in steady state is provided by an EMS while the reduction of transient NOx emissions is achieved through the smoothing of the DE torque demand by utilizing the EM torque as torque compensator. However, the dynamic control law is not robust with respect to exogenous disturbance and unmodeled dynamics that inevitably exist in real-world hybrid electric powertrains.

The rationale behind the work presented in this Thesis, is to reduce the intensity of the transient loading phenomenon in the diesel engine (DE) with the aid of an electric motor (EM). It takes advantage of the rapid conversion between electrical and mechanical energy in EM to assist the DE that has a limited torque delivery during acceleration due to thermodynamic limitations. The EM assists the DE at low-load operation, where the internal combustion engine operates at low efficiency points and produces low torque.

While closed loop control of emissions in DEs has been an active research field for more than fifteen years [4], this Thesis aims to present a novel marine application, where λ-manipulation is achieved only with the additional degree of freedom stemming from the hybridization of the powertrain.

The combustion inside cylinders involves a mixture of air and fuel. For complete combustion, the mixture must be at a precise ratio, known as stoichiometric Air-

to-Fuel Ratio (AFR_{stoich}). λ number is defined as the ratio of the actual to the stoichiometric AFR (AFR/AFR_{stoich}).

In a typical internal combustion engine (ICE) with λ closed loop management, the control is performed through the fuel injection system. In the framework of this Thesis the fueling commands of the Engine Control Unit (ECU) are not overridden, but by applying torque from the EM, the required torque from the DE is reduced, in order for the total torque demand to be met, and in that way the λ is implicitly regulated. In addition, in this Thesis a λ "virtual sensor" is implemented and tested in closed loop, offering the benefit of direct estimation of λ in the cylinder where combustion takes place and that it discards the need for a physical λ sensor in the exhaust duct.

1.1 Diesel Engine Response to Load Transients

A short overview of the diesel engine response to a load increase is described below since it provides useful insights about the physical phenomena that take place in diesel engines during transient conditions. On an engine which is running at steady state and a new higher load is applied, a torque deficit appears and the engine speed drops. The drop in engine speed is sensed by the speed governor which increases the fuel injected into the cylinder by an appropriate amount specified by the ECU (typically derived from a map as a function of various physical variables and limitations).

The higher amount of fuel injected into the cylinder combined with the insufficient air supply, due to thermal and dynamic delays, leads to a drop in the air-to-fuel ratio inside the cylinder and equivalently in the value of λ. The main reason for the mismatch between the air supply and the fueling command is caused from the turbocharger inertia, which results in the compressor operation point moving slowly from a lower air mass flow to higher boost pressure and mass flow.

1.2 Hybrid Testbed Operation During Transients

The rationale behind the approach presented in this Thesis, is to reduce the effect of the transient loading phenomenon in the DE with the aid of an EM. The concept of the above diesel electric hybrid propulsion response methodology is presented schematically in Fig. 1-1, in a typical marine propulsion operation. This figure includes the operating torque envelopes of the DE and EM used in the experimental facility (Hybrid Integrated Propulsion POwertrain - HIPPO 1) and 5 nominal load demand curves of a vessel with fixed pitch propeller. Curve 3 represents the propeller load demand curve that is valid for the design condition; maximum engine power can be utilized in this condition. Propeller curves 1-2 (light) and 4-5 (heavy) show the effect of decreased and increased resistance resulting from off-design conditions.

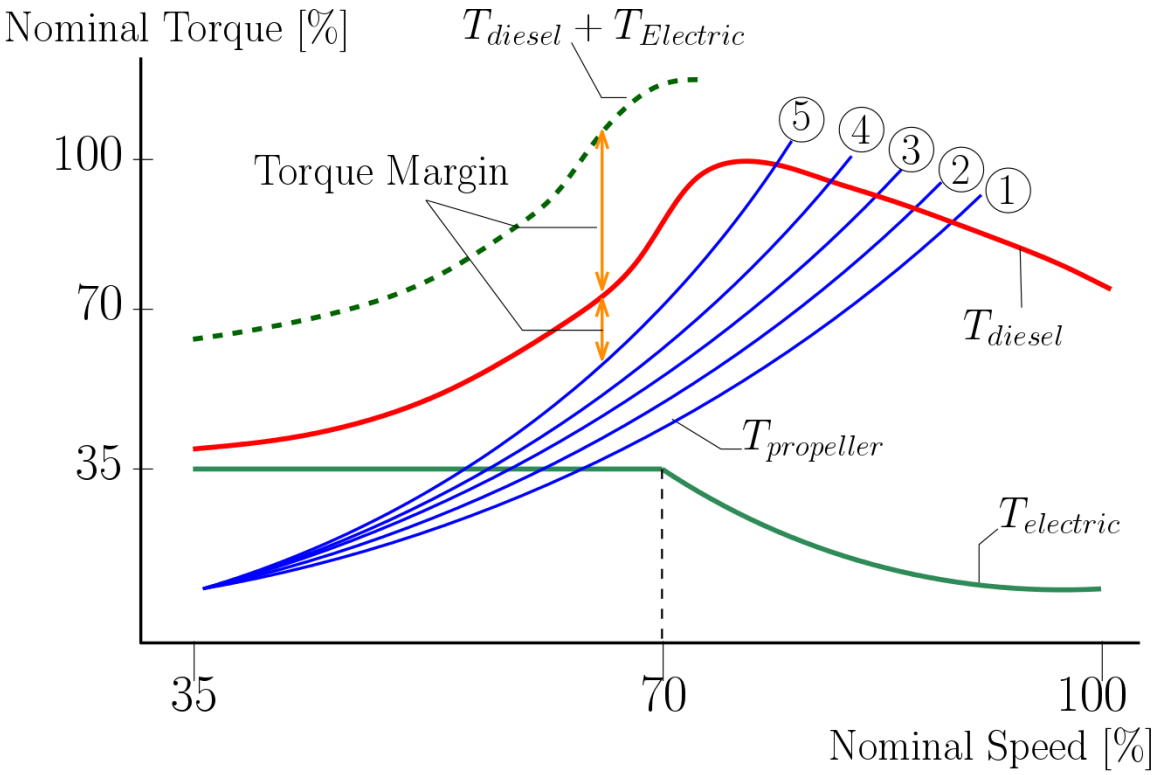

Figure 1-1: Schematic of load acceptance in the Hybrid Integrated Propulsion Powertrain.

Conditions that can lead to steeper load curves are heavy weather, fouled hull, towing a load or driving a power take-out. In the HIPPO-1 configuration, the EM

assists the diesel engine at low-load operation, where the internal combustion engine produces low torque. With this setup the initially small margin between the torque demand from the propeller curve and the available torque from the DE (i.e. the available torque that the propulsion system has available for acceleration during transient operation), can be significantly increased. This can lead to lower emissions of particulate matter (PM) (lower exhaust gases opacity) and lower fuel consumption.

Chapter 2

Experimental Facility

The Hybrid Integrated Propulsion Powertrain (HIPPO-1) testbed built for the purposes of this work, as seen in Fig. 2-1, consists of a diesel engine (DE) in parallel connection to an electric motor (EM). As such, the rotational speeds of DE and EM are identical, whereas the supplied torques add together. The desired torque demand is applied through a water brake (WB).

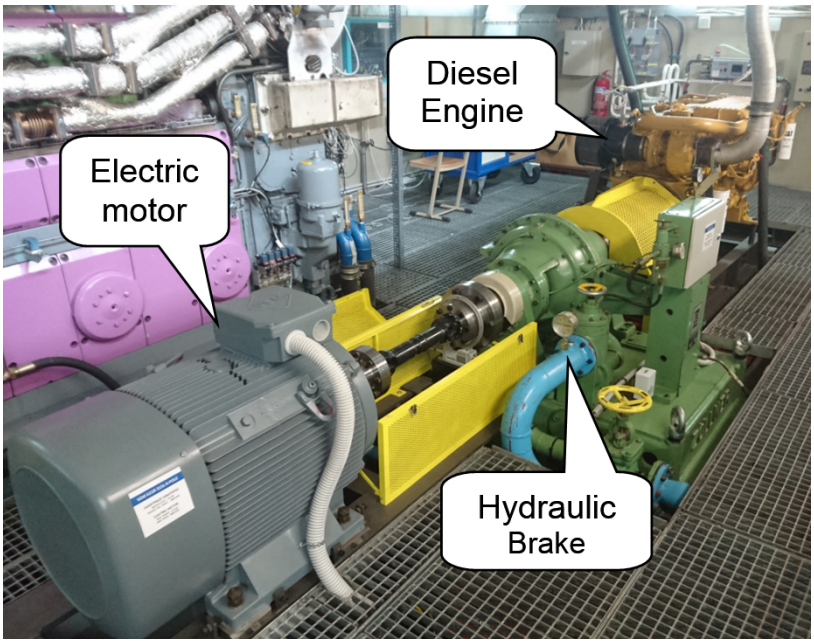

Figure 2-1: The hybrid electric test bed.

The prime mover is a production-type, CATERPILLAR 3176B 6-cyl. 10-liter high speed marine DE, with a rated power output of 425 kW at 2300 rpm. The DE is

coupled to an EM which is a standard 3-phase asynchronous induction motor, with a rated power of 112 kW. The EM is connected to a frequency inverter unit, enabling the torque output regulation of the EM at a predefined rotational speed. Finally, the water brake, which has connection flanges at both ends, has a load capacity of 1200 kW, with maximum speed at 4000 rpm and which is regulated by a separate controller, developed in-house at LME.

2.1 Hardware Implementation

Since the test-bed was a large full-scale facility, with a maximum output capacity of 560 kW, every component of the HIPPO-1 powertrain was designed using 3D CAD software (Autodesk $Inventor^{TM}$) as seen in Fig. 2-2.

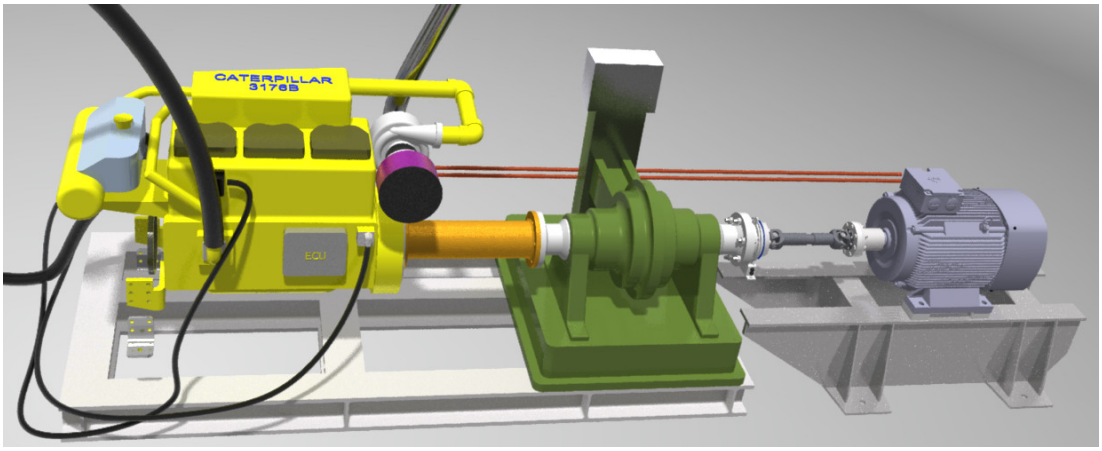

Figure 2-2: Initial 3D drawing of HIPPO-1 testbed.

The first phase included the preparation of the engine room, the manufacturing/ ordering of all the components required for the installation of the DE (i.e. engine mounts, exhaust and water piping, fuel lines) and finally the assembly of the above according to the new powertrain specifications. The DE was connected to the one of the free ends of the WB and the EM to the other. The installation of the sensors and actuators followed.

2.1.1 Electric motor integration to HIPPO-1

In order for the hybrid powertrain to be completed, following a parallel hybrid configuration (mechanical connection between the diesel engine and the electric motor) an AC electric motor(model VEM K21R) was directly connected mechanically to the DE (without a clutch in-between them). The EM is controlled by a frequency inverter. The frequency inverter can be operated in two modes: speed mode, which regulates only the rotational speed of the EM, and torque mode that regulates the torque output of the EM while the EM follows the rotational speed of the DE. The latter was selected due to the architecture of the control scheme of the hybrid testbed, in which the controller output is the torque command to the frequency inverter. The electrical power needed to drive the EM is provided from the grid, while any produced electrical power can be dumped to a pack of installed braking resistors.

The main purpose of the EM in the HIPPO-1 powertrain is to assist the DE at lower speed bands, where the DE produces low torque. Since the torque profile of the DE was known, the EM was chosen so as to produce its full torque up to 1500 rpm, the point at which the CAT engine reaches its maximum torque (Fig. 2-3).

The EM mount was designed in detail as a 3D CAD model, following static stress analysis (Fig. 2-4 and 2-5). Stress analysis was performed for the calculation of an optimal design, with the Stress Analysis toolbox of Autodesk $Inventor^{TM}$ using Finite Element Analysis (FEA) [50].

The toolbox requires the mounting points and the expected force applied on the part. The outcome of this tool is depicted graphically where any flaws in the design of the part can be easily distinguished. The material used for the fabrication of the mount was constructional steel type 50-2, according to DIN 17 100.

The EM mount was placed in the engine room, in line with the mount of the water brake.

For the connection of the EM to the rest of the hybrid powertrain, three connection flanges and one coupling were designed (Fig. 2-6) and manufactured at the workshop of the Laboratory. Also, a cardan shaft (i.e. shaft with universal joints at its ends)

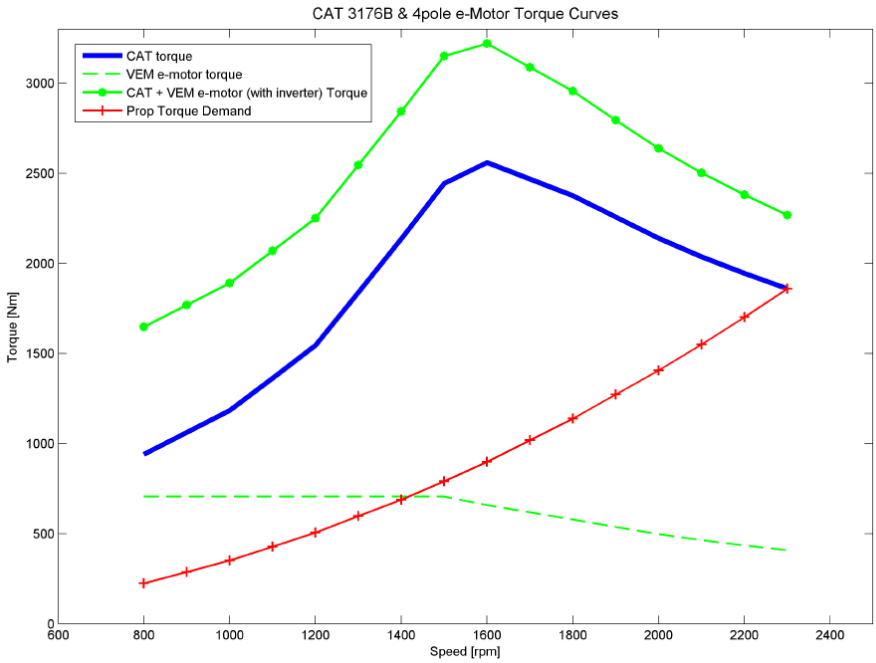

Figure 2-3: Diesel engine (Caterpillar 3176B) and electric motor (VEM K21R) Torque Curves.

was used. The optimum operating length of the cardan shaft is determined by the distance between the driving and the driven units, using the spline it incorporates, within its range. The maximum deflection angle of each joint is 44^o, which permits the driving and driven components to be partially misaligned. The shaft is hollow offering high strength/weight ratio. On both ends of the shaft suitable DIN120 flanges are bolted (Fig. 2-7).

2.1.2 Water Brake

The WB, a Zollner 9n38F, is capable of handling 1200 kW and is equipped with a load cell which monitors the total torque produced by the powertrain, under closed loop control. The load cell signal is transmitted to a load cell amplifier, and then to an analog input of the data acquisition card. From the closed loop controller, a control command is supplied to the outlet analog water valve through an electronic/pneumatic transducer, which converts the electric signal to proportional air quantity as supply to membrane of the water valve. The pressure of water inside the

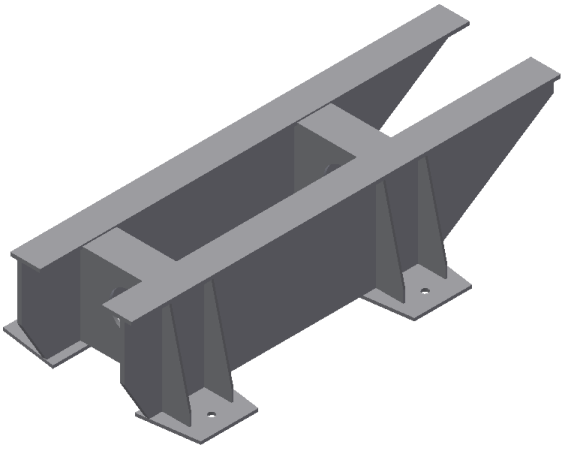

Figure 2-4: 3D model of the EM mount

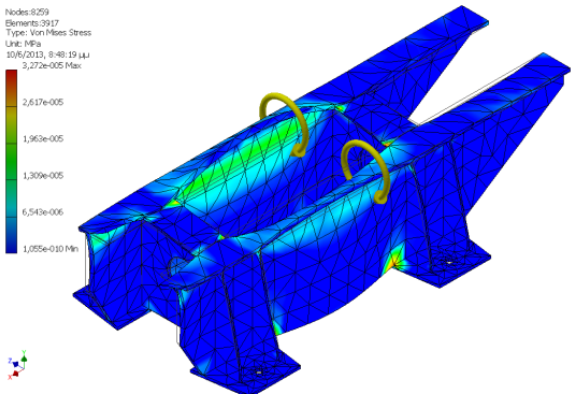

Figure 2-5: Stress analysis of EM mount

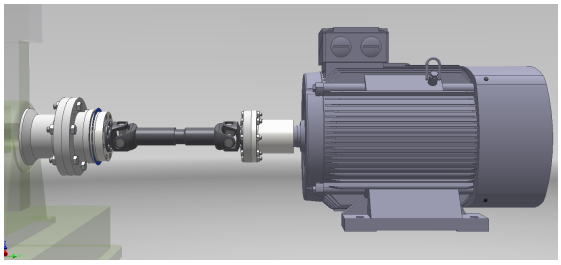

Figure 2-6: 3D CAD drawing of the electric motor and drivetrain.

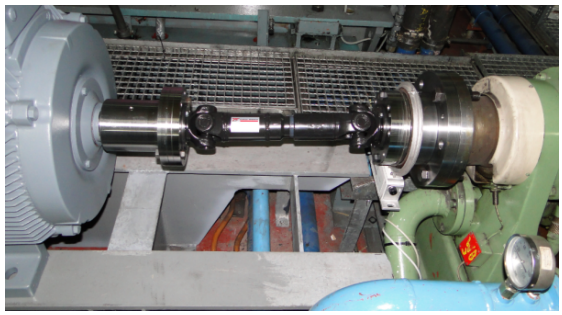

Figure 2-7: Electric motor connected to the water brake (with connection flanges and cardan shaft in place

main dynamometer chamber is also measured, through a pressure sensor installed on the top of dynamometer case.

The WB was modeled via system identification techniques (which are extensively presented in chapter 3) and a robust controller was derived. The designed WB controller shows good tracking performance around its design point. The dynamometer controller has to operate as:

- a regulator i.e. maintaining constant torque (load), under various disturbances like speed changes. This mode simulates an on-board generator which operates with constant rotational speed.

- a servo for tracking torque changes, usually applied either in steps, e.g. load change from 0 to 47% or along a propeller curve, with the torque being propor-

tional to the square of speed.

The propeller loading mode proved to be the most challenging of the above modes. Unlike automotive industry for example where typical loading cycles exist (ECE+EUDC, NEDC), propeller test loading cycles are not established. In that direction measurements on-board ships were taken, as explained in Appendix A. It should also be noted that in the first stages of commissioning the HIPPO-1 testbed, some problems with the WB were present. There is a disparity between the high power capacity of the WB (1200 kW) and the maximum power output of the DE (CAT 3176B - 450 kW). The WB displayed oscillating behavior above 1000 Nm load, and thus the DE could not be operated at full power. The WB displayed hunting behavior in many cases; these problems are presented in detail in Appendix B.

2.2 Testing Facility Measurement System

A schematic representation of the installed sensors and engine parameters is given in Fig. 2-8. Measurements present in the test bed include: NOx/oxygen (Continental Uninox 24V), exhaust gas opacity (AVL 439), fuel mass flow (ABB CoriolisMaster FCM2000). A high precision torque and speed measuring flange, model HBM T10F, is installed on the powertrain, at the EM side. The intake manifold pressure and turbocharger speed (μ epsilon) are also measured. The DE embedded ECU, HIPPO-1 data acquisition system, EM frequency inverter controller, WB water pump and the NOx/lambda sensor are interconnected with a CAN bus network, designed using $Matlab/Simulink^{TM}$.

2.2.1 Control and Data Acquisition System

The whole test bed is controlled and monitored in real time by a $dSpace^{TM}$ DS1103 platform with rapid data prototyping capability. The data acquisition system (DAQ) collects and stores measured data during test runs, which are post-processed after the end of each run. The platform incorporates its own graphical user interface software

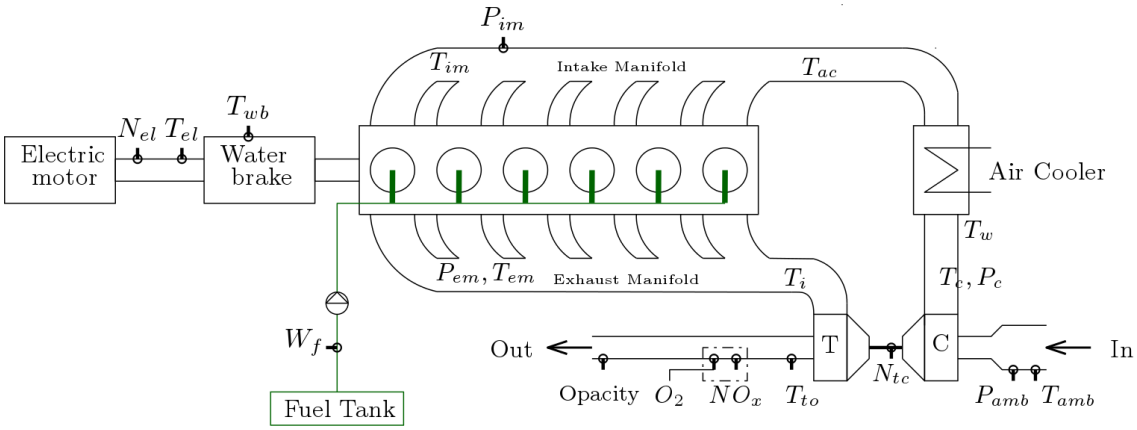

Figure 2-8: Installed sensors (in circle) and engine parameters in experimental diesel engine.

(dSpace NextGeneration), programmed under the $Matlab/Simulink^{TM}$ environment.

The HIPPO-1 DAQ uses a total number of 26 analog input channels, and 12 analog outputs. The analog signals ranges are from -10V to +10V. Another 4 digital inputs and 2 digital outputs as well as a PWM signal for the DE speed setpoint are used. For the measurements presented in this thesis, the $dSpace^{TM}$ system is sampled at 1 kHz. The dSpace DS1103 DAQ and related hardware can be seen in Fig. 2-9.

2.2.2 Lambda and NOx sensor

The wideband lambda sensor proved to be the most important sensor in the experimental setup used for this Thesis, as it was selected to close the control system loop, as is described in more detail in the next chapter.

This sensor is designed to measure the proportion of oxygen in the exhaust gases. It is widely known in the industry as "lambda sensor" (λ sensor), although it provides as output the oxygen concentration from which lambda in the exhaust gases is further calculated considering the stoichiometric air-to-fuel ratio. Since no other chemical process takes place between the combustion in the cylinder and the measurement point of the installed oxygen sensor, we consider the calculated lambda value in the exhaust path to be equal to the lambda value in the cylinder.

This sensor also measures the NO_x content in the exhaust gases. The installed

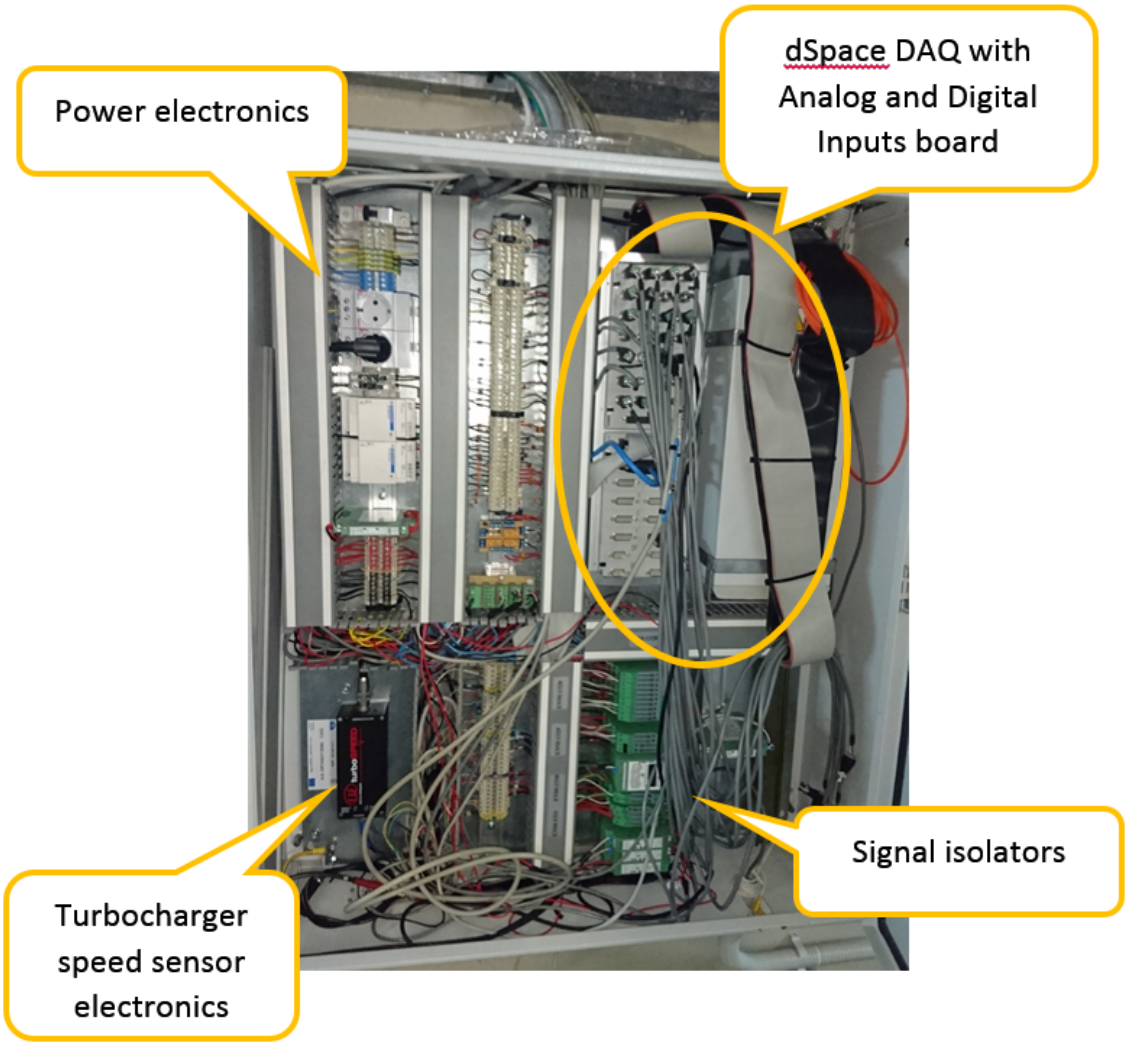

Figure 2-9: HIPPO-1 data acquisition and control module (dSpace DS1103) along with the power electronics and cabling.

unit is a NGK ZFAS-U type SmartNOx wide range linear λ sensor (Fig. 2-10). Not only does this type of sensor have an extended window of measurement and can be used successfully where lean burn strategy is employed, it also provides exceptional accuracy around the stoichiometric point which is useful in the quest for emission reduction. This type of sensor can also be used in conjunction with diesel engines as they operate with an excess air factor.

The temperature of the sensor element is critical, and is regulated by a built-in controller. When the desired temperature of the element has been achieved, around 2 minutes after each power-up, the measurement begins. Also, this sensor measures

the NO_x content in the exhaust gases.

The NGK SmartNOx sensor is connected to the DAQ via CAN bus and a custom made Simulink blockset.

In order to minimize the effect of the exhaust gas pressure which adversely affect its operation (increased time delay constant), the lambda sensor is placed 1 m downstream the turbine (Fig. 2-11). Its response time, i.e. the time interval between a change in the load in the DE and the corresponding lambda change, is measured to be around 120 ms and with the DE at 1600 rpm. The response time is very sensitive to the exhaust gas velocity; lower rpm would lead to higher response times and vice versa. The reason 1600 rpm was chosen as the operating point around which the hybrid testbed is modeled, is because it is the mean value of the rpm spectrum of the DE (800-2400 rpm) and also the point where the DE produces its maximum torque (2500 Nm)

Figure 2-10: The NGK SmartNOx sensor

Figure 2-11: The SmartNOx sensor as installed at HIPPO-1 testbed

2.2.3 Torque Measuring Flange

The HBM T10F Torque Flange is installed on the powertrain on the EM side of the water brake. The torque flange consists of two separate parts: the rotor and the stator. The rotor includes the measuring body and the adapter flange. The measuring body houses strain gauges and electronics. The top surface of the measuring body supports the transmitter coils for contactfree transmission of excitation voltage and

measuring signal. The signals are transmitted and received by a divisible antenna ring (stator). The antenna ring is mounted on a housing that includes the electronic system for voltage adaption and signal conditioning. The stator includes connecting plugs for the torque signal, the power supply and the rotation speed signal with optical measuring system, by means of an infrared beam and slotted disk. The torque meter is rated at 10 kNm. The expected accuracy is 0.1% and the measuring frequency is 1 kHz. The measured torque and speed are connected to the dSpace DAQ as analog inputs. The torque measuring flange can be seen in Fig. 2-12 as installed on HIPPO-1 testbed.

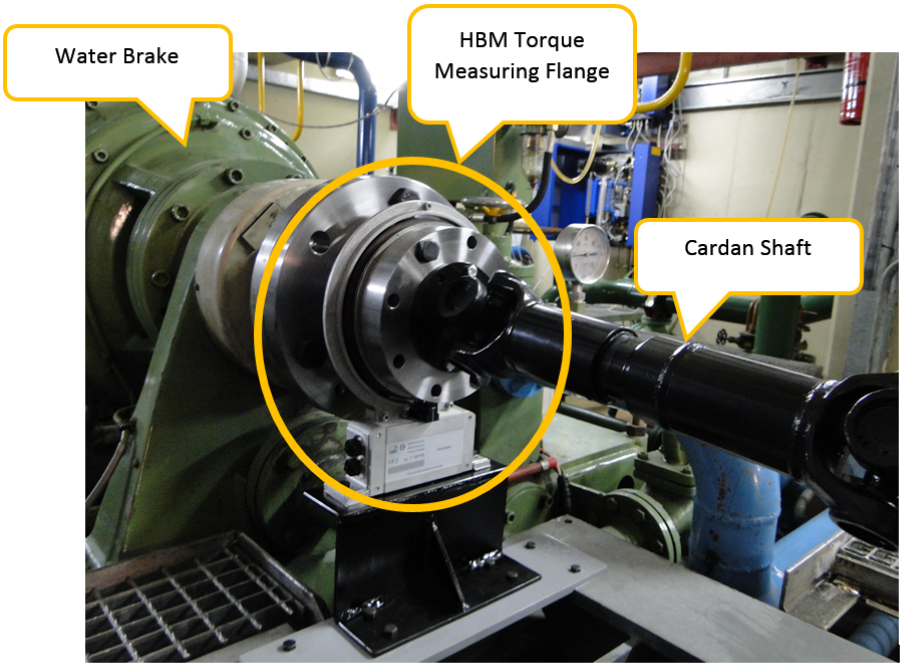

Figure 2-12: Photo of torque measuring meter as installed on HIPPO-1 (HBM T10f).

2.2.4 Opacity sensor

The exhaust gas opacity is measured with an AVL 439 opacimeter. A probe of 1 m length and 10 mm in diameter is mounted in the engine exhaust duct, approx. 1 meter after the exhaust manifold, and draws off sample exhaust gas. The gas is routed to the opacimeter through a conditioning tube. Heated air is supplied around

the tube up to the sensing probe, thus ensuring that the gas sample has constant temperature. The exhaust gas passes through two pumps which maintain a constant measurement flow from 40 to 49 lt/min, before it exits back to the exhaust line.

A 'zeroing' procedure is performed every half hour of measurement in order to evaluate the 'zero intensity value' E_0, required in calculations. The opacimeter is connected via an analog channel to the dSpace DAQ. The output rate is 50 Hz. The opacimeter can be seen in Fig. 2-13 as it is installed on the HIPPO-1 testbed.

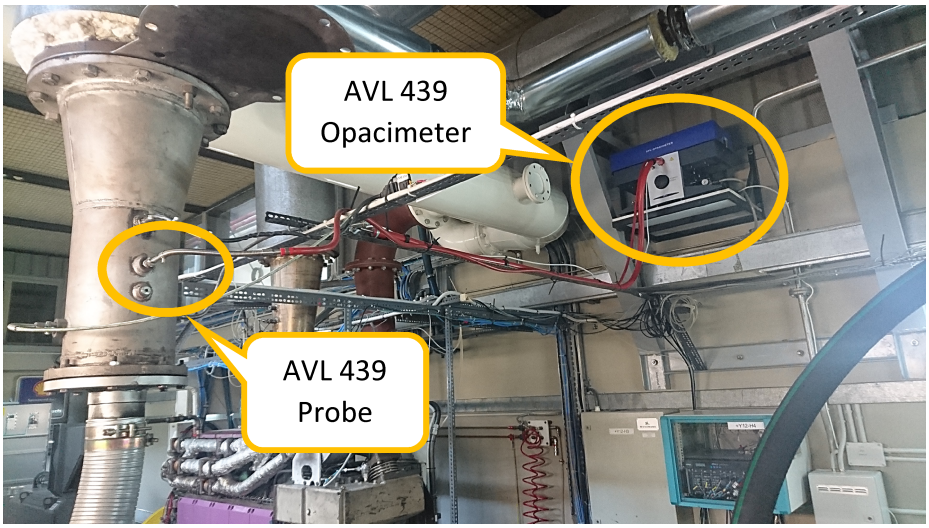

Figure 2-13: Exhaust gas opacity sensor (AVL 439) as installed on HIPPO-1 testbed.

2.2.5 DE turbocharger speed sensor

The DE turbocharger rotational speed is measured with a Micro-Epsilon Turbospeed DZ135 sensor. A very fast proximity sensor detects the tips of the turbocharger aluminum alloy blades passing by. The Eddy current loss principle effects impedance changes in a measuring coil (sensor). The electromagnetic field from the coil generates eddy currents in the turbocharger blade, with every blade generating a pulse. The controller identifies the speed by considering the number of blades. The non-contacting single-channel measuring system consists of a sensor, sensor cable and a controller, installed in a compact aluminum housing.

Figure 2-14: Turbocharger speed measuring sensor as installed on the DE of the HIPPO-1 testbed.

2.2.6 Fuel mass flow sensor

In order to evaluate a controller design at the HIPPO-1 diesel electric hybrid setup, an accurate measurement of fuel consumption is essential. For that purpose, two fuel flow meters were used (ABB CoriolisMaster FCM2000), one at the DE fuel feed line and the other on the fuel return line (Fig. 2-15). These sensors use the Coriolis measuring principle, making them highly accurate (error $<1\%$) and with quick response times. A Coriolis flowmeter requires a force acting on a tube carrying a flowing fluid. This force actually deforms tubes through which the fluid flows (Fig. 2-16). The amount of deformation depends directly on the mass flow rate through the tubes. Signals from sensors measuring this deformation provide a direct indication of the mass flow rate.

Each fuel mass measuring device is connected to an analog input in the DAQ, using a sampling rate of 1 kHz. The data collected from these sensors were used to populate fuel/speed/torque 3D maps in regions of interest, based on experiments at steady state (static) loading conditions, which are utilized by some controlling methods of HIPPO-1. The population of those maps is described in the next chapter.

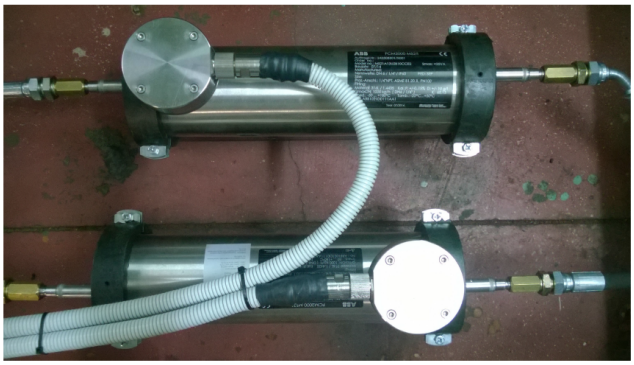

Figure 2-15: ABB fuel mass flow measuring devices as installed at HIPPO-1 testbed

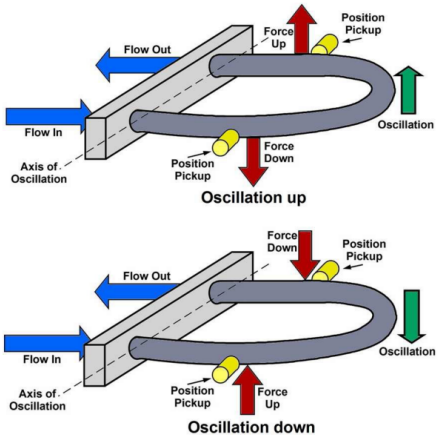

Figure 2-16: Coriolis force measuring principle from [1].

THIS PAGE INTENTIONALLY LEFT BLANK

Chapter 3

System Modeling

Modern control engineering practice includes the use of control design strategies for improving manufacturing processes and the efficiency of energy use, as well as to maintain various safety measures.

A basic requirement for a successful control is to have a suitable model for control. The control plants in process industries are mainly non-linear and continuous-time. The first possibility is to use nonlinear mathematical models of the plants, in the form of partial differential equations. Usage of these models is usually computationally demanding or even not possible in some controller techniques [39]. Therefore it is suitable to use robust control methods based on linearized models. Between the complex physical systems under investigation and the models used for the controllers' synthesis, a design gap exists. The iterative nature of design allows to handle the design gap effectively while accomplishing necessary trade-offs in complexity, performance and cost, in order to meet the design specifications.

A control system is an interconnection of components forming a system configuration that will provide a desired system response [16]. The basis for analysis of a system is the assumption, provided by linear system theory, that it exists a cause-effect relationship for the components of the system. Therefore a process to be controlled can be represented by a single block, as in Fig. 3-1.

In the HIPPO-1 control framework, **the aim** was to create a controller that would perform the **power split** between the DE and EM for a multitude of loading condi-

Figure 3-1: A typical process to be controlled.

tions, mainly focusing on transient operation, in order to reduce exhaust gas emissions (NO_x, PM) and/or fuel consumption.

The main limitation of the experimental facility was that the ECU of the diesel engine CAT 3176B was to be independent so the fueling parameters of the DE could not be directly affected nor measured. Therefore the power output of the DE had to be regulated *indirectly*.

The total load demand on the HIPPO-1 testbed at every time step of the process is

$$T_{load} = T_{DE} + T_{EM} \tag{3.1}$$

where T_{DE} and T_{EM} is the produced torque from the diesel engine and electric motor respectively. In that way, for any given load demand, if the EM would engage, the rest of the total torque would be covered by the DE.

The general controlled plant (system) includes both the EM and DE, where the only input is the EM frequency inverter command. At this point an appropriate measurable signal had to be found that would be suitable as output of the plant, in order to proceed with the modeling.

The signal that was chosen as output of the system, and consequently as the signal that will be used as feedback to the HIPPO-1 controllers, is the value of λ. The main reasons that justify this choice are

- Even though λ is not a measure of emissions itself, it is still a reliable estimate of them. As illustrated in Fig. 3-2, there is a strong correlation between the value of λ and the main emissions formed in diesel engines.

- λ is a suitable signal for control purposes since no significant noise is presented in this value as it is a digital signal acquired using CAN-bus and the dynamics of λ are neither very slow nor very fast [20].

- λ can be quite easily modelled from the air and fuel path dynamics.

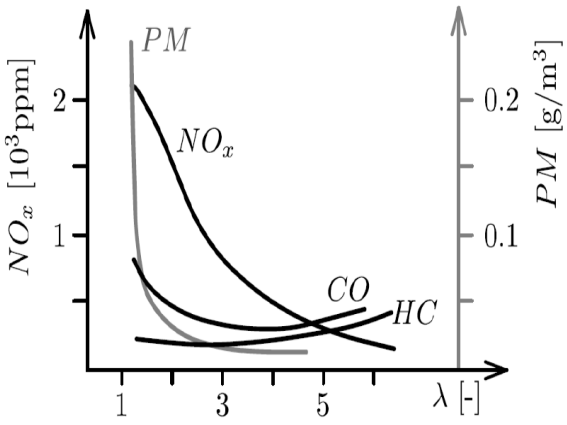

Figure 3-2: NOx and PM as a function of λ -Figure obtained from [20].

The block diagram of the open loop HIPPO-1 system, with the input and output signals is depicted in Fig. 3-3.

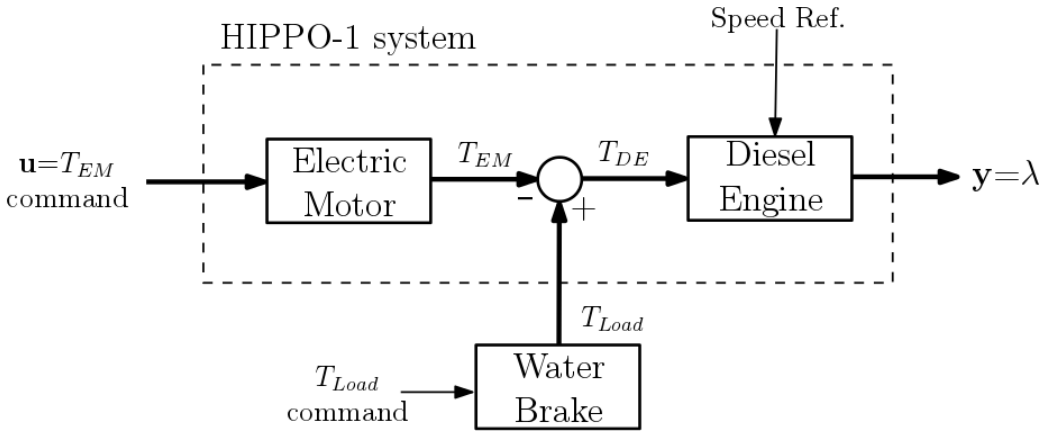

Figure 3-3: HIPPO-1 open loop system

The traditional approach towards the problem of AFR estimation is through phenomenological Mean Value Models (MVM) of the individual engine components, e.g. the intake and exhaust manifolds, the turbocharger, the cylinders etc. Classical first principle methods are extremely useful for their good insight in the operation of the systems, but frequently require too much effort and/or do not achieve the required precision and/or are not suitable for online use [14]. For a turbocharged diesel engine like the one present in HIPPO-1, it is necessary to model

1. the compressor and intercooler
2. turbine performance
3. unsteady-flow effects in the induction system
4. flow through the inlet valves
5. air motion within the cylinder
6. dynamics of the injection system
7. fuel jet interaction with the trapped air to form a spray
8. combustion
9. heat flow within the combustion chamber and the cooling media

For the problem in consideration, linear system identification methods were the preferable option, due to the lack of efficiently detailed information about the engine components. Various models were obtained around an appropriate engine operating point. Linear control-oriented models for AFR dynamics in internal combustion engines based on identification have been used successfully in the past; see [18] and [21].

3.1 Identification Methods

Most methods of system identification rely on iterative, nonlinear optimization to fit parameters in a pre-selected model structure, so as to best fit the observed data [33]; these are known as *parametric* methods. An alternative class of identification methods is the *subspace methods*, which are 'one-shot' rather than iterative and rely on linear algebra rather on optimization. They are particularly effective for multivariable systems and can be used with arbitrary input-output-data and not just with pulse responses. For the case that a non-linear model is required, Hammerstein-Wiener models are commonly used.

One can use also Instrumental Variables, Maximum Likelihood, Impulse response analysis (Markov parameters) or others. In the following sections the methods applied for the identification of models used in this Thesis are presented.

3.1.1 Parametric Identification

In general, the estimating algorithm performs two major tasks. At first the parameters for estimation are initialized and then updated. The details of the algorithms used to perform these tasks vary depending on a variety of factors, including the sampling of the estimated model and the estimation data [34].

The method for estimating the vector of θ parameters has the general term *prediction error* method, PEM. Prediction error ϵ is defined as

$$\epsilon(t, \theta_*) = y(t) - \hat{y}(t|\theta_*) \tag{3.2}$$

between the measured output and the predicted output of the model. Norm V_N is used

$$V_N(\theta, z^N) = \frac{1}{N} \sum_{t=1}^{N} l(\epsilon_F(t, \theta)) \tag{3.3}$$

Then the estimate $\hat{\theta}_N$ is defined as the minimization of function $V_N(\theta, z^N)$. Typical solution method is *least squares*.

With parametric estimation, process models were derived for inputs and outputs. This model type is chosen for its advantages: the model coefficients have a physical interpretation and it provides delay estimation.

Different model structures were created by the selection of the number of poles, and zeros and the addition of time delay.

3.1.2 Subspace Identification

The term subspace identification refers to a class of algorithms with main characteristic the approximation of subspaces generated by the rows or columns of some block matrices of the input and output data.

Popular subspace identification method is Numerical algorithm for Subspace System IDentification (N4SID), implemented in the Identification toolbox of MATLAB [35].

A major advantage is that *N4SID* algorithms are non-iterative with no nonlinear

optimization part involved [44]. This is why they do not suffer from the typical disadvantages of iterative algorithms, e.g. no guaranteed convergence local minima of the objective criterion and sensitivity to initial estimates. For classical identication an extra parametrization of the initial state is needed when estimating a state space system from data measured on a plant with an non-zero initial condition. Another advantage of the *N4SID* algorithms is that there is no difference between zero and non-zero initial states.

3.2 Experimental Identification Input Signals

System identification can be defined as the process of obtaining a model for the behavior of a plant, based on input and output data. A fundamental decision that has to be made in terms of the identification process concerns the type of signal that will be used. The requirement is that during system identification in open loop, the input should be persistently exciting, i.e. it should contain sufficiently many distinct frequencies. The identification experiment has to distinguish different models in the set of all possible models used.

Also, for linear system identification, it is desired to achieve a desired input spectrum for a signal with as small crest factor as possible. Crest factor (C_r), is a measure of a waveform, showing the ratio of peak values to the effective value [32]. The desired property of the waveform used for identification is defined in terms of

$$C_r^2 = \frac{\max\limits_{1\leq t\leq N} u^2(t)}{\frac{1}{N}\sum\limits_{t=1}^{N} u^2(t)} \tag{3.4}$$

where u is the input signal. A good signal waveform is one that has a small crest factor. The theoretical lower bound for C_r is 1, which is achieved by binary symmetric signals.

In this section two choices for input signals are presented.

3.2.1 White Noise

White noise is a random signal that contains all frequencies uniformly, with a constant power spectral density. Because white random noise has an inherently flat frequency spectrum, it can be used to characterize the frequency response of systems such as filters. Theoretically white noise is a preferable input signal, that provides uniform fit at all frequencies, but it has a high crest factor.

3.2.2 Pseudo-Random Binary Signal

A Pseudo-Random Binary Signal (PRBS) is a periodic deterministic signal with white noise-like properties. It has been widely used for system identification as well as for spread spectrum wireless communications and GPS. PRBS can be easily generated with a shift register that circulates its output to the input gate, and thereby generates a periodic, long sequence binary signal. It is generated by the difference equation

$$u(t) = rem(A(q)u(t), 2) = rem(a_1 u(t-1) + ...a_n u(t-n), 2) \tag{3.5}$$

Here $rem(x, 2)$ is the remainder as x is divided by 2. Also, $u(t)$ only assumes the values of 0 and 1. Of course after u is generated, it can be changed to any level. In our case the maximum input to the frequency inverter is 0.1 V.

PRBS has the lowest crest factor and gives control over the shaping of its spectrum [47], making it the signal of choice for this Thesis. Its disadvantage is that only a full period of PRBS signal bears the desired properties.

3.3 Experimental Identification Tests

Based on the crest factor (C_r) criteria, the method employed to measure input and output data for system identification was to apply several full length PRBS at the HIPPO-1 testbed. The PBRS signal was chosen to be 9-bit with a full length of around 450 sec per period.

The design of a PRBS signal involves the determination of its switching time,

order of excitation, magnitude and clock period. The magnitude of the PRBS signal can be chosen so that the crest factor obtains its maximum value with consideration of the physical limitations of the system ([32], p. 415).

The order of PRBS was selected so that the dominant frequencies of the identified system were covered [11]. The system identification procedure has a natural logical flow: at first the data are collected, then a set of models is selected and finally the "best" model in this set is picked, based on the fit percentage of the model versus the measured data. It is quite likely though, as it happened most of the times during the identification process described in this Thesis, that a particular model obtained would not pass the typical model validation tests.

Three separate identification test sets are shown below under open loop operation, each containing a different excitation signal (EM command, engine speed and WB load), in order to extract a wide spectrum of models describing the powertrain.

3.3.1 Identification Set 1: Alternating EM Torque

A PRBS signal was imposed at the frequency inverter of the electric motor as torque command (EMcmd), and the resulting λ values of the diesel engine were measured; thus $[u; y] = [EMcmd; \lambda]$.

The identification experiment was carried out with constant torque demand at T_d= 500 Nm, as imposed by the water brake dynamometer, and constant shaft speed N_e= 1600 rpm. In Fig. 3-4 the PRBS excitation signal on the EM (top) and the resulting DE λ values (bottom) can be seen. Data was collected with a rate of 1 kHz, low-pass filtered and divided in two sets, one for identification and the other for validation purposes.

3.3.2 Identification Set 2: Alternating Speed

For this session, a suitable PRBS signal was imposed at speed governor of the DE (PWM signal), and the measured variable was the resulting λ values; thus $[u; y] = [\mathrm{N}_E;\ \lambda]$. The identification experiment was carried out with constant torque

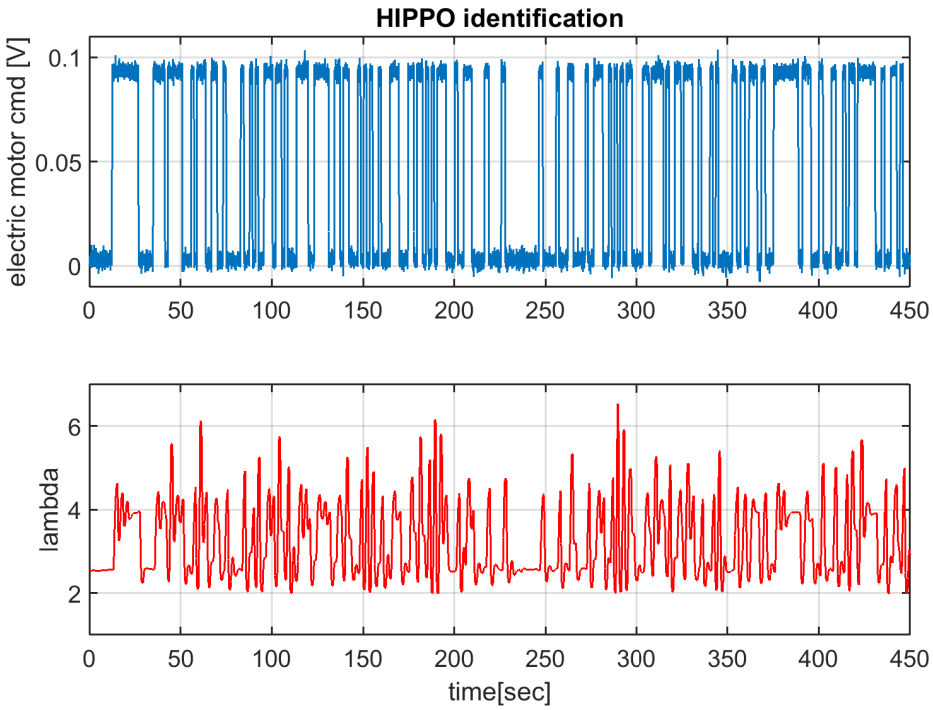

Figure 3-4: PRBS (top) imposed on the EM command and resulting λ values (bottom), used for identification purposes of HIPPO-1.

demand at T_d= 500 Nm, as imposed by the water brake dynamometer, without any torque coming from the EM T_e= 0 Nm (Fig. 3-5). It can be observed that the measured total torque (third subplot) displays some fluctuations due to the speed change, whereas the EM command is zero (fourth subplot) for the purposes of this identification experiment.

3.3.3 Identification Set 3: Alternating WB Load

For the final identification session, the water brake dynamometer was excited with a suitable PRBS signal, as can be seen in Fig. 3-6. The command affects the position of the pneumatic water valve, which defines the volume of water inside the WB. As descibed in the previous chapter, the amount of water dictated the applied torque at the testbed. Thus $[u; y] = [TorqueWB; \lambda]$. The identification experiment was carried out with constant shaft speed N_e= 1600 rpm, as can be seen in the third subplot of the same figure, and the EM not producing any torque.

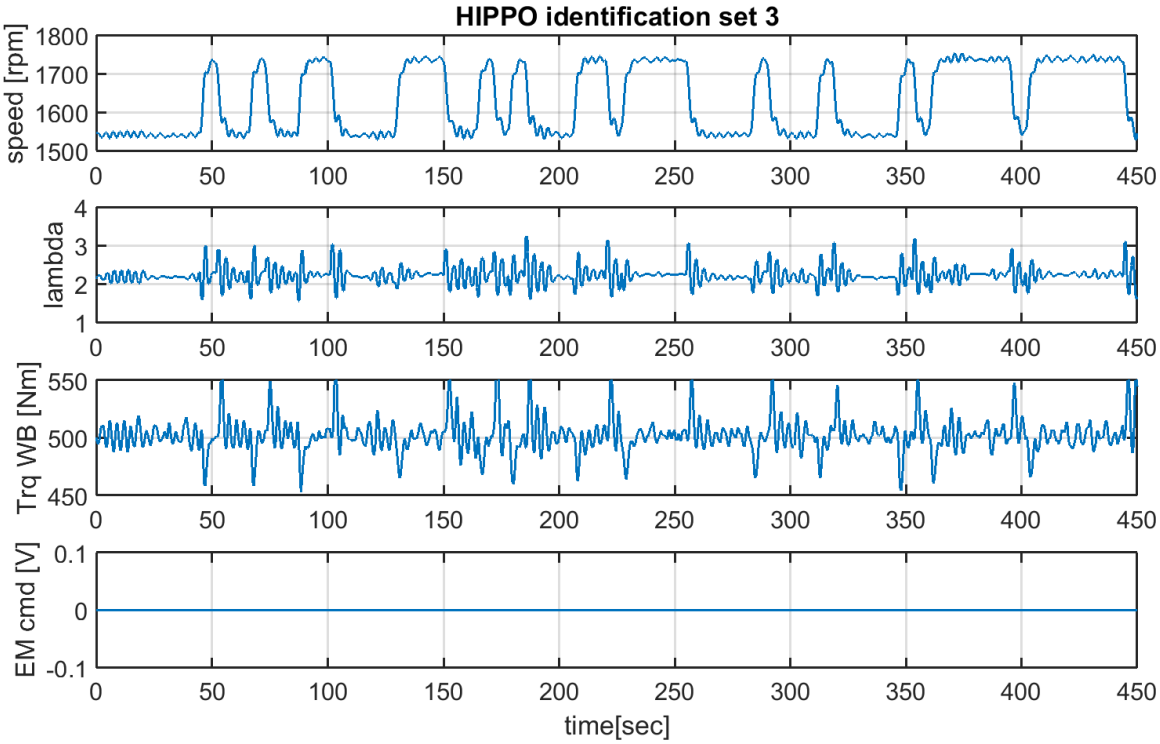

Figure 3-5: PRBS imposed on the DE speed, used for identification purposes of HIPPO-1.

3.4 HIPPO-1 Models

In this section, the two basic forms of model structures that are the outcome of the identification methods are presented. Model 1 uses only one of the identifications timeseries (alternating EM command) and Model 2 utilizes all three identification timeseries for a global model.

A wide range of identified models were derived. The dominant models with the corresponding input-output variables can be seen in Table 3.1. These models are presented in detail in the following subsections.

3.4.1 Model 1

In the case of a first-order system a process model in continuous time is

$$G(s) = e^{-sT_d} \frac{K_p}{1 + sT_p} \tag{3.6}$$

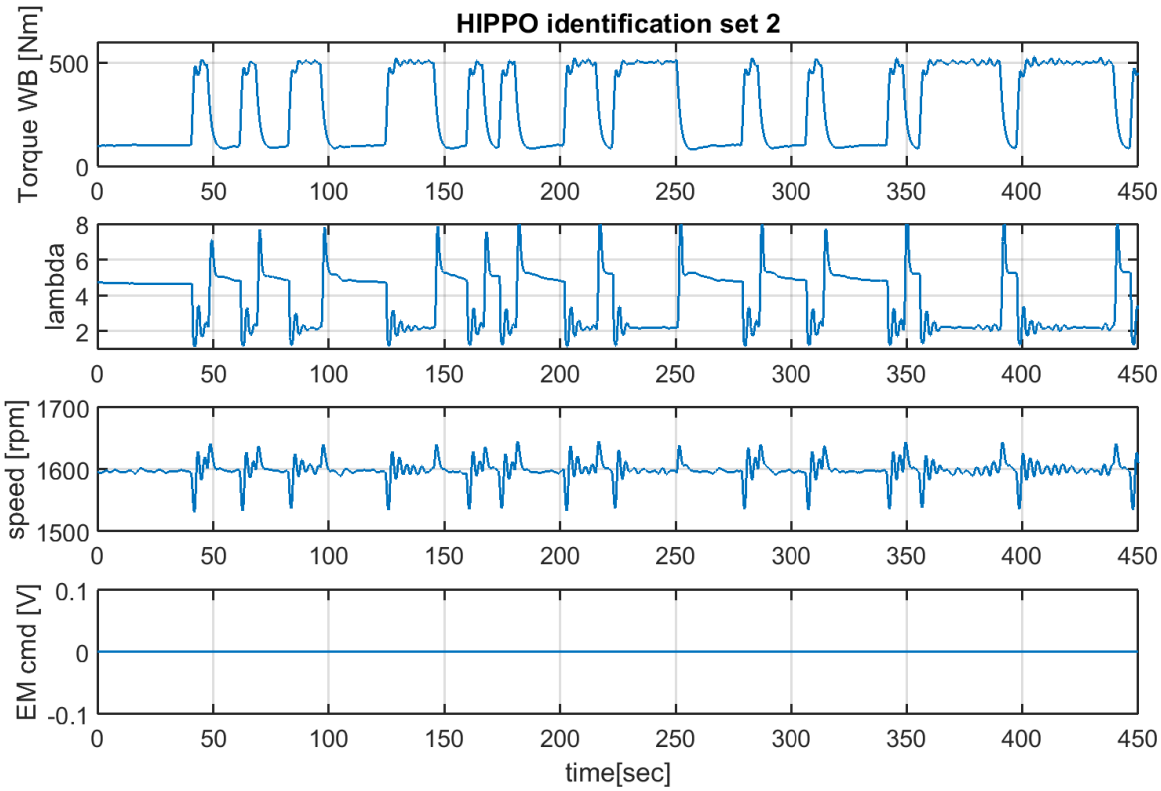

Figure 3-6: PRBS imposed on the WB valve, changing the load demand of the powertrain, used for identification purposes of HIPPO-1.

where K_p is the static gain, T_p is the time constant, T_d is the time delay.

The poles of a linear system are the roots of the denominator of the transfer function G. The poles have a direct influence on the dynamic properties of the system. The zeros are the roots of the denominator of G. Poles are associated with the output side and zeros are associated with the input side.

The identification of the transfer functions was carried out with the Matlab/System Identification Toolbox, [35], and more specifically with the toolbox command **tfest**. *tfest* uses the prediction error minimization (PEM) approach to estimate transfer function coefficients [32], as presented in Section 3.1.1.

In this case, continuous-time transfer functions were estimated, using time-domain data with a sampling time of 0.001 seconds. The estimation algorithm initializes the estimable parameters using the method specified by the *InitMethod* estimation option, which is used to initialize the values of the numerator and denominator of the output of tfest. The 'n4sid' initialization option estimates a discrete-time model, using the

CONTROL ORIENTED MODELS										
NAME	TYPE	INPUT					OUTPUT			
		EMcmd	MAP	SPEED	$\Delta SPEED$	lambda	lambda	MAP	NOx	F.O.C.
model 1	LINEAR MODEL	x					x			
model 2	LINEAR MODEL	x			x		x			
mMAP	LINEAR MODEL	x		x				x		
mNOx	LINEAR MODEL		x			x			x	
mCons	LINEAR MODEL		x	x						x
SIMULATION ORIENTED MODELS										
NAME	TYPE	INPUT					OUTPUT			
		EMcmd	Tdiesel	SPEED			lambda	MAP	Telectric	
mTel	LINEAR MODEL	x							x	
model 3	NARX MODEL		x	x			x	x		

Table 3.1: The identified models used for controller synthesis and simulation purposes, with their input-output variables.

N4SID estimation algorithm, which transforms it to continuous-time using function *d2c*.

The initialized parameters are updated using a nonlinear least-squares search method, specified by the *SearchMethod* estimation option. The objective of the search method is to minimize the weighted prediction error norm.

The transfer function G_l from identification with input the command to the frequency inverter, $u = EMcmd$; and output $y = \lambda$ is presented in Eq. 3.7. Time delay is in sec.

$$G_l = \frac{(16.1s^4 + 134.2s^3 + 376s^2 + 1455s + 1628)}{s^5 + 4s^4 + 25.4s^3 + 50.4s^2 + 108.7s + 101.3}^{-0.79s} \tag{3.7}$$

Fig. 3-7 shows the nominal model and other similar identified models (i.e. with variation in number of poles and zeros) compared with actual step response of λ.

For the identification of the transfer function only the first half of the whole experimental set of data was used. The second half was used to validate the identified transfer function.The output of the nominal model 1 was compared to the output of actual λ values from time series data, as shown in Fig. 3-8. Model 1 fit was about 71 %, capturing the dominant dynamics of the process under control.

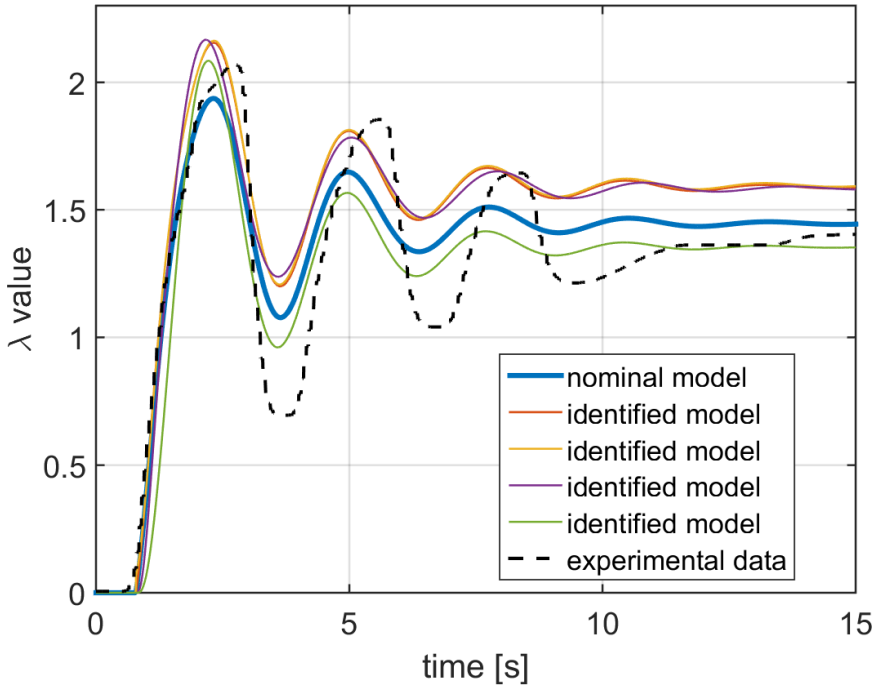

Figure 3-7: Model 1 family step response.

3.4.2 Model 2

With the use of all three engine identification datasets, multiple kinds of models were identified, according to their input-output attributes. Emphasis was given to low-order models which give a close description of the oscillating dynamics of the engine.

From the identification process, state-space models using subspace method (N4SID) algorithms (as described in Section 3.1.2) and ARX models (Linear AutoRegressive models with eXogenous input) were derived in order to describe the engine transient dynamics during step loading.

The SS models in discrete time, have the structure

$$\begin{aligned} x(k+1) &= Ax(k) + Bu(k) \\ y(k) &= Cx(k) + Du(k) \end{aligned} \tag{3.8}$$

Multi Input Single Output (MISO) models with inputs the EM Frequency Inverter Command ($EMcmd$) and the error between the measured engine speed (N_E) from

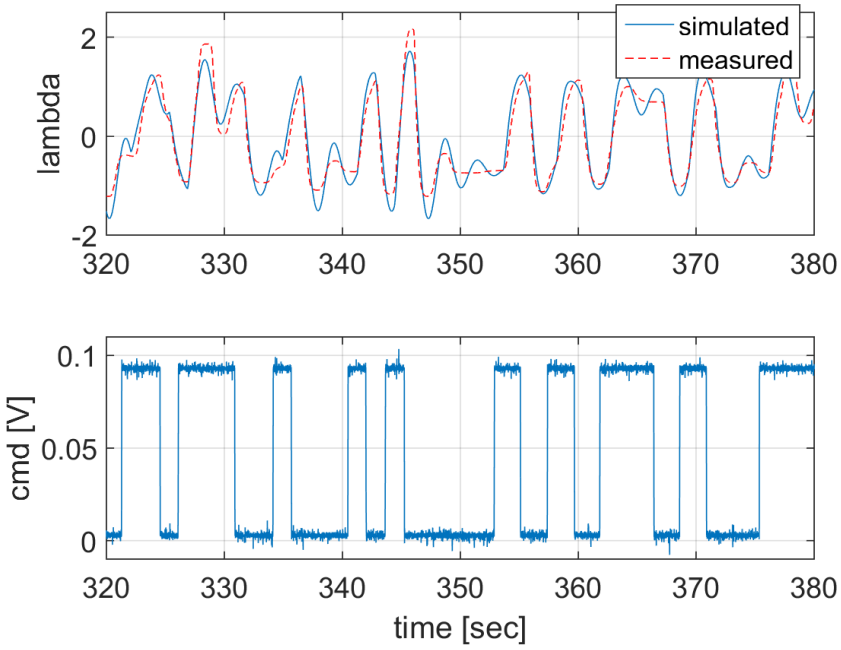

Figure 3-8: Model 1 output and measured λ comparison (top); The input PRBS signal.

a reference value ($dN_E = N_E - N_E Ref$) as inputs were derived are described in Eq. (3.9).

$$\lambda = f(EMcmd, dN_E) \tag{3.9}$$

The matrices A, B, C and D of the state space form, as were generated from the system identification are described in Eq. (3.10).

$$A = \begin{bmatrix} 0.07556 & -1.739 \\ 3.093 & -1.946 \end{bmatrix} \qquad B = \begin{bmatrix} 0.3254 & 0.001003 \\ -0.7647 & 0.0005494 \end{bmatrix}$$
$$C = \begin{bmatrix} 30 & 1.166 \end{bmatrix} \qquad D = \begin{bmatrix} 0 & 0 \end{bmatrix} \tag{3.10}$$

Engine emissions and fuel consumption models were also modeled at the operating point of $N_E = 1600$ rpm. Low-order NOx (NOx) and fuel consumption (FOC) models depending on engine parameter measurements engine speed (N_E), engine inlet manifold pressure (MAP) and λ were extracted from the available measured data, as

described in Eq. (3.11)-(3.12).

$$NOx = f(\lambda, MAP), \tag{3.11}$$

$$FOC = f(MAP, N_E) \tag{3.12}$$

Finally, models of Eq. (3.9) - (3.12) were combined so as to make a MIMO model, as shown in Eq.(3.13) and used in MPC design in order not only to control λ but also comply with emission restrictions and fuel consumption limitation. In these models the Input Attributes are not independent from each other, so a state feedback is needed in order to predict accurately the engine behavior and get proper values of the output prediction trajectories.

$$\begin{Bmatrix} \lambda \\ NOx \\ F.O.C. \end{Bmatrix} = f(EMcmd, dN_E, N_E, MAP, \lambda) \tag{3.13}$$

A state feedback signal structure assumes that a system output value is treated also as input for the system, as shown in Fig. 3-9. The need of the state feedback manipulation is shown in Fig. 3-10, which shows the controller performance (*model 2* as internal model), with and without the use of state feedback.

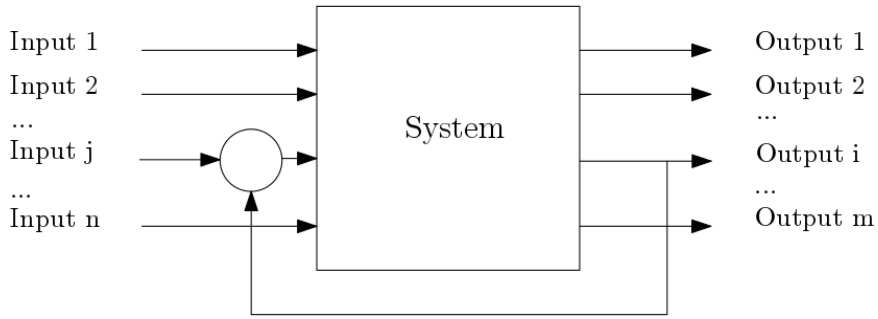

Figure 3-9: State feedback formulation.

For example λ and MAP are treated as output of $EMcmd$ and also as input for NOx.

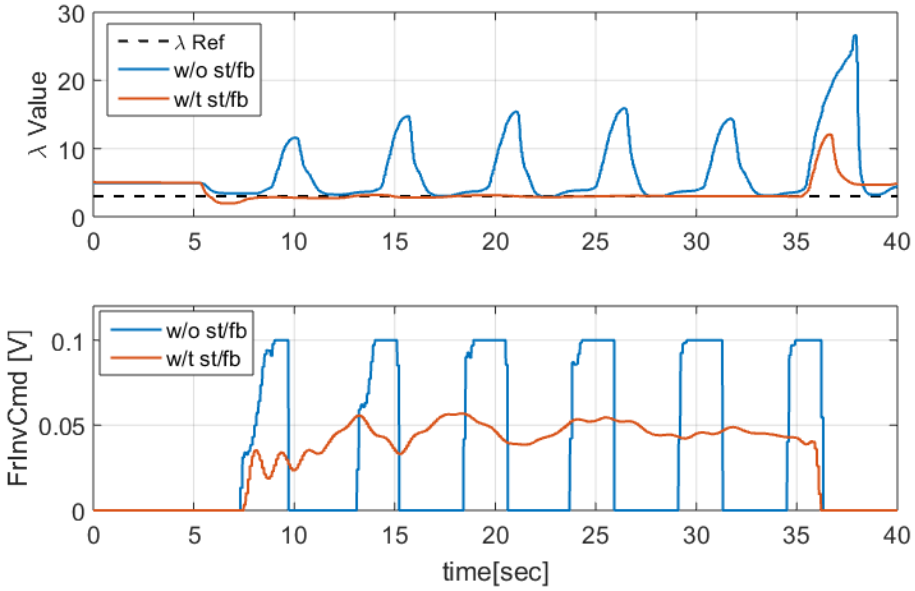

Figure 3-10: Evaluation of state feedback implementation.

3.4.3 Model 3

For simulation purposes, a non-linear ARX model was derived. An ARX model is a linear autoregressive model which additionally has exogenous inputs. This means that the model relates the current value of a time series in a way so that it is possible to explain or predict current and past values of the driving (exogenous) series.

For a SISO system, the ARX model structure is

$$y(k) + a_1 y(k-1) + ... + a_{na} y(k-n_a) = b_1 u(k-n_k) +$$

$$+ ... + b_{nb} u(k - n_b - n_k + 1) + e(k) \tag{3.14}$$

where

- $y(k)$ - Output at time t.
- n_a - Number of Poles.
- n_b - Number of zeros plus 1.
- n_k - Number of input samples that occur before the input affects the output, also called the dead time in the system.

- $y(k-1), ..., y(k-n_a)$ - Previous outputs on which the current output depends.
- $u(k-n_k), ..., u(k-n_b-n_k+1)$ - Previous and delayed inputs on which the current output depends.
- $e(k)$ - White-noise disturbance value.

The above consideration can be easily extended for MIMO systems.

The nonlinear ARX model computes the output y in two stages as seen also in Fig. 3-11

1. It Computes regressors from the current and past input values and past output data. In the simplest case, regressors are delayed inputs and outputs, such as $u(t-1)$ and $y(t-3)$ called standard regressors. Custom regressors can also be specified, which are nonlinear functions of delayed inputs and outputs. For example, $tan(u(t-1))$ or $u(t-1) * y(t-3)$. By default, all regressors are inputs to both the linear and the nonlinear function blocks of the nonlinearity estimator. A subset of regressors as inputs to the nonlinear function block can also be specified.
2. The nonlinearity estimator block maps the regressors to the model output using a combination of nonlinear and linear functions. Non-linearity estimators, such as tree-partition networks, wavelet networks, and multilayer neural networks can also be chosen. Either the linear or the nonlinear function block from the nonlinearity estimator can be excluded.

The nonlinearity estimator block can include linear and nonlinear blocks in parallel. The application of the above model is further described in Chapter 4.

3.4.4 Time delay

The physical lambda sensor is installed in the exhaust duct, approximately 1 m after the exhaust manifold of the diesel engine. Consequently, a deviation/error in λ will be sensed only after the exhaust gas has arrived at this point. The time that elapses

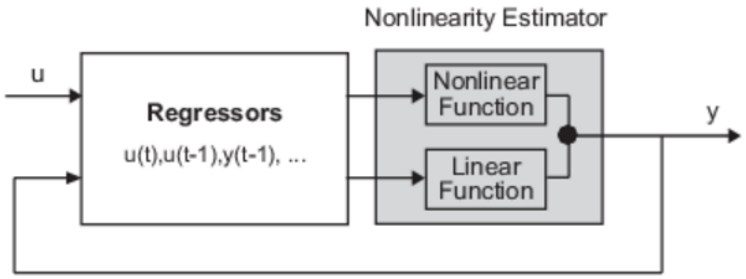

Figure 3-11: Non-linear ARX structure from [35].

between the end of the combustion cycle and the measuring of λ for the exhaust gas of the corresponding cycle is the time interval that the the sensed signal is close to the reference value while the the value of λ inside the cylinder may be below the reference value. If the measured λ is used for controller purposes, then the error signal for the feedback controller is approximately zero during this time interval; thereby, the command to the electric engine is zero too.

Measured time delay between a change at the command of the frequency inverter and the corresponding change in λ equal to 0.79 s. at 1600 rpm was directly imported into the models. This transfer delay is directly affected by the engine speed. The transfer delay of the physical λ sensor alone is around 0.1 sec.

Controllers used in this Thesis require a linear, finite dimensional system model. For this purpose, the time delay was replaced with a 20-th order Padé element [1], adopting the approach where for delays up to 40 ms a first order approximation is chosen, and for every additional 40 ms, one order is added [53].

The Bode diagram in Fig. 3-12 shows the nominal model and other similar identified models along with the model with Padé approximation. It can be noted that the identified models show similar frequency response over a wide frequency region and with the choice of the nominal model for robust controller design, the whole set can be stabilized.

[1]Pade approximation: rational representation of the time delay factor

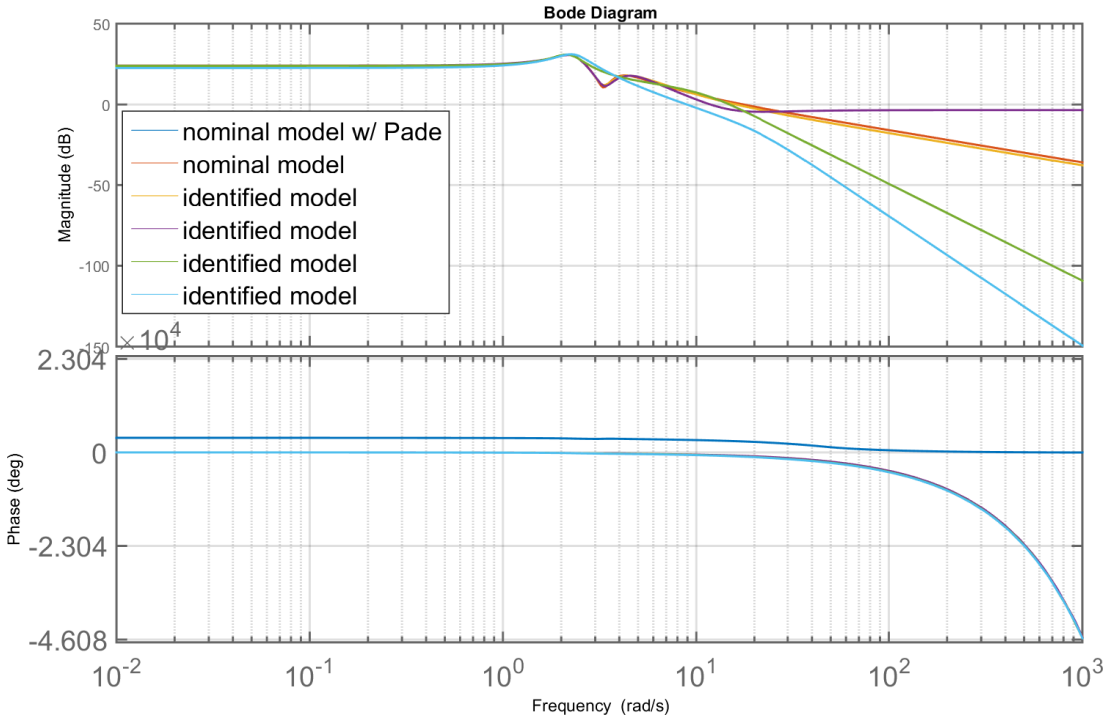

Figure 3-12: Bode diagram from identified model with delay and with Padé element.

3.5 Lambda Virtual Sensor

Quite frequently NOx, PM and virtual lambda (λ) sensors are used in controllers when either no physical sensors are available or the layout and the installation of the sensor introduces filtering effects and time delays thus, posing limitations in the efficiency of feedback control, i.e. the achievable bandwidth.

The process of deriving a virtual PM sensor based on a mean value phenomenological model is described in [27]. Another alternative is the development of virtual sensors by "black-box" modeling principles with neural networks or genetic algorithms as in [22] and [15], respectively. A category that lies in-between is "gray-box" virtual sensors, see for example [23], [9] and [63].

In HIPPO-1, the physical oxygen sensor is installed in the exhaust duct of the diesel engine, 1 m after the turbine outlet, which introduces an additional delay to that of the sensor itself (approx. 120 ms). With the oxygen concentration in the exhaust gases, the λ is calculated, as is explained in more detail in Chapter 2. Also,

during fast load reductions, the ECU senses the acceleration and drastically reduces the injected fuel or even stops fueling, causing large spikes in the measurement of λ. When such signal is fed to the controller, the command will display undesirable oscillatory behavior.

In order to eliminate such problems, a λ *virtual* sensor was developed and used in the control loop [6]. The main parts of the virtual sensor model consist of the *fuel path*, the *air path* and *gas mixing*, as shown in the block diagram of Fig. 3-13. The λ virtual sensor model makes use of the physical variables which are available through measurements, namely the rotational speed of the engine N_e, the turbocharger speed N_{tc}, the pressure at the air cooler inlet p_{im} and through map (look-up table) like the torque T_e produced by ICE. The validation results of the created λ virtual sensor are presented in Appendix C.

Fuel Path Model

The engine is approximated as a Willans machine [52], where the engine is assumed to be an energy converter which converts the available fuel chemical energy W_{in} into output flow $\phi_{out} = \omega_e$ and effort variables $\epsilon_{out} = T_e$. Although the energy conversion is non-linear, an affine relationship between the input power and the output effort variables is a fair approximation for a specified engine speed.

For each time instant, the following equation holds

$$T_e = \frac{e(\omega_e) \cdot \dot{m}_f \cdot H_{LV}}{\omega_e} - T_{loss}(\omega_e) \tag{3.15}$$

where ω_e is the engine speed in rad/s, H_{LV} is the lowest heating value of the fuel and e is the thermodynamic efficiency of the thermodynamic cycle.

The injected fuel will affect the torque output of the engine only after the injection to power cycle [20]. For this reason, a time delay is introduced into Eq. 3.15 which is transformed to

$$T_e(t) = \frac{e \cdot \dot{m}_f(t - t_{inj \to PC})}{\omega_e(t)} \cdot H_{LV} - T_{loss} \tag{3.16}$$

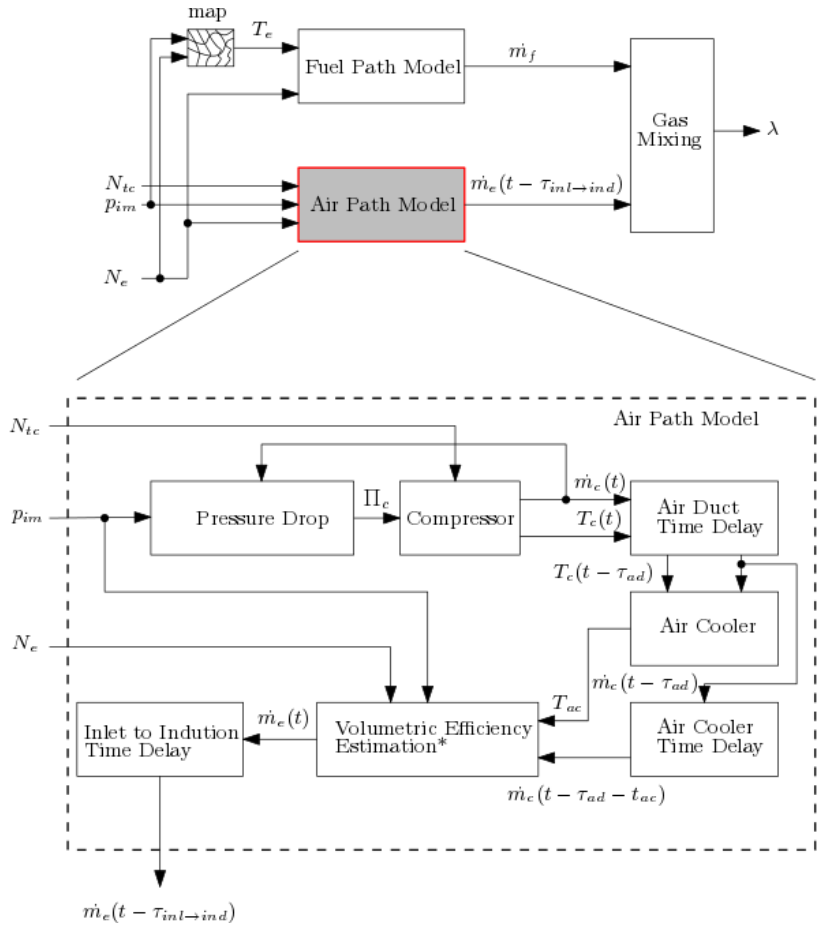

Figure 3-13: Virtual sensor model fundamental components.

Equation 3.16 can be written as

$$\dot{m}_f(t) = \frac{\omega_e(t+\tau_{inj\to PC})\cdot(T_e(t+\tau_{inj\to PC})+T_{loss})}{H_{LV}\cdot e} \tag{3.17}$$

so that the unknown output is the fuel flow.

The rotational speed of the engine at time instant $t+\tau_{inj\to PC}$ is replaced by a first-order Taylor approximation

$$\omega_e(t+\tau_{inj\to PC}) = \omega_e(t) + \frac{d\omega_e}{dt}(t)\cdot\tau_{inj\to PC} \tag{3.18}$$

Regarding the torque output at the time instant $t+\tau_{inj\to PC}$, the assumption that the inertial torque $J\frac{d\omega_e}{dt}(t)$ is converted to torque output within the time interval

$\tau_{inj\to PC}$ is adopted; thus:

$$T_e(t+\tau_{inj\to PC}) = T_e(t) + J_e\frac{d\omega_e}{dt}(t) \tag{3.19}$$

Air Path Model

The air path model is composed of blocks which calculate the volumetric efficiency, the pressure drop in compressor and air cooler, the compressor performance, the conditions in the outlet of air cooler as well as the time delays of air through the air duct, the air cooler and induction in the cylinders. At this part of the model, the conversion from crank-angle to time also takes place.

The output of this model is the air mass flow aspirated by the engine, $\dot{m}_e$, while the inputs are the engine speed N_e, the turbocharger speed N_{tc} and the pressure at the air cooler inlet p_{im}.

In-cylinder Gas Mixing

At each time instant, the value of λ for the fresh charge mixture of air and fuel is given by

$$\lambda = \frac{AFR}{AFR_{st}} = \frac{\dot{m}_e/\dot{m}_f}{AFR_{st}} \tag{3.20}$$

However, a part of the exhaust gases remains inside the cylinder and is mixed with the fresh air charge. The final value of $\lambda(t)$ would be a weighted average of $\lambda(t-\tau_{ieg})$ which is the value of λ for the previous cycle and of $\lambda_{fc}(t)$ which is the value of λ for the new air that is aspirated inside the cylinder. The derived relationship is

$$\lambda(t) = \frac{\lambda(t-\tau_{ieg})\cdot m_{res}(t) + \lambda_{fc}(t)\cdot[m_e(t)+m_f(t)]}{m_e(t)+m_f(t)+m_{res}(t)} \tag{3.21}$$

where the masses that appear in the equation above can be computed from the corresponding mass flows using the integration formula

$$m(t) = \dot{m}(t - \tau_{ieg}) \cdot \tau_{ieg} \tag{3.22}$$

The interval of integration is the time between the induction and the exhaust cycle

$$\tau_{ieg} = \frac{2\pi \cdot 2}{\omega_e \cdot z} \tag{3.23}$$

3.6 Diesel Engine Maps

A wide range of look-up tables (maps) were created from experimental data collected from the HIPPO-1 powertrain, under steady state operation [41]. The data for the maps in this work have been obtained with the conventionally calibrated and controlled engine. After data processing, two-dimensional (Fig. 3-14) and three-dimensional maps (Fig. 3-15) were populated, with the DE parameters. These look-up tables have 2 inputs and 1 output each time. The same method is used by [62] and [36].

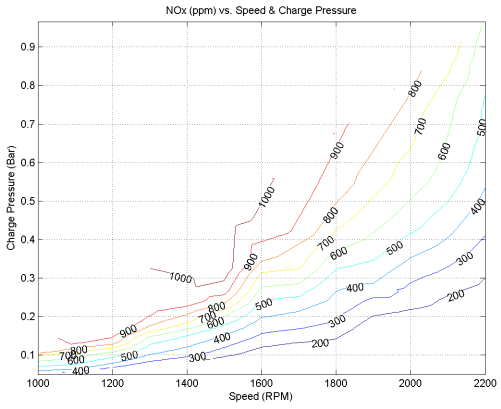

Figure 3-14: 2D map.

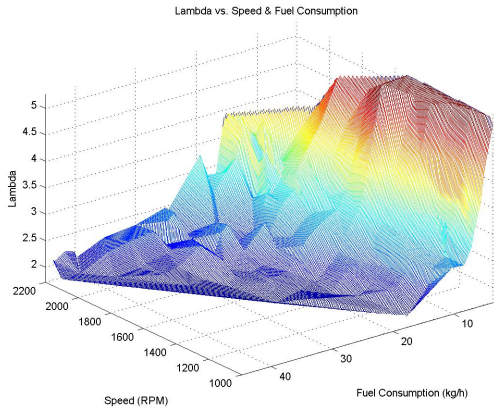

Figure 3-15: 3D map.

The selection of the data that were used for the population of one of the look-up tables is depicted in Fig. 3-16. A suitable Matlab algorithm was synthesized that selected the appropriate recorded samples. The basic requirement for this selection was the DE to be in steady state operation, so when the reference and recorded torque values were only 3% apart for a time window of *2 s.* which equals to 2000 samples

on HIPPO-1 DAQ, the next sample was selected by the algorithm.

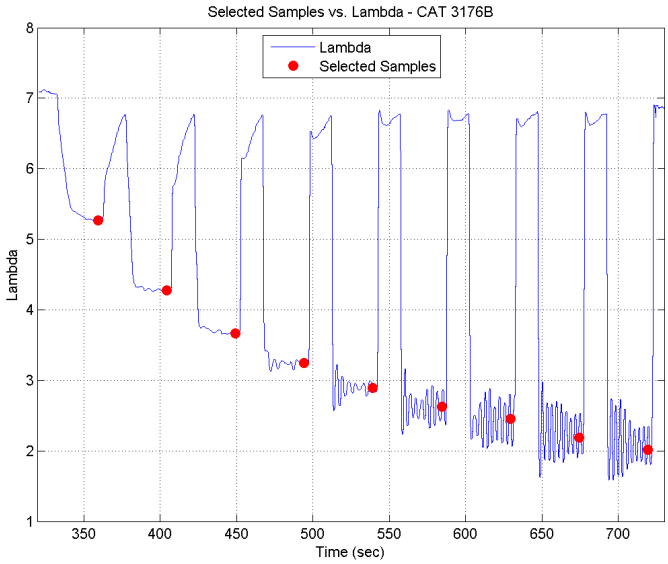

Figure 3-16: λ value selected samples from experimental data for the population of the look-up tables.

Separate sets of experimental data were used to evaluate the map output values (Fig. 3-17), within the same operating region. The data generated from the look-up tables display good performance, maintaining acceptable deviations from the measured values in steady state condition. The main contribution of the created maps to the HIPPO-1 testbed, is the derivation of λ reference values for the controllers.

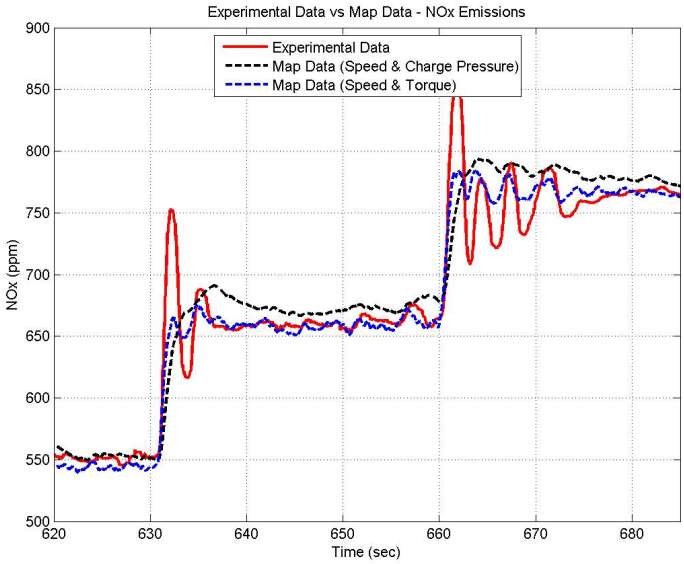

Figure 3-17: Comparison of measured (experimental) NOx vs NOx derived from the created look-up tables.

THIS PAGE INTENTIONALLY LEFT BLANK

Chapter 4

Robust Controller Design

The performance of a hybrid powertrain in terms of reducing both exhaust gas emissions and fuel consumption, critically depends on the performance of the power management strategy, i.e. the control algorithm that controls how the power demand will be split between the DE and EM.

In this Thesis the first method applied was H_∞ robust control, which was adopted and investigated with direct application. The H_∞ method as introduced by Doyle, Glover, Khargonekar and Francis (1989) is a model based method for designing robust linear controllers, based on linear models. In a broad sense this type of control allows to shape the transfer functions that affect the behavior of the plant under control, during disturbance rejection and command tracking. In practice, the robust controller is designed for a particular nominal operating point of the plant and is expected to behave in an acceptable way in a region around the nominal plant.

The robust controller for λ closed loop control is obtained as an H_∞ mixed sensitivity controller, as in [17]. Mixed sensitivity H_∞ controllers have been implemented successfully in diverse diesel engine applications, see for example [3] and [45].

The main control objective is to minimize the infinity norm [1] of the transfer function between w and z, by designing a controller capable of eliminating the influence of the exogenous inputs w to the exogenous outputs z, using the sensed outputs

[1]The infinity norm of a vector x is defined as $\|x\|_\infty = max(|x_i|)$. Hence it is the maximum entries' magnitude of the vector.

contained in v to produce the control signal u.

A transfer function-shaping philosophy is adopted, in order to force the shape of the magnitude and the phase of specific transfer functions in the frequency domain. The transfer functions that are under examination include

- L: the open loop transfer function
- S: the sensitivity function
- T: the complementary sensitivity function
- KS: the control sensitivity function

These functions, as will be later explained, define greatly the behaviour of the system which is under control. Being able to directly force the shapes of these functions, forms a controller that influences the physical system in a way that specific performance requirements are fulfilled "on demand". By this it is implied that shaping the magnitude of the sensitivity function, giving to it a specific form in the frequency domain, one directly forces a certain behavior of the error signal in the whole frequency and magnitude spectrum of a possible reference input. In that way, a controller can be designed, which achieves fast or slow reaction to the reference inputs, or demands specific range of the steady state error and even limits the amount of energy contained in the control signal, by taking under consideration all the limitations imposed by the mathematical interpretations of the physical system to be controlled.

4.1 Plant model

The robust control system considered the case of a linear, time-invariant (LTI) plant. However, in real applications plants are rarely linear, their parameters vary with time, measurements are contaminated with noise, the plant model is approximate representation of the true plant, etc. The model used for this robust controller is Model 1, as described in Chapter 3.

4.1.1 Data Scaling

Scaling is very important in practical applications as it makes the model analysis simpler and helps to avoid numerical errors [54]. The idea is to make input and output data of similar order, usually less than one in magnitude. A judgment is made from the start of the design process about the required performance of the control system. The references and disturbances were divided by their maximum expected values and the outputs by the maximum allowed change. These values were, for the EM frequency inverter command $FrqInvCmd$ =0.1 V, for DE torque=600 Nm, and for λ =10.

4.2 H_∞ Controller Design

In this work, the S/KS/T weighting scheme is implemented for the shaping of the frequency response of the closed loop transfer functions, where the performance, stability and robustness specifications are specified by the appropriate choice of the weighting parameters.

The H_∞ mixed sensitivity is suitable when dealing with modelling uncertainties, since they can be compensated in the specifications of the complementary sensitivity T weight. In addition to the sensitivity S and the complementary sensitivity T, the transfer KS from r to u is incorporated in the scheme, so as to restrict the size and the behavior of the input signals.

Following the determination of the closed loop response weights, the controller derivation can be formulated as a solution to a minimization problem. In this stage, a stabilizing controller K is obtained, so that the H_∞ norm of the extended plant transfer function T_{zw} between the exogenous inputs to the system (d, r, n) and the exogenous outputs (z_1, z_2, z_3), where d are the disturbances, r is the reference signal, n is the noise signal, e is the error and u is the control output, is minimized as in Eq. 4.1.

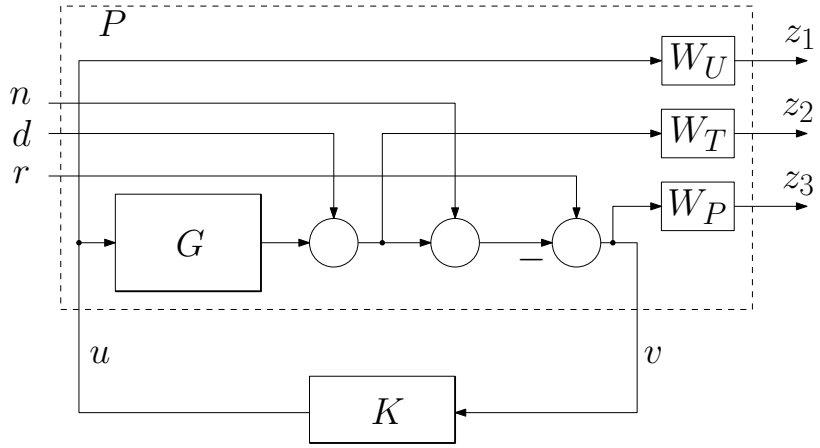

Figure 4-1: The S/KS/T weighting scheme.

$$\|T_{zw}\|_\infty = \left\| \begin{bmatrix} W_P S \\ W_U K S \\ W_T T \end{bmatrix} \right\|_\infty \leq \gamma \tag{4.1}$$

The shaping of S, KS, T was achieved by defining specific weight bounds W_P, W_T and W_U, that set for each frequency a specific upper limit that the corresponding transfer function was not allowed to surpass. These weights determine the frequency response of S, T, K and are chosen as in Eqs. 4.2-4.4

$$W_P(s) = \frac{s/M_P + \omega^\star_{BP}}{s + \omega^\star_{BP} \cdot A_P} \tag{4.2}$$

$$W_T(s) = \frac{s + \omega^\star_{BT}/A_T}{s \cdot M_T + \omega^\star_{BT}} \tag{4.3}$$

$$W_U(s) = \frac{s + \omega^\star_{BU}/A_U}{s \cdot M_U + \omega^\star_{BU}} \tag{4.4}$$

where the parameters A_i and M_i correspond to the asymptotic behavior of the weighting functions W_i for $s \to 0$ and $s \to \infty$, respectively.

Typically $\gamma = 1$ so that the closed loop transfer functions are limited by the inverse of the weighting functions W_i for the entire spectrum of frequencies.

At steady state it is desirable that the plant output closely follows the reference command and the controller rejects the exogenous disturbances. For this reason A_T

$\simeq 1$ and A_P is chosen as small as possible. Integral action with a value of A_P=0 is avoided due to the numerical instabilities in the H_∞ synthesis algorithm.

The requirements for small overshoot and robustness with respect to uncertainty is lumped into the condition of small weighting parameter W_P. Furthermore, the selected bandwidths $\omega^\star_{BT}$ and $\omega^\star_{BP}$ have to compromise the conflicting requirements of fast rise time and low noise sensitivity.

The controller weight W_U is specified in such way so as to allow tight control at low frequencies and noise attenuation at high; the physical limitations of the system are also taken into account. Weight W_T is chosen so that complementary sensitivity T is limited to avoid unnecessarily high bandwidth of the control system. Various cases were examined in order to evaluate controller performance and robustness (model order, dead times, un-modelled dynamics, disturbances).

The parameters of controller weights are described in Table 4.1.

Table 4.1: Controller Weight Parameters

Weight/Specification	A	M	$\omega^\star_B$ [rad/s]
W_P	0.01	1.5	0.07
W_T	0.9	0.0014	24
W_U	2.1	0.03	11

The H_∞ controller was designed using graphical programming, in the Matlab/Simulink environment. The controller is then compiled in C++ language using the built-in functions, and then downloaded to the real-time dSpace platform.

Using Robust Control Toolbox of Matlab [5], the mixed sensitivity controller is obtained with the command **mixsyn** with a value of γ of 1.06. The controller was implemented in discrete state-space form, with sampling time of 1 ms, in Simulink. Due to the Pade approximation of the delay, the order of the controller rises with increasing delay.

The Bode diagram of the frequency response of S, KS and T of the nominal model with the selected weights is given in Fig. 4-2.

The Bode diagram of the frequency response of closed loop system T for the nominal model and various identified plant models is shown in Fig. 4-3. Robustness

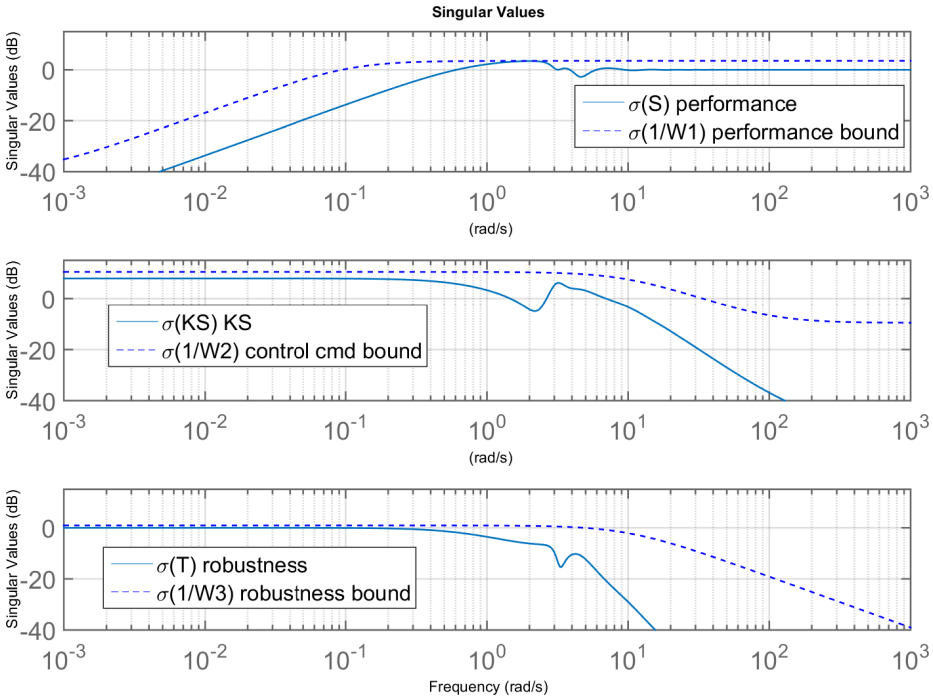

Figure 4-2: Bode diagrams of S/KS/T.

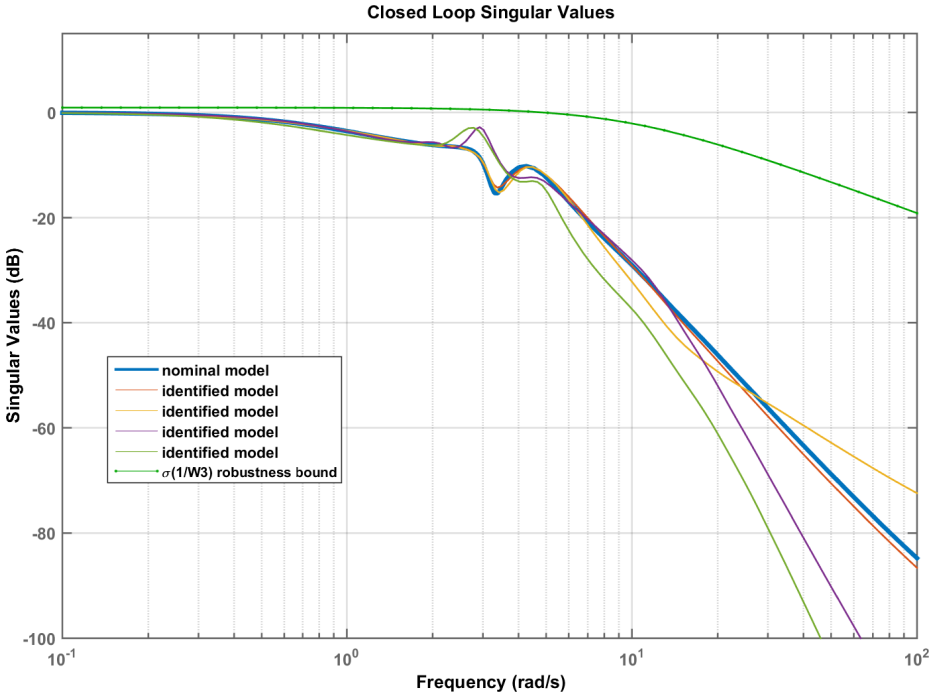

Figure 4-3: Singular values for T, with nominal model (bold) and other identified models.

with respect to modeling errors can be observed, as the various models show similar behavior with the nominal model and its controller.

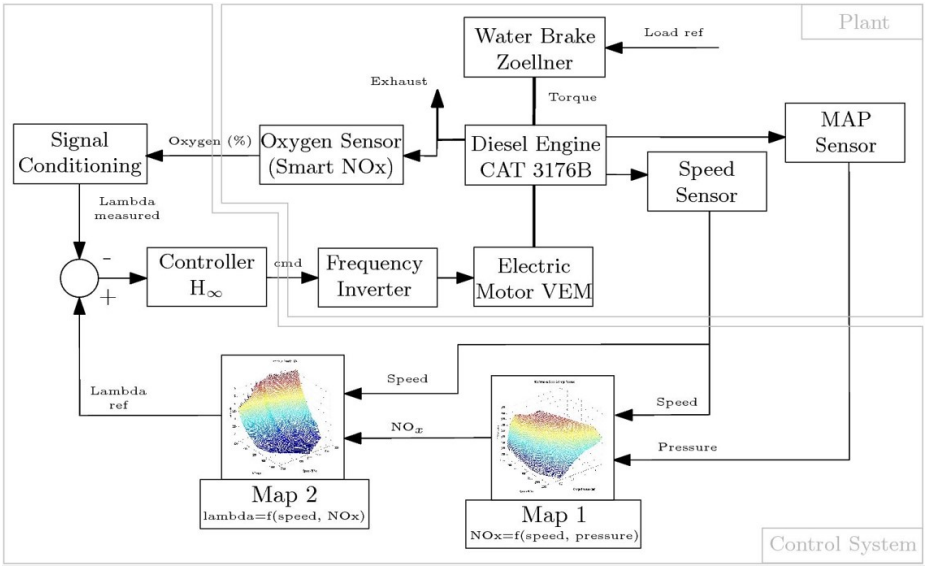

Figure 4-4: The closed loop system with installed sensors and lambda reference options.

The block diagram for the closed loop system is shown in Fig. 4-4. The controller receives the measured λ values and a reference value, which depending on the mode of operation, is either a constant (static reference) or a dynamic one (from look-up tables). The main sensors for feedback control are the oxygen sensor, the engine speed sensor and the intake manifold pressure. With the availability of a λ virtual sensor, the λ measurement is replaced by λ calculations in closed loop. The resulting controller command is the input to the frequency inverter of the EM.

4.3 H_∞ Experimental Results

Various experiments were conducted on the HIPPO-1 powertrain, in order to evaluate the performance of the load share strategy.

These are divided in three sections, as follows. At first, the proposed robust controller was tested and evaluated in closed loop simulation, using the non-linear DE model as described in Chapter 3. The second set of experiments resembles a generator-set on-board a ship, where the engine operates at constant speed (1600 rpm) and with alternating electrical load. In this case the controller receives a static lambda reference value. In the third set of experiments the engine operates in a

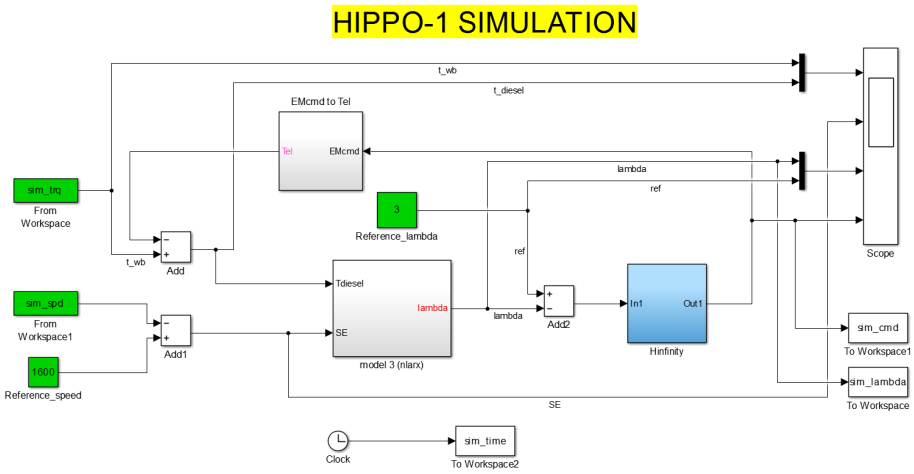

Figure 4-5: Simulink block diagram for simulation purposes of HIPPO-1, using H_∞ control.

propulsion arrangement and propeller loading, with simultaneous variations on speed and torque. In this case a set of look-up tables for the λ reference points was used. In both loading scenarios, the performance is assessed when the controller receives λ feedback from the physical sensor or the virtual one.

4.3.1 Closed Loop Simulation

The above methodology for engine modelling and controller design with robustness measures was at first tested in simulation. For the validation in simulation of the proposed control scheme, a non-linear ARX model of the plant was derived through system identification, model 3, as described in more detail in Chapter 3. The Simulink program used for modeling of HIPPO-1 can be seen in Fig. 4-5.

The λ model was compared with measurement data obtained from the test bed while operating under closed loop control. Fig. 4-6 shows the λ values and the hybrid controller command for two load steps, from 100 Nm to 300 Nm and back to 100 Nm, and from 100 Nm to 500 Nm, at 1600 rpm. The λ values predicted by the model decrease fast during loading and display almost identical behavior when compared to the measured values. The corresponding controller command values, depict the small reaction time of the controller and the slightly oscillating performance when the command rises.

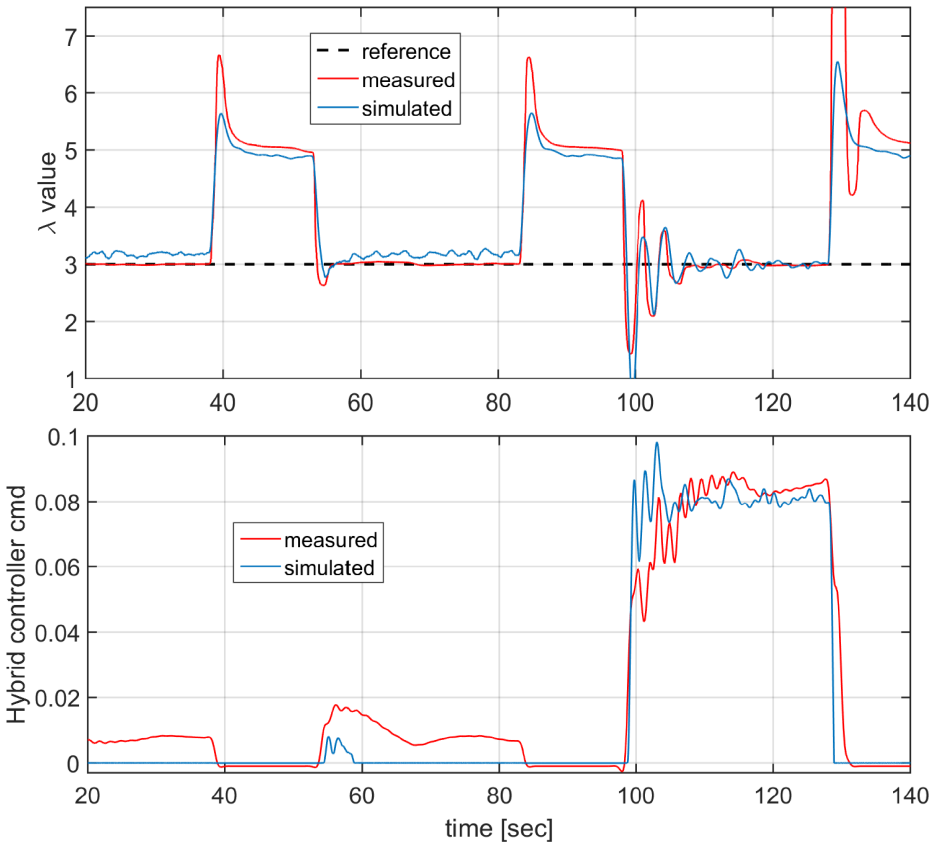

Figure 4-6: Measured and simulated data from the hybrid system under closed loop control.

4.3.2 Generator mode

An experiment with load steps from 100-300 Nm and 100-500 Nm, at 1600 rpm, is shown in Fig. 4-7. The static λ reference was set at $\lambda_{ref} = 3$, after repetitive experiments of the same loading cycle. As can be seen in the second subplot, the purpose of the proposed controller is to track the imposed λ setpoint by engaging the EM. The controller output and the resulting torque provided by the EM, can be seen in the third and fourth subplots of the same figure. The use of the virtual sensor in the control loop gives less oscillatory command and the EM reaches its maximum torque faster than the hybrid setup with the physical sensor. Also, the proposed controller provides good tracking performance during changes in the load, for both cases of feedback.

The λ set point represents the only parameter needed for tuning the strategy for a specific loading profile. As soon as there is a rising edge in the applied total torque, the measured λ drops almost instantly, creating an error between the measured and static λ values. The controller uses this error as input and engages the EM, producing torque. It can be observed that the proposed controller provides good tracking performance during the load change and at steady state. To avoid any performance deterioration in case of the inverter command saturation, all integrators are implemented with anti-reset-windup. The hybrid setup with the virtual sensor provides slightly faster command output to the electric motor, compared to the physical sensor, due to the delays of the installed λ sensor.

In Fig. 4-8, the impact of the hybrid powertrain on the produced NO_x, exhaust gas opacity and measured fuel consumption, as compared to the conventional setup can be noted. The total torque demand is still met, but the electric motor assists the ICE while it is accelerating, in order to reduce exhaust opacity, NO_x content and fuel consumption. Both sensor setups show almost the same behavior. It is shown that during acceleration, the produced exhaust gas opacity values are significantly lower, by almost 25%. The NO_x content is slightly decreased during the first moments of the load change (first "spike"), but is greatly reduced once the EM engages and

contributes to the total load demand. Regarding the fuel consumption, it is around 20% lower with the hybrid setup than the conventional one for the same loading cycle.

4.3.3 Propeller mode

In order to assess the proposed power split methodology against realistic data from ships, appropriate measurement equipment was installed on-board a high-speed vessel with waterjets, so as to gather actual engine performance and emissions data during normal service, as described in Chapter 3. The voyage included high speed cruising, port approaching at low speed and maneuvering, idling for unloading and loading of the vessel and immediate departure afterwards, as shown in Fig. 4-9.

There is a common relation between the torque (power) and speed in ship propulsion, known as the *propeller law* [64]. From experience it is known that shaft rotational speed (n_p) is almost linearly proportional to the ship's speed (V_s)

$$n_p = c_1 \cdot V_s \tag{4.5}$$

The power required to tow the ship at ship speed V_s with resistance R, is the effective (towing) power P_E (eq. 4.6). Using the assumed proportionality of resistance and ship speed squared, effective speed is, as a first approximation, proportional to the cube of speed V_s.

$$P_E = R \cdot V_s \tag{4.6}$$

$$P_E = c_2 \cdot V_s^3 \tag{4.7}$$

For a ship equipped with a fixed pitch propeller or waterjets, the necessary power requirement, P, is proportional to shaft speed, n, to the power of three (propeller law), by combining equations 4.5-4.7

$$P = c_3 \cdot n^3 \tag{4.8}$$

where c_3 is a constant number. In our case, $c_3 = 1.56 \cdot 10^{-4}$, which was derived from

the on-board measurements and utilized for the experimental propeller curve.

This data, after appropriate scaling, was utilized as reference for the design and evaluation of loading profiles during experiments, as in Fig. 4-10. The torque changes from approx. 120 Nm to 700 Nm and the engine speed from 1100 rpm to 1850 rpm.

The λ set point for these experiments is derived from a set of two static maps, with the independent variables N_e and P_{inlet}, as seen in Fig. 4-4. The output of the first map (Map 1) is the expected NO_x value for any given engine speed and inlet manifold pressure. This NO_x value is then multiplied by the desired NO_x reduction percentage (in the form of a gain) and used as input for the second map (Map 2), which in turn gives the λ set point (reference) value. A delay of 1000 ms is also imposed at the λ set point, before is enters the controller block.

The induced reduction of NO_x values between the two maps, leads to higher reference λ values. If this reduction was not present, the λ measured and reference values, would be almost identical and thus the controller would perform no action.

The gain values used in this work come after trial end error, but a future optimization work will be able to provide appropriate numbers. The two maps are created from experimental data collected from the hybrid propulsion powertrain, under steady state operation (see Fig. 4-11).

The main idea of dynamic λ reference points is to shift the DE to more efficient operating points only during transient loading, where the measured λ drops rapidly, by engaging the EM. The EM command is imposed by a positive error between the reference λ value and the measured one, while in steady state condition, the error would be minimized and thus the EM would switch off. The designed controller leads to observable reduction of NO_x emissions, exhaust gas opacity and fuel consumption, with respect to the conventional (non-hybrid) powertrain, during acceleration. The electric power consumption is not taken into account, as this work focuses only on the transient loading phenomena. Also, further studies have shown that, in general, more than 50% of total medium sized diesel engines pollutant emissions can be attributed to transient effects [42].

The corresponding λ values, controller command and the resulting EM torque

are depicted in Fig. 4-12. The recorded λ values are higher using the hybrid setup (leaner combustion) than using the conventional one (i.e. without EM assistance), as the controller tracks the reference λ values imposed by the look-up tables. As the virtual sensor is based on the air path of the engine, which is faster than the exhaust path used by real sensor, the λ value derived by the virtual sensor drops faster than the physical one, thus creating a bigger error when compared to the reference λ value. In turn, this leads to faster engagement of the EM by the controller.

Fig. 4-13 shows the measured gas emissions of NO_x,exhaust gas opacity and measured fuel consumption. For the NO_x emissions of the hybrid setup with the physical sensor, a reduction of 16% was recorded during acceleration, while the use of the virtual sensor saved another 5%. The measured opacity was about 20% less during transient loading for both sensor setups, when compared to the conventional powertrain. As for the fuel consumption, both sensor setups show almost the same behavior. It can be observed that during acceleration, the fuel consumption values are significantly lower, while in steady state operation (EMcmd=zero) the fuel consumption is identical.

In steady state operation, the dynamic λ setpoints as imposed by the look-up tables, and the measured/calculated λ values converge, and the EM switches off.

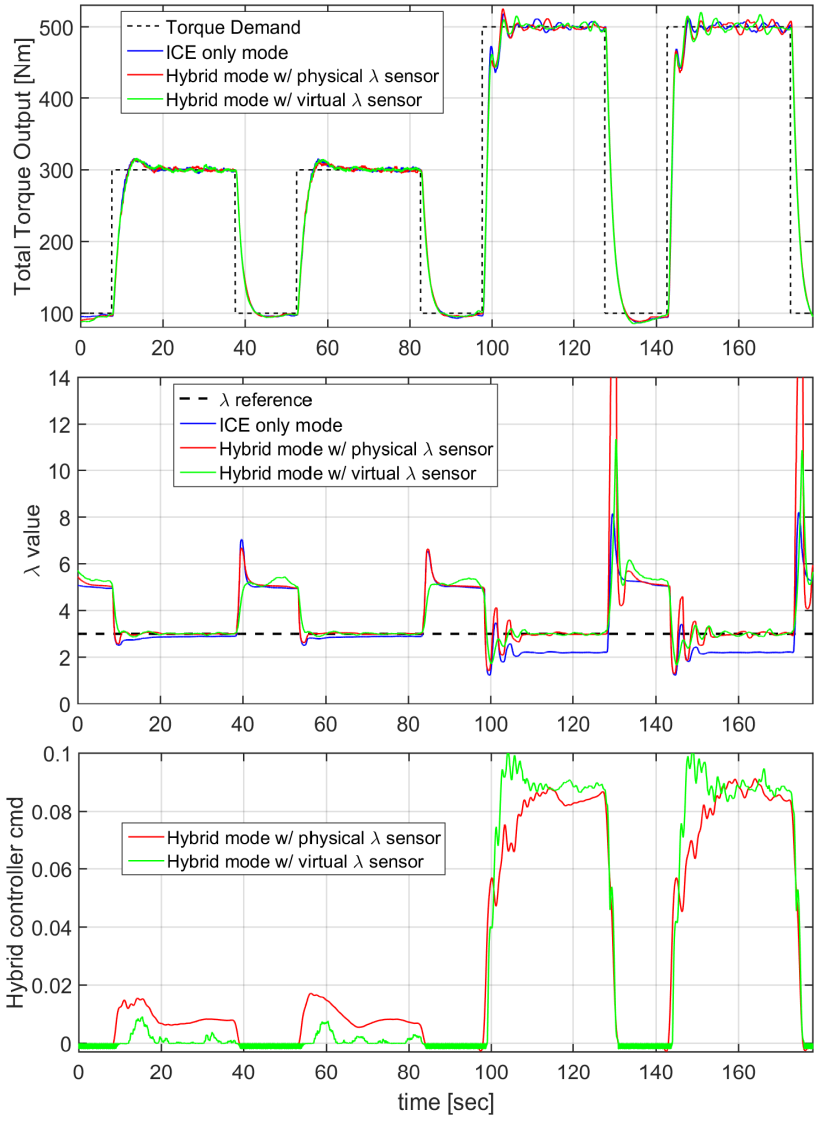

Figure 4-7: Effect of the hybrid powetrain on λ value during generator mode with static reference point.

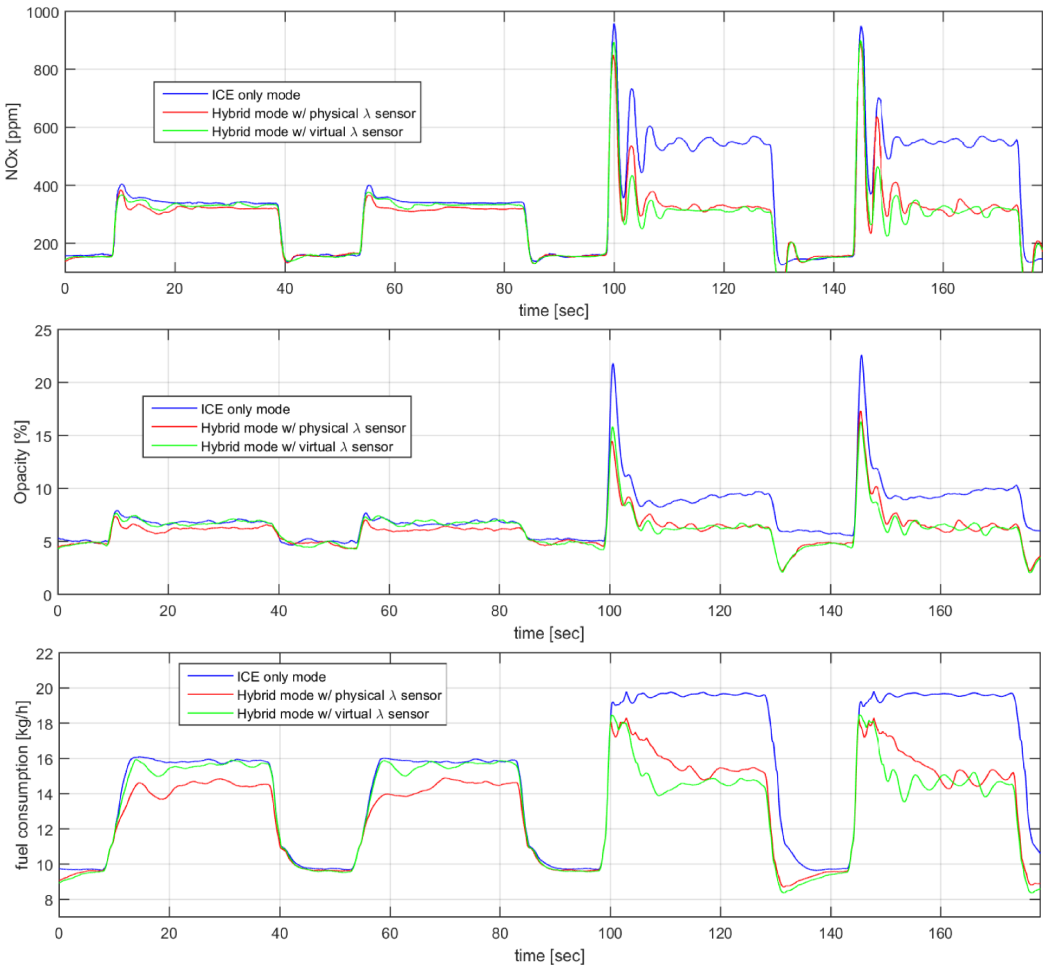

Figure 4-8: Effect of the hybrid powetrain on NO_x, exhaust gas opacity and fuel consumption, during generator mode with static lambda reference point.

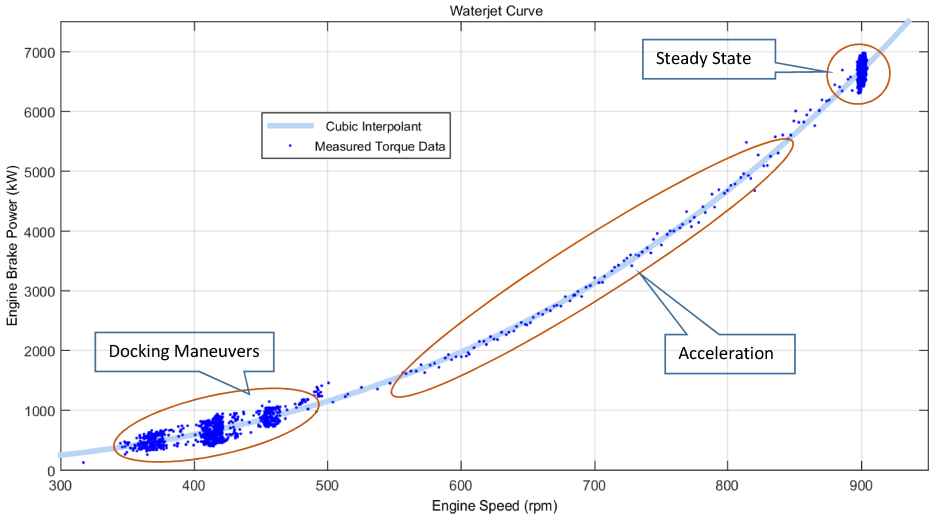

Figure 4-9: Measured water-jet power demand curve from on-board data.

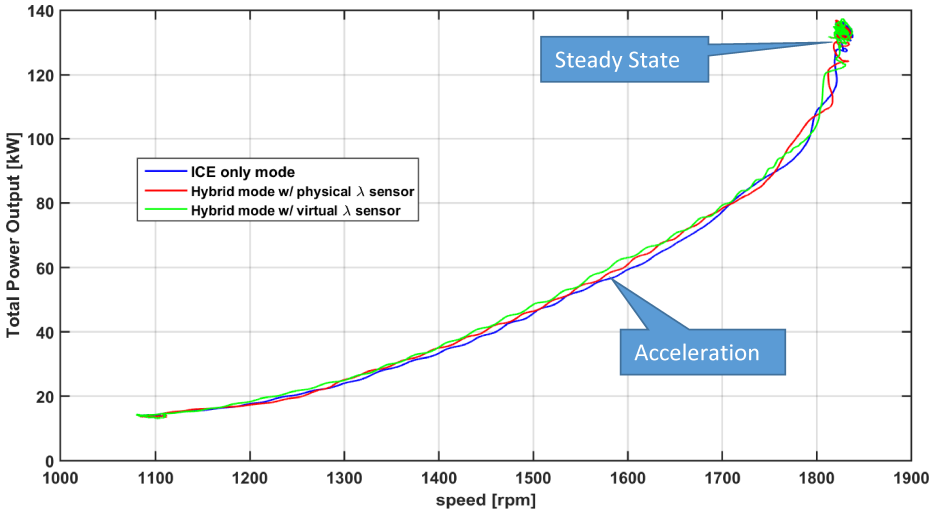

Figure 4-10: Propeller power demand curve on test bed.

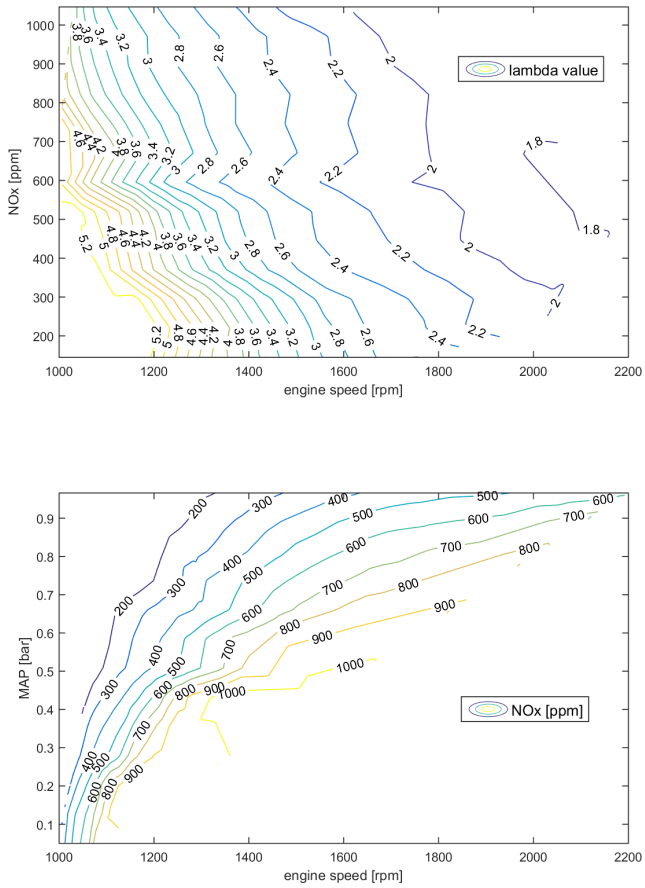

Figure 4-11: Reference maps for λ based on NOx, engine speed (top) and for NOx based on MAP, engine speed.

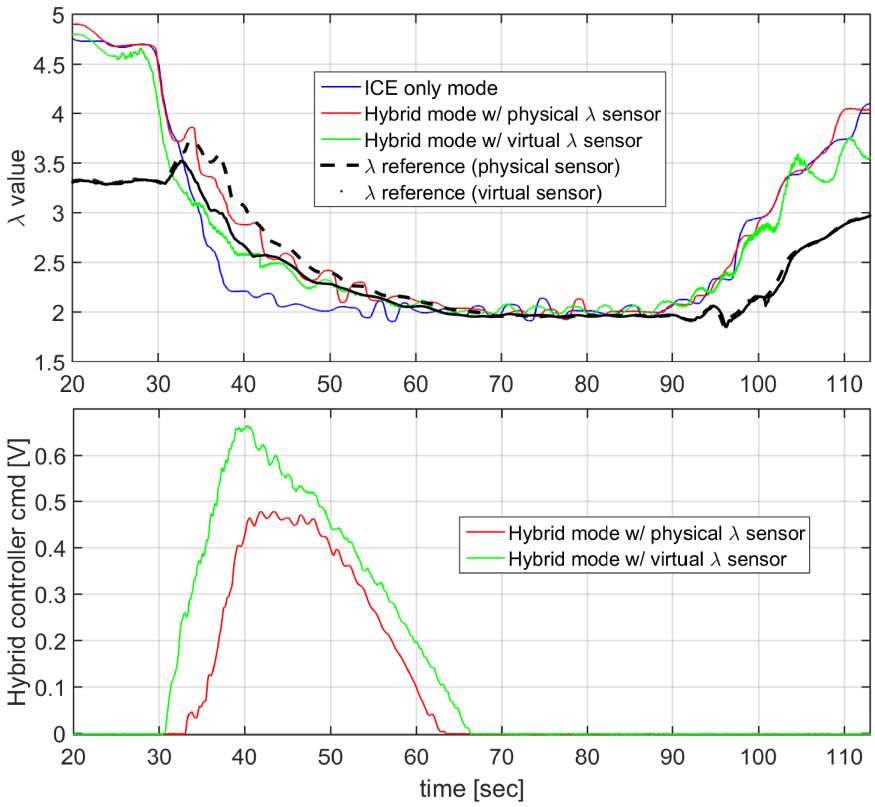

Figure 4-12: Lambda values and resulting controller command, with physical and virtual sensor, during a propeller loading curve.

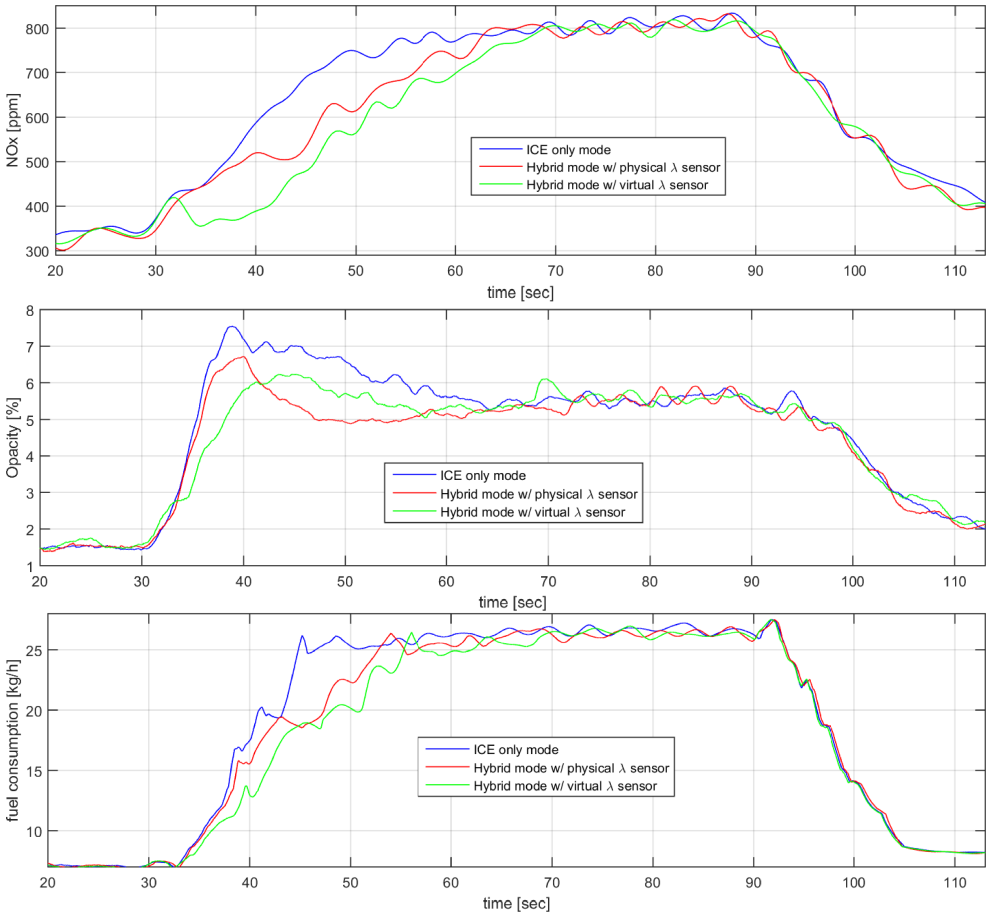

Figure 4-13: Effect of the hybrid powetrain on NOx, exhaust gas opacity and fuel consumption during a propeller loading curve.

Chapter 5

Model Predictive Controller Design

Predictive control, or model based predictive control (MPC) as it is sometimes known, is one of the few advanced control techniques to have had a significant and widespread impact on industrial process control. The main reasons for this success are [37]

- It handles multivariable control problems.
- It can take account of actuators limitations.
- It allows operation of the controlled plant closer to its limitations, which can prove to be more efficient in many cases.

MPC controllers incorporate constraints present in the plant, and hence react very differently in the presence of disturbances, when compared to linear optimal control techniques. It is possible to operate the plant with a setpoint very close to the constraint, with an acceptable small probability of violating the constraint. An MPC controller, unlike other controller strategies, usually includes minimum and maximum values of parameters as constraints, without the need of specifying a setpoint.

The basic idea of MPC is depicted in Fig. 5-1. The time is discrete, with the current sampling instant labeled as integer k. Then at current time k, the plant output is $y(k)$ (also it is the latest measurement available), with $y(k-1)$, $y(k-2)$, the previous history of the output trajectory. Also shown is the set-point trajectory,

which is the trajectory that the output should follow, the values of which are marked as $s(t)$.

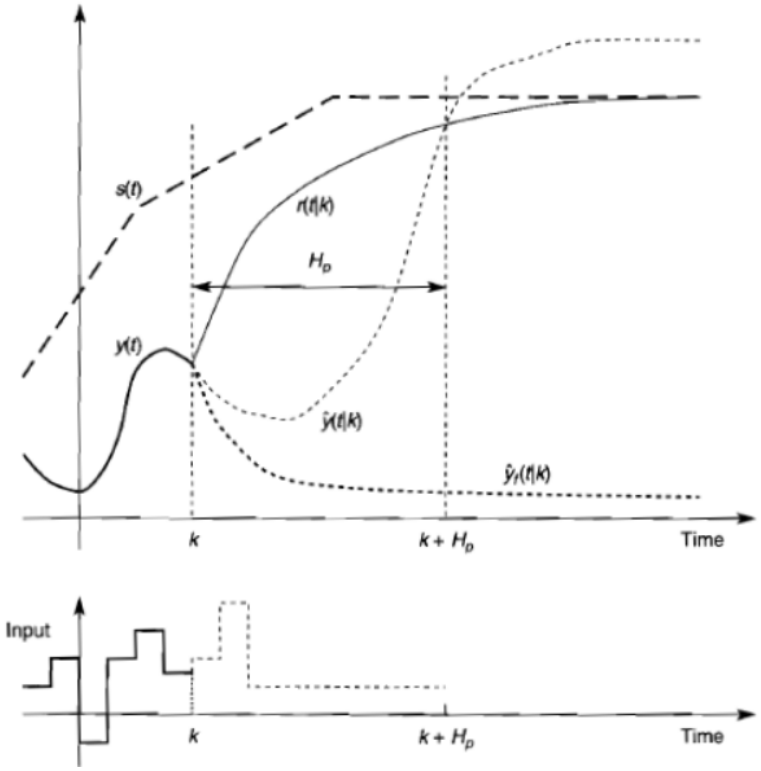

Figure 5-1: The basic idea of predictive control, displaying the prediction horizon, from [37].

Optionally, there is the *reference trajectory*, marked as $r(t|k)$. This starts at current output $y(k)$ and is defined as an ideal trajectory along which the plant should return to the set-point trajectory, in the case for example that a disturbance occurs. It is frequently assumed that the reference trajectory approaches the set-point exponentially from the current output value, where the time constant of the exponential defines the speed of the response.

A predictive controller utilizes an internal model to predict the behavior of the plant, starting at the current time, over the prediction horizon, H_p. This predicted behavior depends on the assumed input trajectory $\hat{u}(k+i|k)$, with $i = 0, 1, ..., H_p - 1$. It is assumed that the internal model is linear. The notation $\hat{u}$ is used instead of u to denote that at time k there is only prediction of what the input at time $k+i$ shall

be; the actual input at that time, $u(k+i)$, shall probably be different from $\hat{u}(k+i|k)$.

The input trajectory is chosen so as to bring the plant output at the end of prediction horizon $k + H_p$ to the required value $r(k + H_p)$.

The notation $(k + i|k)$ indicates that the future value of a signal is depended on the conditions at time k. The trajectory $\hat{y}(k + i|k)$ is the controller prediction of the output value according to its internal model responding to the future sequence of the inputs $\hat{u}(k + i|k)$, $i = 1 : H_u$ of the controller, where $H_u \leq H_p$ is the control horizon and defines the acceptable control moves within the prediction horizon. The indication $\hat{u}$ means that the estimated value of $u(k + i|k)$ may be different from the actual input value $u(k + i)$ that will be applied at time interval $k + i$.

The aim of an MPC is to fit the output trajectory as well as possible to its reference, according to the conditions at time k.

Once the optimal input trajectory has been selected, the first control move $u(k) = u(k|k)$ is applied to the plant, until the new measurement $y(k + i)$ of the output is available in order to devise the new optimal control strategy at time $(k + 1)$ over the new horizon $i = 2 : (H_p + 1)$. This strategy, where the H_p-length horizon slides by one sample interval at each step, is called *receding horizon strategy* [13]. If we suppose that, according to the internal model of MPC, the free response of the system is $\hat{y}_f(k + i|k)$ and S_u is the step input response of the system, then the estimation of the future output trajectory values at the end of prediction horizon can be expressed as

$$\hat{y}(k + H_p|k) = \hat{y}_f(k + H_p|k) + \sum_{i=0}^{H_u} S_u \Delta\hat{u}(k + i|k) \tag{5.1}$$

Once the future input trajectory has been chosen, only the first element of that trajectory is applied as input signal to the plant. Then the complete cycle of the output measurement, prediction, and input trajectory determination is repeated, one sampling interval later. Since the prediction horizon maintains the same length as before, but slides along by one sampling interval at each step, the *receding horizon* control strategy applies.

Constraints are the other major characteristic of an MPC. This affects the choice of future input trajectory $\hat{u}(k+i|k)$, with $i = 0, 1, ..., H_p - 1$, in such a way that the input signals and their rates remain within allowed constraints and such that the outputs, and possibly *inferred* variables in the case that these are not measured directly, also remain within allowed constraints. Assume the following sequence

- Obtain measurements $y(k)$
- Compute the required plant input $u(k)$
- Apply $u(k)$ to the plant

Proper choice of prediction and control horizons are crucial for the system performance. A common choice of parameters is first to choose the control interval as 20-30 sampling periods, and then choose prediction horizon H_p equal to that number. In the case of constraints, a long prediction horizon allows the controller to anticipate the constraint and avoid it or minimize its effects. In the case of non-minimum phase plants (those with zero at right half plane and initial response to the opposite direction of the command) a long prediction horizon would allow the controller to move in longer-term direction.

The output variables are referred to as controlled variables (CV), while the input variables are called manipulated variables (MV). Measured disturbances are called disturbance variables (DV).

5.1 Unconstrained MPC

It is standard to assume a linear and time-invariant plant, which after discretisation of time at a single sampling rate, gives the following state-space system

$$x(k+1) = Ax(k) + Bu(k) + Ew(k) \tag{5.2}$$

$$y(k) = C_y x(k) + v(k) \tag{5.3}$$

$$z(k) = C_z x(k) \tag{5.4}$$

where x is the state vector, u is the control input vector, y is the measured output vector, z is the vector of outputs to be controlled and w, v are the vectors of unknown state disturbances and measurements errors respectively. A, B, C_y, C_z and E are constant matrices.

For the solution of the optimization problem, quadratic programming (QP) is used in order to minimize the cost function $J(z_k)$ by computing the optimal sequence of the MV $(EMcmd)$ as it moves over the Control Horizon (H_P) [8]. The cost function J penalizes deviations of the predicted controlled outputs $\hat{z}(k+i|k)$ from a reference trajectory $r(k+i|k)$. The cost function is defined as

$$V(k) = \sum_{i=H_w}^{H_p} \|z(k+i|k) - r(k+i|k)\|^2 Q(i) + \sum_{i=0}^{H_u-1} \|\Delta u(k+i|k)\|^2 R(i) \tag{5.5}$$

where H_p and H_u are the prediction and control horizons respectively, H_w is the window parameter, Q and R are weights.

If the plant has a linear model and a quadratic cost function like above, then the problem that has to be solved is a standard finite-horizon linear quadratic (LQ) problem [28]. The idea is to pose control problems as problems of constrained optimization. The 'classical' theory of Optimal Control, mainly developed between 1955 and 1970, was driven by problems coming from the needs of aerospace industry, namely by the problems of launching, guiding and landing space vehicles and also of needs in flight and missile control [37].

The optimal value of the cost is

$$J^0 = x_k^T P x_k \tag{5.6}$$

where P is symmetric positive semi-definite solution of the algebraic Riccati equation

$$P = A^T P A - A^T P B (B^T P B + R)^{-1} B^T P A + Q \tag{5.7}$$

The cost equation is rewritten in

$$V(k) = \|Z(k+i|k) - T(k+i|k)\|_Q^2 + \|\Delta U(k+i|k)\|_R^2 \tag{5.8}$$

Recall that Z has the form

$$Z(k) = \Psi x(k) + \Upsilon u(k-1) + \Theta \Delta U(k) \tag{5.9}$$

for suitable matrices Ψ, Υ and Θ.

Then the error $\mathcal{E}$ can be defined as

$$\mathcal{E}(k) = \mathcal{T}(k) - \Psi x(k) + \Upsilon u(k-1) \tag{5.10}$$

5.2 Constrained MPC

Inequality constraints on input and output variables are important characteristics for MPC applications and formed a motivation during the early developments of MPC. Input constraints (or manipulated variables) can be considered as a result of physical limitations of plant equipment, like frequency command limit or rate-of-change in variables like actuator movement or flow rates. Output constraints are related to the plant operational strategy.

In constrained MPC, the control action can be computed subject to hard constraints on the manipulated variables and/or the outputs.

Manipulated variable constraints

$$u_{min}(l) \leq u(k+l) \leq u_{max}(l) \tag{5.11}$$

Manipulated variable rate constraints

$$|\Delta u(k+l)| \leq \Delta u_{max}(l) \tag{5.12}$$

Output variable constraints

$$y_{min}(l) \leq y(k+1|k) \leq y_{max}(l) \tag{5.13}$$

The cost function is defined as

$$V(k) = \sum z(k+i|k) - r(k+i|k)^2_{Q(i)} + \sum \Delta u(k+i|k)^2_{R(i)} \tag{5.14}$$

which is a standard optimization problem known as the *Quadratic Programming* (QP) [12].

A major problem that may occur with constraint optimization is that the problem may be unfeasible; in which case the solver stops. Various approaches are used in practice, such as avoiding hard constraints, actively manage constraint definition in every step k or actively manage horizons in every step k.

Several types of future behaviour of controlled variables (CV) exist [48]. Usually the CV are set to a *fixed set point*, and the deviations on both sides are penalized by the cost function. A drawback of this type is that the control action can be very aggressive, with large input adjustments; with a possible remedy to detune the controller.

Another option is the *zone* control, where upper and lower boundaries are defined and are usually implemented as upper and lower soft constraints. This is the case when the objective is to keep CVs within boundaries, neglecting their exact values. A third option is to define the CV as a *reference trajectory*. From the current CV to the setpoint, a curve of first or second order is specified and a quadratic cost function penalizes deviations. Finally objectives are represented as *funnels*, which are similar to zones but become narrower over the prediction horizon.

5.3 MPC Optimization Problem

MPC solves at each control interval an optimization problem [8], with the use of quadratic programming (QP). QP solver determines the MV moves over the control

horizon. From the QP decision, only the first move is applied until the next control interval. The QP problem deals with the following issues

- the cost function, which is a scalar non-negative measurement of controller performance to be minimized,
- constraints, which are the operational conditions of the plant that the solution must satisfy, such as te physical bounds of MV and the plant output variables.

Finally, the decision of QP solver includes the MV adjustments that minimize the cost function over the prediction horizon and, at the same time, satisfy the constraints.

The MPC QP solver converts an MPC optimization problem to the general QP form.

$$\min_{x}(\frac{1}{2}xHx + fc)$$

such that

$$Ax \leq b$$

where

- x is the solution vector.
- H is the Hessian matrix.
- A is a matrix of linear constraint coefficients.
- b and f are vectors.

H and A matrices are constants. The controller computes these constant matrices during initialization and retrieves them from computer memory when needed. It computes the time-varying b and f vectors at the beginning of each control instant.

KWIK (Knows What it Knows) algorithm [56] is used to solve the QP problem, which requires the Hessian to be positive definite. In the first control step, KWIK uses as initial guess is the unconstrained solution. If x satisfies the constraints, it is the optimal QP solution, x*, and the algorithm terminates. Otherwise at least one of

the linear inequality constraints must be satisfied as an equality. In this case, KWIK uses an efficient, numerically robust strategy to determine the active constraint set satisfying the standard optimization conditions.

A KWIK algorithm begins with an input set X and output set Y. The hypothesis class H consists of aset of functions from X to Y $: H \subseteq (X \rightarrow Y)$ [8]. The target function $h^* \in H$ is unknown to the learner. The hypothesis class H and parameters ε and δ are known to both the learner and environment. The environment selects a target function $h* \in H$ adversarially.
The agent then repeats the following

1. The environment selects an input $x \in X$ adversarially and informs the learner

2. The learner predicts an output $\hat{y} \in Y \cup \perp$ where $\perp$ means "I don't know".

3. If $\hat{y} \neq \perp$, it should be accurate: $|\hat{y} - y| \leq \varepsilon$ where $y = h^*(x)$. Otherwise the entire run is considered a failure.

4. If $\hat{y} = \perp$, the learner makes an observation $z \in Z$ of the output, where $z = y$ in the deterministic case, $z = 1$ with probability y and 0 with probability $1 - y$ in the Bernoulli case, or $z = y + n$ for the zero-mean random variable n in the additive noise case.

In the following control steps, the active constraint set determined at the previous control step becomes the initial guess for the next.

5.4 Design of Model Predictive Controllers

The objective in the present work is the reduction of DE exhaust gas emissions and/or fuel consumption, by utilizing appropriate control strategies for the hybrid diesel electric power-split. This chapter describes the development of two different MPCs. The aim of the controller is to ensure reference tracking of the control object (λ value) and disturbance rejection during transient loading conditions mainly, but also

during steady state operation. The application can be used as a retrofit solution to an existing engine, as the fuel control system is not altered.

The λ value is controlled by changing the EM frequency inverter command value (EMcmd), so EMcmd is the only manipulated variable (MV). The other system inputs are treated as measured disturbances (DV) and are used in order to provide a better output trajectory prediction over the prediction horizon (H_p).

In MPC, an explicit linear model is required to predict expected plant outputs, within a predefined time horizon. For this purpose, **Model 2**, as described in Chapter 3, was used. For the solution of the optimization problem, quadratic programming (QP) is used that aims to minimize the cost function over the prediction horizon by computing the control horizon (H_u) optimal sequence of the *MV*. The cost function [46] of the MPC controller is described in Eq. 5.15

$$J(z_k) = \underbrace{\sum_{i=1}^{p} \left\{ \frac{w_\lambda}{s_\lambda} \left[\lambda_{Ref}(k) - \hat{\lambda}(k+i|k) \right] \right\}^2}_{J_y} +$$

$$\underbrace{\sum_{i=0}^{p-1} \left\{ \frac{w_u}{s_u} u(k+i|k) \right\}^2}_{J_u} +$$

$$+ \underbrace{\sum_{i=0}^{p-1} \left\{ \frac{w_{\Delta u}}{s_u} \Delta u(k+i|k) \right\}^2}_{J_{\Delta u}} + \underbrace{\rho_\epsilon \varepsilon_k^2}_{J_{cst}} \quad , \tag{5.15}$$

where

z_k - Optimization process decision, given by

$$z_k^T = \begin{bmatrix} u(k|k)^T & u(k+1|k)^T & ... & u(k+p-1|k)^T & {}_k \end{bmatrix}$$

k - Current control interval.

p - Number of prediction intervals.

$\lambda_{Ref}(k)$ - Reference value for λ value at current control interval.

$\hat{\lambda}(k+i|k)$ - Predicted value of λ at ith prediction horizon step.

$u(k+i|k)$ - Optimal $EMcmd$ value predicted for $(k+i)$th control interval, given by z_k function.

$\Delta u = u(k+i|k) - u(k+i-1|k)$ - As control horizon is smaller than prediction horizon, Δu is constrained to zero for certain steps in the prediction horizon.

w_j - Tuning weight of jth variable of the controller

s_j - Scale factor for jth variable of the system, in engineering units.

ε_k - Slack variable at control interval k.

ρ_ϵ - Constraint violation penalty weight.

The first term of the cost function (J_y) includes the error between the λ reference value and the calculated one, and tries to minimize that. The second term (J_u) includes the EMcmd with an appropriate weight (W_u). The third term incorporates the rate of change of EMcmd with the tuning weight ($W_{\Delta u}$).

The relative weighting between the reference tracking (w_λ), the command value (w_u) and the rate of the command change ($w_{\Delta u}$) was selected so that the controller response is relative to the dynamics of the EM. The problem is hard constrained by the physical limits of the electric motor system, with the EM command being constrained as follows

$$\frac{u_{min}}{s_u} \leq \frac{u(k+i|k)}{s_u} \leq \frac{u_{max}}{s_u},\ i = 0 : p-1 \tag{5.16}$$

EM frequency inverter command must also remain within $[0, 0.1]$ V, due to hardware restrictions. Two MPC controllers were formulated and tested on the HIPPO-1 testbed as presented in Table 5.1.

		INPUTS / SCALE FACTOR	DV / SCALE FACTOR				OUTPUTS / SCALE FACTOR			CONSTRAINTS	
CONTROLLER NAME	MPC MODEL	EMcmd	MAP	SE	dSE	lambda	NOx	FOC	lambda	MV CONSTRAINTS	OUTPUT CONSTRAINTS
MPC 401	model 2	0.1	-	-	300	-	-	-	10	[0∼0,1]	-
MPC 900	model 2, mMAP, mNOx, mCons	0.1	0.25	300	300	10	20	30	10	[0∼0.1]	NOx:[0∼400] FOC:[0∼14]

Table 5.1: A summary of the characteristics of the created model predictive controllers.

Both controllers take into account the error between the engine speed setpoint and the measured rotational speed. This proved to be a good choice as a DV, because when a load is applied on the DE, the engine speed drops almost instantly.

One of the formulated controllers receives the measured λ values and a reference value, with the latter depending on the mode of operation. The reference value can be either a constant (static reference) or a dynamic one (from look-up tables).

The main sensors used for feedback control are the λ sensor, the engine speed sensor and the intake manifold pressure sensor. The resulting controller command is the input to the frequency inverter of the EM (EMcmd).

The choices of controller parameters like prediction horizons, weight matrices and sampling times, have a considerable effect on the performance and stability of the MPC. For more information regarding tuning of MPCs, see [24].

The controller tuning parameters are selected so that they display the desirable response characteristics. The sampling time of the MPC controllers' was set to $T_s = 0.1\ s.$ in order to have acceptable computational times. The selected controller timing is also faster than the controlled plant, which has an experimentally verified response time of 0.79 s., from a change to the EMcmd to the corresponding measured λ value.

The Prediction Horizon (H_p) was selected as the 20 % of the time duration of the transient phenomenon; Control Horizon (H_u) was selected between 5-30 % of H_p.

5.4.1 MPC 401 Design

MPC 401, is an un-constrained model predictive controller that utilizes the error of the measured engine speed against the reference value as a measured disturbance

(DV). The block diagram for the MPC 401 closed loop system is shown in Fig. 5-2.

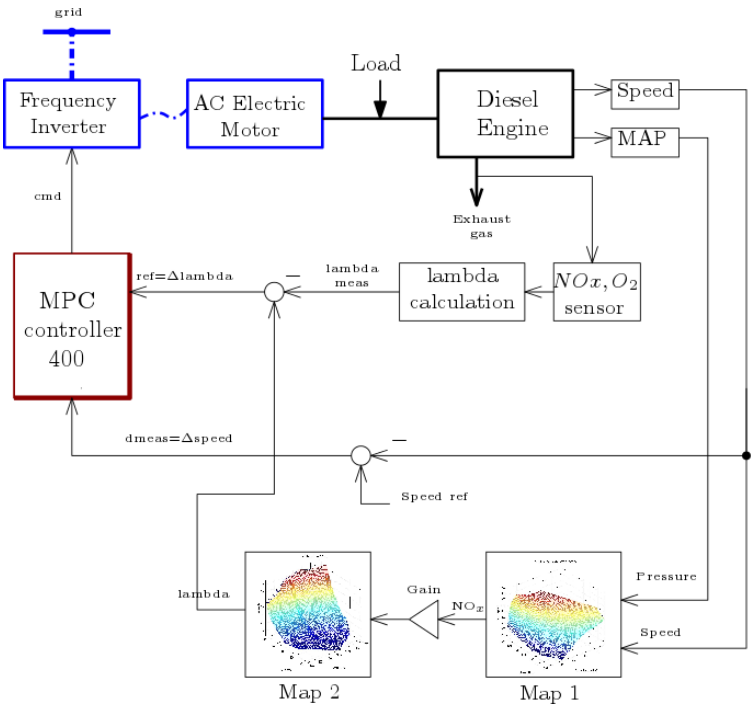

Figure 5-2: The closed loop system of the unconstrained MPC 401 scheme, with installed sensors and lambda reference options.

5.4.2 MPC 900 Design

MPC 900 is a constrained model predictive controller, that tracks the λ reference value, but also tries to cope with NOx and FOC upper limits.The block diagram for the MPC 900 closed loop system is shown in Fig. 5-3.

NO_x emissions and Fuel Oil Consumption (FOC) are also taken into account and soft constraints are applied in order to cope with environmental and operational limitations regarding these system outputs. When exceeding these softened limits a cost is added to the cost function forcing the controller, with the purpose if it is possible, to restore the system within the limits. Soft constraints' penalty is described with "J_{cst}" term of the cost function and is applied when

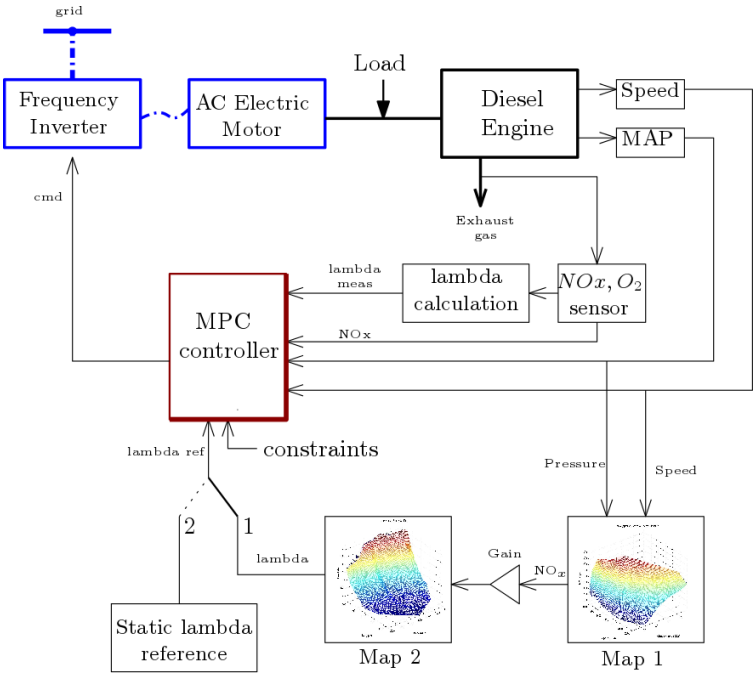

Figure 5-3: Constaint controller MPC 900 closed loop system with installed sensors and lambda reference options.

$$\frac{y_{NOx}(k+i|k)}{s_{y_{NOx}}} \leq \frac{y_{NOx,max}}{s_{y_{NOx}}} + \epsilon_k V_{NOx,max}, \tag{5.17}$$

$$\frac{y_{FOC}(k+i|k)}{s_{y_{FOC}}} \leq \frac{y_{FOC,max}}{s_{y_{FOC}}} + \epsilon_k V_{FOC,max}, \tag{5.18}$$

$$i = 1 : p$$

where

- $y_{j,max}$ - Upper bounds for jth plant output
- ϵ_k - Scalar QP slack variable used for constraint softening.
- $V_{j,max}$ - Dimensionless controller constants for jth plant output used for constraint softening and expresses the softened limits of the specific system's variable.

MPC 900 controls the λ value and also tries to cope with NOx and FOC upper limits. When the output values are within the desired limits, setting $w_u > 0$ forces

the controller to provide a zero command to the electric motor actuator as a result of the cost optimization.

5.5 MPC Experimental Results

The performance of the proposed predictive control structures have been tested and validated with a number of experiments. Performance evaluation of the designed MPC controllers was firstly conducted through step response simulation against each controller's internal model, in order to fine tune its parameters and ensure the system stability. The control structure is designed for the combined control of exhaust gas opacity and NO_x emissions. Such regions are found in the lower speed and lower load range of the given DE.

The experiments conducted on the HIPPO-1 powertrain, in order to evaluate the MPC controllers, are similar to those used for the evaluation of the robust controllers in Chapter 4. Reduction in exhaust gas emissions and fuel consumption was verified by comparison of the same parameters achieved when using the HIPPO-1 testbed with MPCs, to those corresponding to the conventional powertrain (DE only).

5.5.1 Simulation results

The controllers were evaluated through simulation using open-loop experimental data and the non-linear DE model presented in Chapter 3. During simulation the controller's performance was evaluated against reference tracking, disturbances rejection and keeping the system within desired limits in real environment. The Simulink program used for modeling of HIPPO-1 can be seen in Fig. 5-4, for two loading scenarios, a step loading from 100 to 400 Nm and a step loading from 100 to 500 Nm.

The assessment of MPC 401 performance during simulation in relation to experimental results is shown in Fig. 5-5. A disturbance is applied on the load demand T_{WB}. The torque demand data, as applied on the WB, is collected from experimental open-loop data. The corresponding lambda values and controller command are recorded. It can be observed that the simulated curves display similar behavior to the

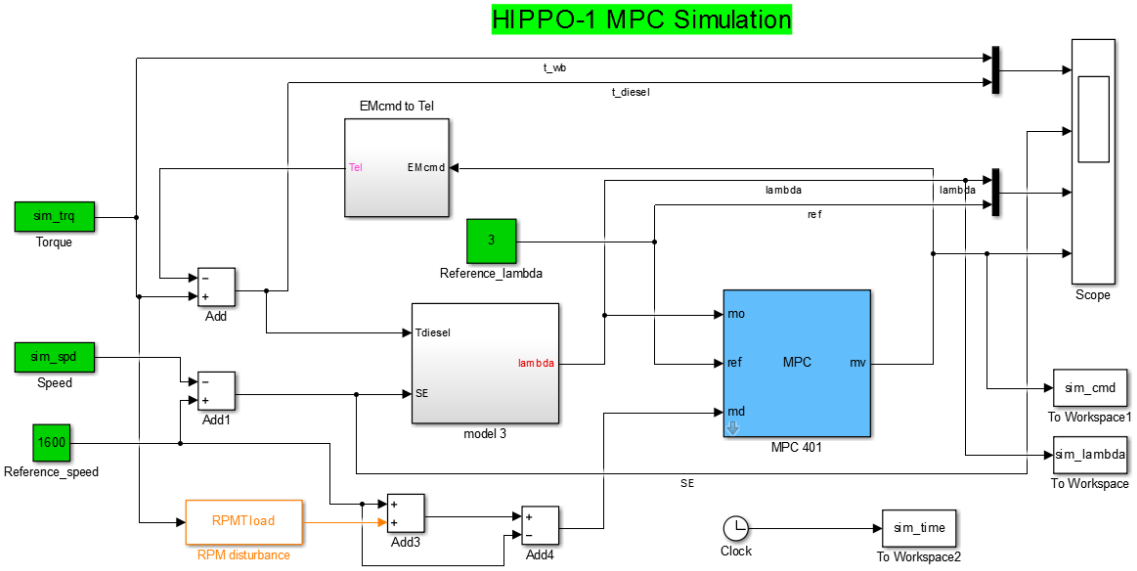

Figure 5-4: HIPPO-1 simulation setup using MPC control, as presented in a Simulink block diagram.

experimental data obtained under closed loop control, thus verifying the successful design of the simulation models.

5.5.2 Step Loading

The first set of experiments included step loading from 200-500 Nm, with constant engine speed ($N_E = 1600\ rpm$, simulating an on-board generator-set). Two controllers were tested, MPC 401 and MPC 900. The purpose of the proposed controllers is to track the imposed λ setpoint by engaging the EM. Results can be seen in the first subplot of Fig. 5-6. The measured lambda can be seen in the second subplot of the same figure, both with the conventional and hybrid setups. The reference λ values are derived from static look-up tables (maps) that utilize the measured intake manifold pressure and engine speed. These maps were created from experimental data of the DE, under a wide range of operation, as presented in detail in Chapter 3.

The control can be considered satisfactory. It can be observed that both MPC controllers display good tracking performance of the reference λ, during load change and at steady state. The conventional powertrain leads to much lower λ values (richer combustion) than the proposed hybrid solution.

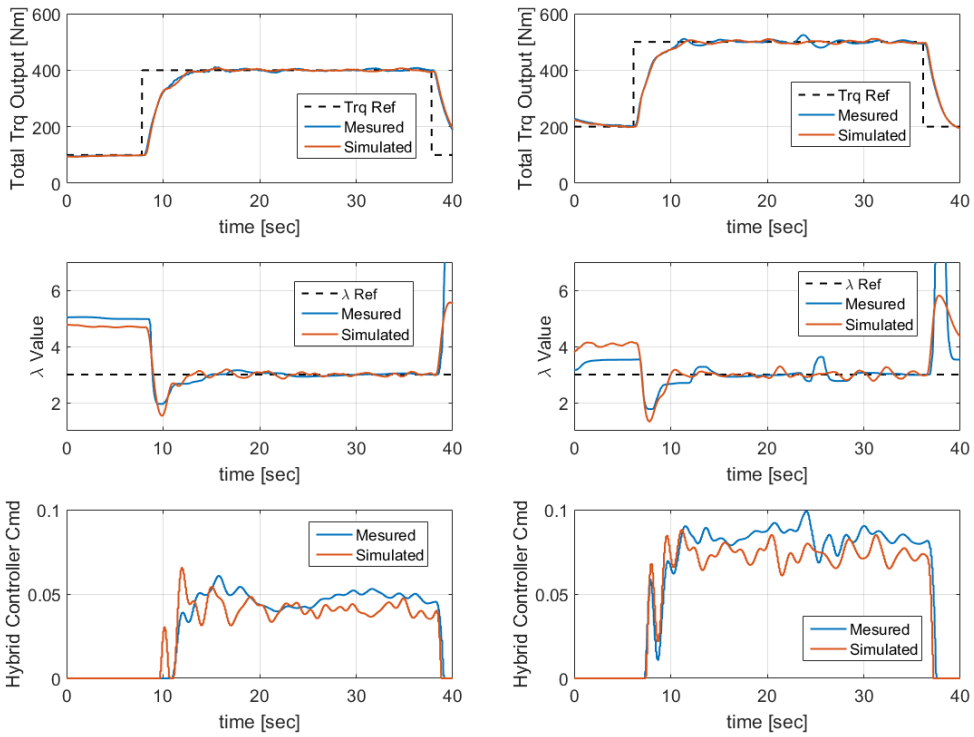

Figure 5-5: MPC 401 simulation and experimental data comparison, for two distinct loads.

As soon as there is a rising edge in the applied total torque, λ value drops rapidly and an error appears between the measured and reference lambda values. The controller engages and the EM produces torque, which is added to the torque produced by the DE, in order to meet the total torque demand. The controller command to the frequency inverter of the EM can be seen in the third subplot of Fig. 5-6. There is significant difference in the way the proposed two MPC designs behave. MPC 401, that utilizes the speed error, engages a few ms before lambda drops, because the speed of the DE drops almost instantly when a load is applied. After the initial command spike, the controller can predict that a "big" command will lead to an overshoot, and the command value drops once again. It can also be seen that generally the MPC 900 design produces higher command values than the MPC 401, although the model of the plant used is the same in both, due to the addition of constraints in MPC 900 for NOx content and fuel consumption.

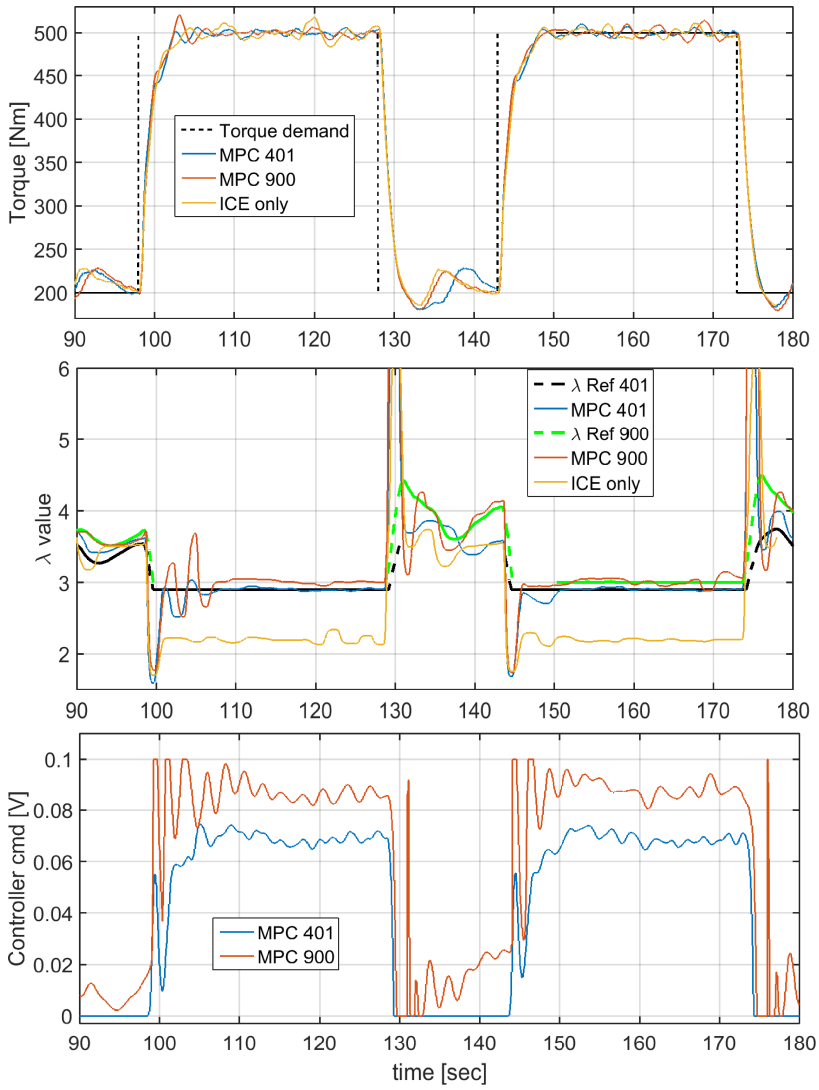

Figure 5-6: Measured total torque output, corresponding lambda values and controller command to the EM.

In Fig. 5-7 the torque output of the EM, the ICE intake manifold pressure and the powertrain's rotational speed is presented. In the first subplot it can be seen that the shape of the EM torque is generally the same for both controller designs, with MPC 900 producing more torque due to the limitations it offers in exhaust emissions and fuel consumption. In the second subplot, the intake manifold pressure is significantly higher with the conventional powertrain than with the hybrid, due to the EM taking part of the total applied torque. Again, MPC 900 leads to lower pressure because it engages the EM more than MPC 401. In the last subplot of the same figure, the

engine speed (and consequently of the whole powertrain) can be seen.

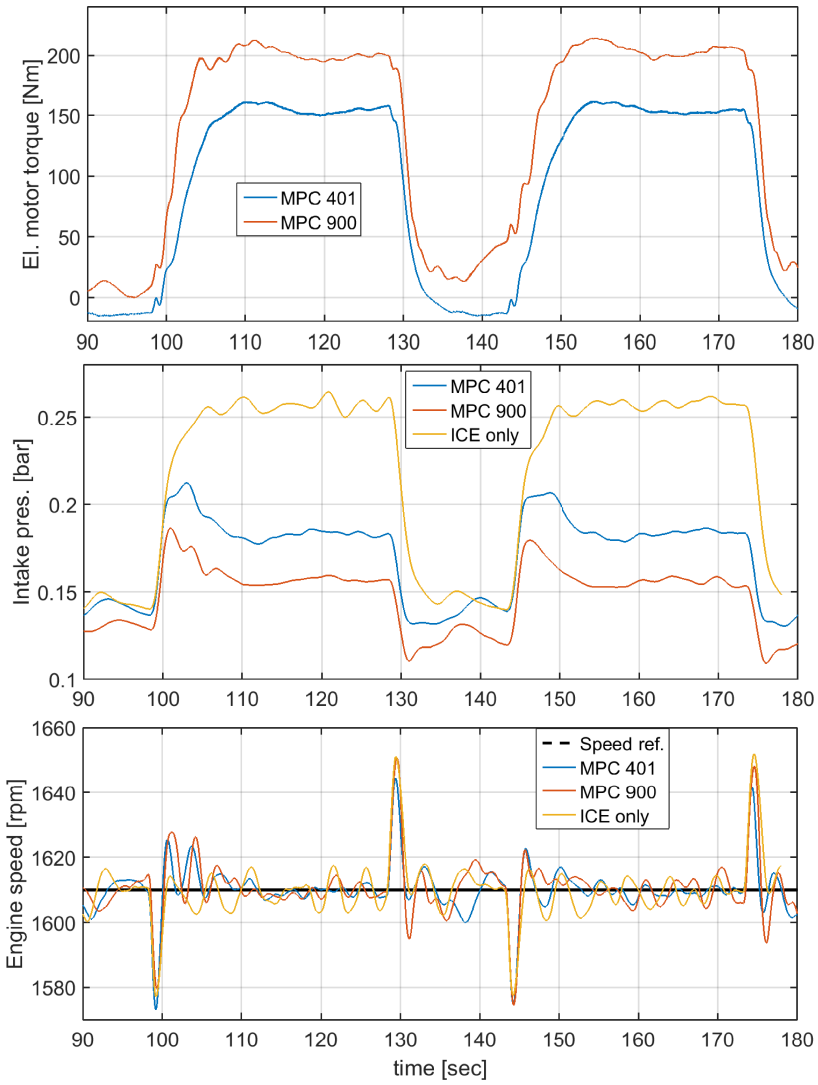

Figure 5-7: Hybrid controller command and torque split during step loading.

The λ set point represents the only parameter needed for tuning the strategy for a specific loading profile. In Fig. 5-8, the impact of the hybrid powertrain on the produced NO_x, measured exhaust gas opacity and fuel consumption, as compared to the conventional setup can be seen.

It can be noted that with the hybrid powertrain setup, both controllers offer the same gains in terms of the NOx content, which is around 40 % less during steady state than the conventional system. The first NOx spike during the load change, cannot be avoided due to the dynamics of the control system, but it can be observed that MPC

900, which incorporates the NO_x dynamics of the plant and has a soft constraint over it, manages to reduce the NO_x content by about 10 % during transient loading. During the load change, the NO_x content rises rapidly, and the soft constraint of 500 ppm is only violated during the first 1.5 seconds of the new applied load. The violation of the NO_x soft constraint causes the MPC 900 to generate a higher EMcmd.

Regarding the measured exhaust gas opacity, both MPC designs show the same behavior, with a reduction of 25 % when compared to the conventional powertrain for the same loading scenario. The third subplot of the same figure depicts the measured fuel consumption of the ICE. It can be seen that for the conventional powertrain the fuel consumption is around 20 kg/h, while with MPC 401 and 900 is around 16 kg/h (20% reduction) and 12 kg/h (40% reduction) respectively. The big difference between the two controller designs is due to the higher engagement that MPC 900 causes to the actuator (i.e. EM frequency inverter), as compared to MPC 401.

5.5.3 Propeller Loading

In the second set of experiments, the engine simulates a propeller loading operation, with alternating speed and torque. For more information on the loading scheme and reference λ values, see Chapter 4, experimental results section.

The λ reference points used, come from a set of maps, as a function of engine speed and inlet manifold pressure. The feedback from the λ virtual sensor was also used for these sets of experiments, but it displayed similar results to those presented in Chapter 4, so for illustration purposes are not displayed again in this section.

Figure 5-9 depicts the measured propeller loading curve during these experiments. The torque changes from approx. 120 Nm to 700 Nm and the engine speed from 1100 rpm to 1850 rpm.

The designed controllers lead to observable reduction of NO_x emissions, exhaust gas opacity and fuel consumption, with respect to the conventional (non-hybrid) powertrain, during acceleration. The electric power consumption is not taken into account, as this research focuses only on the transient loading phenomena of the DE. Also, further studies have shown that, in general, more than 50% of total diesel

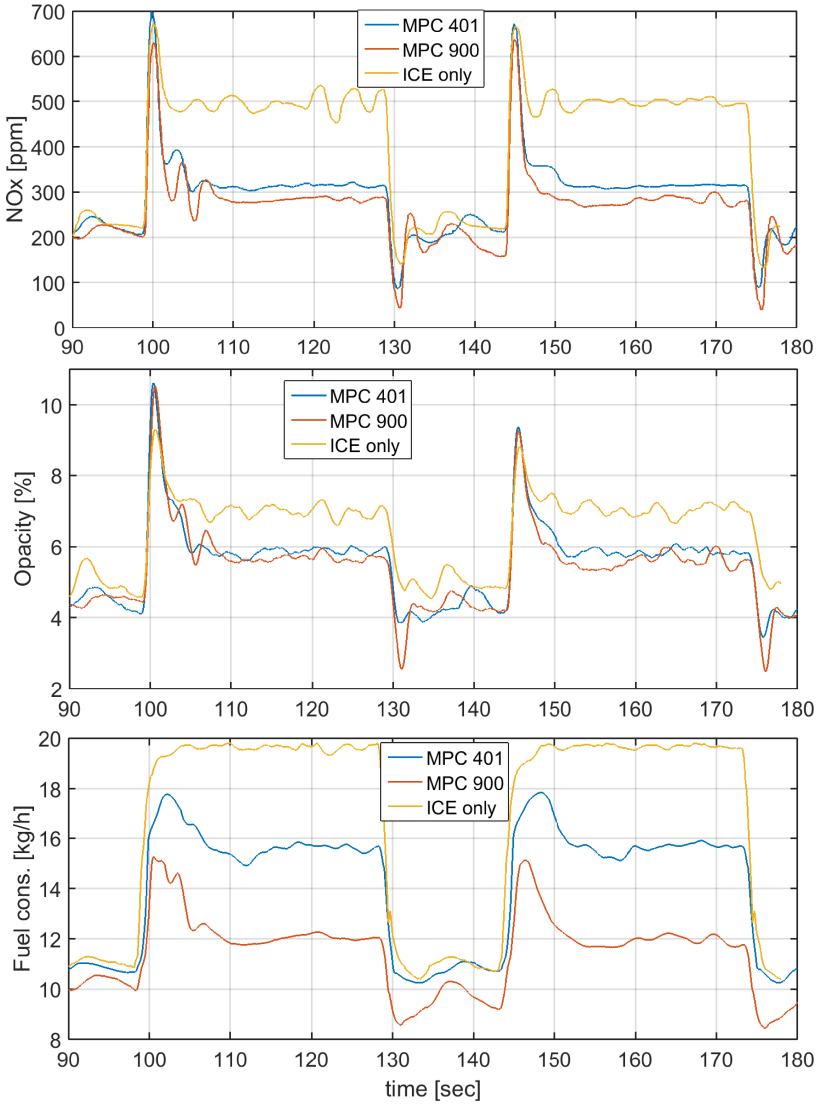

Figure 5-8: Effect of the hybrid powetrain on exhaust NO_x, opacity and fuel consumption, during step loading with dynamic λ reference.

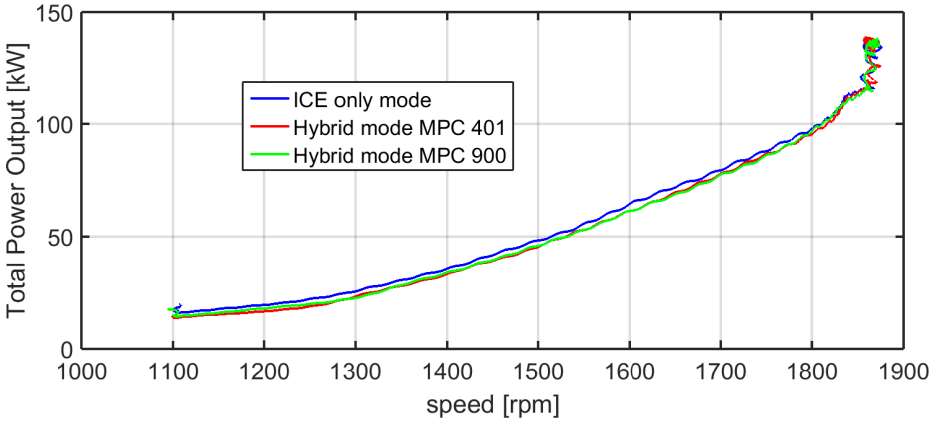

Figure 5-9: Propeller power curve on test bed.

engines pollutant emissions can be attributed to transient effects [42].

The comparison of the power-split on the conventional powertrain and HIPPO-1 and corresponding λ values are depicted in Fig. 5-10. The recorded λ values are higher using the hybrid setup (leaner combustion) than using the conventional one (i.e. without EM assistance), as the controller tracks the reference λ values imposed by the look-up tables. Fig. 5-11 shows the controllers' command values during the propeller loading scenario.

Fig. 5-12 shows the measured gas emissions of NO_x, exhaust gas opacity and measured fuel consumption. For the NO_x emissions of the hybrid setup a reduction of 16% was recorded during acceleration.

The measured opacity was about 20% less during transient loading when compared to the conventional powertrain.

As for the fuel consumption, it can be observed that during acceleration, the fuel consumption values are significantly lower with the hybrid setup.

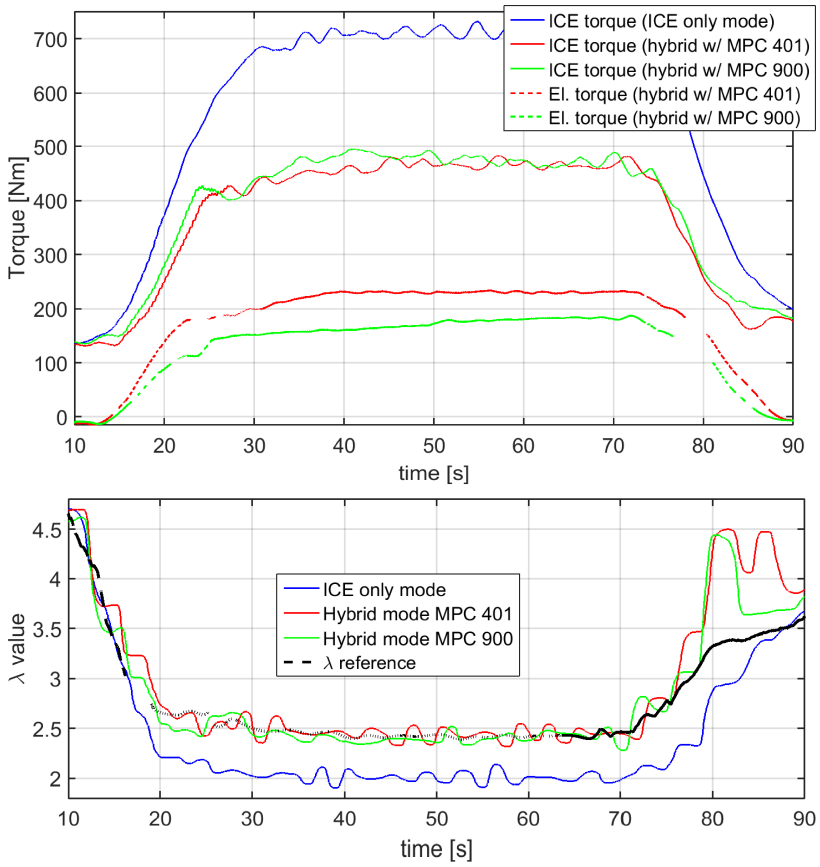

Figure 5-10: Torque power split along a propeller loading curve, with physical λ sensor.

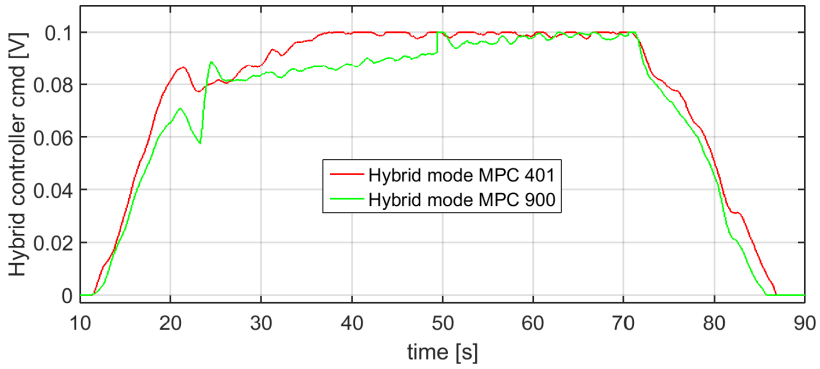

Figure 5-11: MPC controller command during a propeller loading curve.

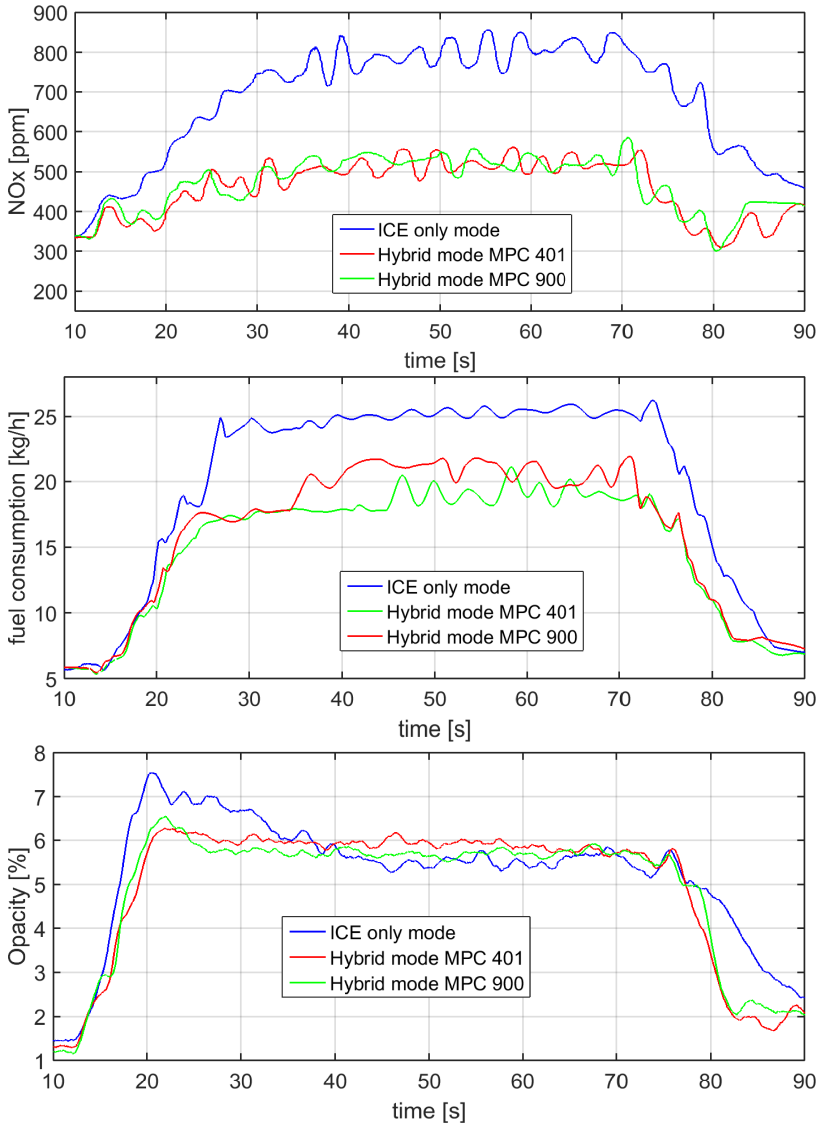

Figure 5-12: Effect of the hybrid powetrain on NOx, exhaust gas opacity and fuel consumption during a propeller loading curve.

Chapter 6

Conclusions and Future Work

In this research work, the aim was to develop a controller that would perform the **power split** between the DE and EM of a hybrid diesel electric powertrain for a multitude of loading conditions, mainly focusing on transient operation, in order to reduce exhaust gas emissions (NO_x, PM) and/or fuel consumption. A full scale test-bed (HIPPO-1) was built to test the proposed controllers.

Model derivation from experimental data, based on system identification, provided successful models for the design of the controllers. The models captured the dominant dynamics of the process under control.

Three different power management controllers (one robust and two model predictive) for the HIPPO-1 powertrain were investigated, where both a commercial λ sensor and a λ virtual sensor provided feedback.

Simulations with the model inputs and outputs in closed loop, allowed for appropriate choices of tuning parameters for the controllers. The most important variables tuned were control and prediction horizons, controller weights and sampling times. The simulations validated the design of the controllers, ensured the safety of the test-bed operation and decreased the test-bed operation time.

Different sets of experiments were conducted on the hybrid propulsion powertrain. The first set of experiments used a static λ reference value and the engine operating at constant speed and with alternating load, which corresponds to the load profile of a generator on-board a ship.

In the second set of experiments the engine was operated with changing speed and torque, simulating the load demand of a propeller. The proposed controllers provided good tracking performance, both with static reference points and with dynamic ones, as imposed by the created look-up tables.

The controllers, tested under the presence of exogenous disturbances, demonstrated their ability to reduce NO_x and particulate matter (PM) that were emitted by the internal combustion engine in transient loading and verified the choice of λ as feedback signal.

It was shown that the integration of feedback of λ of a diesel engine in a marine hybrid setup, during acceleration, via controlling the electric motor, can lead to improved performance and lower exhaust gas emissions during the load transient. The λ virtual sensor exhibited a performance which was matching that of the commercial physical sensor, and at some instances was even better, due to the smaller response time it offered. The virtual sensor utilized only of the turbocharger speed measurement and not the shaft torque measurement. Considering the limited availability of the shaft torque measurement in marine applications, the potential applicability of this method in standard-marine plants is widened.

The drawback of such an approach is the needed modeling of the plant, the increased complexity of the resulting controller and the added cost that comes when hybridizing a powertrain.

6.1 Future Work

- In the particular setup of the present work, envisioned as a possible retro-fit application for smoke reduction, the fueling parameter of the engine was considered to be an independent control variable, manipulated by the engine's ECU. In a possible alternate setup, the engine speed control could be incorporated in the controller.

- In this Thesis, the main focus has been the is emission and fuel consumption change during transient loading operation. One objective was to prove the

feasibility of the concept of controlling the EM via the DE λ value. In that regard, the EM current drawn was not taken into account. In a future research work, the energy balance of the EM and DE could be calculated or actually measured.

- In this work, various controllers using linear SISO and MIMO internal models were tested. The use of adaptive models or linear parameter-varying models can be suggested, in order to deal with the plants' non-linearities.

- The MPC controllers in this work seem to handle exhaust emission limits better than the H_∞ robust controller. The standard MPC uses an online optimizer at every control step, which requires a lot of computational power. A possible turnaround for that could be the use of Explicit-MPC, where the QP problem is solved off-line and stored in look-up tables.

- In this work, the reference λ values that were utilized in many cases by the designed controllers, were obtained from look-up tables. In a future application of the method this reference value could be derived by an optimization algorithm, taking into account exhaust emissions and/or fuel consumption.

THIS PAGE INTENTIONALLY LEFT BLANK

Bibliography

[1] ABB. Technical description td/flow/003en. *ABB Measurement Products, Coriolis mass flowmeters*, 2014.

[2] S. Adachi, M. Iwadare, and M. Ueno. Multi-variable air-path management for a clean diesel engine using model predictive control. *SAE International*, 2009.

[3] E. Alfieri, A. Amstutz, and L. Guzzella. Gain-scheduled model-based feedback control of the air/fuel ratio in diesel engines. *Control Engineering Practice*, 17(12):1417–1425, December 2009.

[4] A. Amstutz and L. K. Del Re. Ego sensor based robust output control of egr in diesel engines. *IEEE Transactions on Control Systems Technology*, 3(1):413–420, 1995.

[5] G. J. Balas, R. Chiang, A. Packard, and M. Safonov. *Robust Control Toolbox*. The MathWorks, Semptember 2015.

[6] K. Bardis. *Robust Controller Design for a Hybrid-Electric Marine Propulsion Plant*. Diploma Thesis, School of Naval Architecture and Marine Engineering, National Technical University of Athens, 2015.

[7] B. M. Baumann, G. N. Washington, B. C. Glenn, and G. Rizzoni. Mechatronic design and control of hybrid electric vehicles. *IEEE/ASME Trans. on Mechatronics*, 5:58–72, 2000.

[8] A. Bemporad, M. Morari, and N. L. Ricker. Model predictive control toolbox user's guide. 2015.

[9] M. Benz, C.H. Onder, and L. Guzzer. Engine emission modeling using a mixed physics and regression approach. *International Journal of Control*, 132, 2010.

[10] E. Boletis. Integration of propulsion system from the point of view of efficiency optimization. *In Proceedings of the 28th CIMAC World Congress 2016, Helsinki, Finland*, 2016.

[11] M. Braun, D. Rivera, W. Foslien, and C. Hrenya. Multi-level pseudo-random signal design and model-on-demand estimation applied to nonlinear identification of a rtp wafer reacto. In *Proceedings of the 1999 American Control Conference*, volume 3, pages 1573–1577. IEEE, 1999.

[12] A. E. Bryson and Yu-Chi Ho. *Applied Oprimal Control*. Taylor and Francis Group, 1975.

[13] D.W. Clarke and R. Scattolini. Constrained receding-horizon predictive control. *IEEE Control Theory and Applications*, 138(4), 1991.

[14] H. Hjalmarsson D. Alberer and L. del Re. Identification for automotive systems. *Springer-Verlag Ltd*, 2012.

[15] L. del Re, P. Langthaler, C. Furtmueller, S. Winkler, and M. Affenzeller. NOx virtual sensor based on structure identification and global optimization. (2011-01-0627), April 2005.

[16] R. C. Dorf and R. H. Bishop. *Modern Control Systems*. Prentice Hall, 2001.

[17] J. C. Doyle, K. Glover, P. P. Khargonekar, and B. A. Francis. State-space solutions to standard H_2 and H_∞ control problems. 34(8):831–847, August 1989.

[18] R. De Filippi and R. Scattolini. Idle speed control of a F1 racing engine. *Control Engineering Practice*, 14:251–257, 2006.

[19] O. Grondin and L. Thibaultand C. Quérel. Transient torque control of a diesel hybrid powertrain for NOx limitation. In *Proceedings of the 2012 IFAC Workshop on Engine and Powertrain Control, Simulation and Modeling*, volume 3, pages 286–295, 2012.

[20] L. Guzzella and C. Onder. *Introduction to Modeling and Control of Internal Combustion Engine Systems*. Springer, London, 2nd edition, 2004.

[21] S. Hashimoto, H. Okuda, Y. Okada, S. Adachi, S. Niwa, and M. Kajitani. An engine control systems design for low emission vehicles by generalized predictive control based on identified model. In *Proceedings of the IEEE International Conference on Control Applications*, pages 2411–2416, 2006.

[22] M. Henningsson, P. Tunestål, and R. Johansson. A virtual sensor for predicting diesel engine emissions from cylinder pressure data. In *2012 IFAC Workshop on Engine and Powertrain Control, Simulation and Modeling*, pages 424–431. International Federation of Automatic Control, 2012.

[23] M. Hirsch, D. Alberer, and L. del Re. Grey-box control oriented emissions models. In *Proceedings of the 17th World Congress, Seoul, Korea*, pages 1573–1577. The International Federation of Automatic Control, July 2008.

[24] M. Huzmezan and J.M. Maciejowski. Rcam design challenge presentation document: the model based predictive control approach. *Technical Report GARTEUR/TP-088-20*, 1997.

[25] V. H. Johnson, K. Wipke, and D. Rausen. Hev control strategy for real-time optimization of fuel economy and emissions. *SAE 2000 Transactions Journal of Engines*, 109(2000-01-1543), 2000.

[26] Y. Kim, A. Salvi, J. Siegel, Z. Filipi, A. Stefanopoulou, and T. Ersal. Hardware-in-the-loop validation of a power management strategy for hybrid powertrains. *Control Engineering Practice*, 29, 2014.

[27] P. Kirchen. *Steady-State and Transient Diesel Soot Emissions: Development of a Mean Value Soot Model and Exhaust-Stream and In-Cylinder Measurements*. PhD thesis, Swiss Federal Institute of Technology Zurich, 2008.

[28] D. E. Kirk. *Oprimal Control Theory, An Introduction*. Dover Publications, Dover Books on Electrical Engineering edition, 2004.

[29] C. Lin, H. Peng, and J. W. Grizzle. A stochastic control strategy for hybrid electric vehicles. *Proceedings of American Control Conference*, (5):4710–4715, 2004.

[30] C. Lin, H. Peng, J. W. Grizzle, and J. Kang. Power management strategy for a parallel hybrid electric truck. *IEEE Transactions on Control Systems Technology*, 11(6):839–849, 2003.

[31] C. C. Lin, J. M. Kang, J. W. Grizzle, and H. Peng. Energy management strategy for parallel hybrid electric truck. In *Proceedings of the American Control Conference*, pages 2878–2883, 2001.

[32] L. Ljung. *System Identification, Theory for the User*. Prentice Hall, Upper Saddle River, NJ, 2nd edition, 1999.

[33] L. Ljung. Perspectives on system identification. In *In Plenary talk at the proceedings of the 17th IFAC World Congress, Seoul, South Korea*, 2008.

[34] L. Ljung. Experiments with identification of continuous time models. In *15th IFAC Symposium on System Identification, Saint-Malo, France*, May 2009.

[35] L. Ljung. *System Identification Toolbox*, September 2015.

[36] N. D. Vaughan R. Ceen T. Hale G. Kennedy M. C. Ward, C. J. Brace. Investigation of sweep mapping approach on engine testbed. *SAE Technical Paper 2002-01-0615*, 2002.

[37] J.M Maciejowski. Predictive control with constraints. *Prentice Hall*, 2004.

[38] P. Majecki, G.M. van de Molen, M. Grimble, I. Haskara, and C.F.Chang Y. Hu. Real-time predictive control for si engines using linear parameter-varying models. *IFAC-PapersOnLine*, 2015.

[39] J. Mikles and M. Fikar. *Process Modelling, Identification and Control*. Springer, 2007.

[40] J. M. Miller. Propulsion systems for hybrid vehicles. *The Institution of Engineering and Technology*, 2008.

[41] D. Mytilinis. *Mapping of a Diesel Engine Parameters for Controlling a Hybrid Electric Ship Propulsion Powertrain.* Diploma Thesis, School of Naval Architecture and Marine Engineering, National Technical University of Athens, 2015.

[42] T. Nuesch, M. Wang, P. Isenegger, C. H. Onder, R. Steiner, and L. Guzella. Optimal energy management for a diesel hybrid electric vehicle considering transient pm and quasi-static nox emissions. *Control Engineering Practice*, 29:266–276, 2014.

[43] P. Ortner and L. del Re. Predictive control of a diesel engine air path. *EEE TRANSACTIONS ON CONTROL SYSTEMS TECHNOLOGY*, 15(3), 2007.

[44] P. Van Overschee and B. De Moor. N4sid: Subspace algorithms for the identification of combined deterministic-stochastic systems. *Automatica, Special issue on statistical signal processing and control*, 30(1), 1994.

[45] G. Papalambrou, E. Karlis, and N. Kyrtatos. Robust control of manifold air injection in a marine diesel engine. In *8th IFAC Symposium on Robust Control Design ROCOND 2015 Bratislava*, volume 48, pages 438–443, July 2015.

[46] N. Planakis. *Predictive Control of a Hybrid Diesel-Electric Marine Propulsion Plant.* Diploma Thesis, School of Naval Architecture and Marine Engineering, National Technical University of Athens, 2016.

[47] T. Poloni, T. A. Johansen, and B. Rohal'-Ilkiv. Modeling of air-fuel ratio dynamics of gasoline combustion engine with arx network. *Journal of Dynamic Systems, Measurement, and Control*, 130(6), 2008.

[48] S. Qin and T. badgewell. A survey on industrial model predictive control technology. *Control Engineering Practice*, 2003.

[49] M. Ramsbottom and F. Assadian. Use of approximate dynamic programming for the control of a mild hybrid. In *Proceedings of WMG Hybrid Conference*, December 2006.

[50] J.N. Reddy. An introduction to the finite element method (third ed.). *McGraw-Hill*, 2006.

[51] G. Ripaccioli, A. Bemporad, F. Assadian, C. Dextreit, S. Di Cairano, and I. Kolmanovsky. Hybrid modeling, identification, and predictive control: An application to hybrid electric vehicle energy management. In *Hybrid Systems: Computation and Control*, volume 5469, pages 321–335. Springer-Verlag, 2009.

[52] G. Rizzoni, L. Guzzella, and B. Baumann. Unified modeling of hybrid electric vehicle drivetrains. *IEEE/ASME Transactions on Mechatronics*, 4:246–257, September 1999.

[53] C. Roduner, C. Onder, and H. Geering. Automated design of an air/fuel controller for an si engine considering the three-way catalytic converter in the $h\infty$ approach(1997). *In Proceedings of the fifth IEEE Mediterranean Conference on Control and Systems, Paphos, Cyprus*, 1997.

[54] I. Postlethwaite S. Skogestaad. Multivariable feedback control. *John Wiley and Sons, Ltd*, 2005.

[55] M. Salman, N. J. Schouten, and N. A. Kheir. Control strategies for parallel hybrid vehicles. *Proceedings of the American Control Conference*, 1:524–528, 2000.

[56] C. Schmid and L.T. Biegler. Quadratic programming methods for reduced hessian sqp. *Computers Chemical Engineering*, page 817832, 1994.

[57] N. Schouten, M. Salman, and N. Kheir. Fuzzy logic control for parallel hybrid vehicles. *IEEE Transactions on Control Systems Technology*, 10:460–468, 2002.

[58] A. Sciarretta and L. Guzzella. Control of hybrid electric vehicles. *IEEE Control Systems Magazine*, pages 60–70, April 2007.

[59] A. Stefanopoulou and R. Smith. Maneuverability and smoke emission contraints in marine diesel propulsion. *Control Engineering Practice*, pages 1023–1031, 2000.

[60] A. Taghavipour, N. L. Azad, and J. McPhee. Real-time predictive control strategy for a plug-in hybrid electric powertrain. *Mechatronics*, 29, 2015.

[61] E. D. Tate, J. W. Grizzle, and H. Peng. SP-SDP for fuel consumption and tailpipe emissions minimization in an evt hybrid. *IEEE Transactions on Control Systems Technology*, 18(3):673–687, 2010.

[62] A. Thiruvengadam, S. Pradhan, P. Thiruvengadam, M. Besch, D. Carder, and O. Delgado. Heavy-duty vehicle diesel engine efficiency evaluation and energy audit. *Report, Center for Alternative Fuels, Engines and Emissions, West Virginia University*, 2014.

[63] F. Tschanz, A. Amstutz, C. Onder, and L. Guzzella. A real-time soot model for emission control of a diesel engine. In *6th IFAC Symposium Advances in Automotive Control, Munich, Germany*, pages 222–227. International Federation of Automatic Control, 2010.

[64] H.K. Woud and D. Stapersma. Design of propulsion and electric power generation systems. *The Institue of Marine Engineering, Science and Technology*, 2003.

Appendices

Appendix A: On-board Performance and Exhaust Emission Measurements

In order to acquire loading curves as realistic as possible that were to be used on the test-bed, measurements were conducted on-board two fast ferries equipped with waterjets. In Fig. A-1 the installation procedure of the power measuring equipment in the engine room of one of the ferries is shown.

Exhaust emissions and performance measurements were conducted concurrently. LME has undertaken, in cooperation with the shipowner company, the installation of experimental equipment on-board two of the companys ships and collect data during normal service. This included a circular route from Piraeus port to three islands. The entire voyage lasted approximately 9 hours in the Aegean Archipelago and it included high speed cruising, port approaching at low speed, maneuvering and immediate departure afterwards. The collected data refer to the composition of the exhaust gas ($CO_2, O_2, CO, HCs, NO_x, SO_2$), the opacity of the exhaust gas at the open end of the exhaust gas stack, the torque and speed on the engines shaft and the in-cylinder pressure.

The use of the on-board performance parameters and exhaust emission measurements (Fig. A-2) conducted within the scope of this Thesis was two-fold: at the first place they were utilized to show that during the departure from a port (transient loading) the DE produces visible black smoke at the exhaust (opacity), and secondly the data were used to produce propeller torque demand curves, used after appropriate scaling during the experiments on the HIPPO-1 test-bed.

Figure -1: Installation of the torque measuring device on the shaft of one of the main engines.

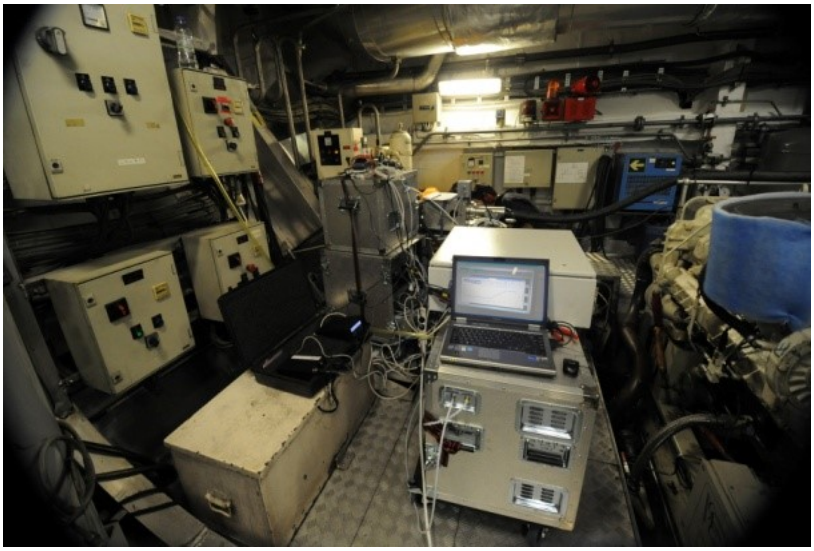

Figure -2: The emission analyzers in the engine room of one of the ferries.

Appendix B: Water Brake Problems

During the first stages of the HIPPO-1 commissioning, the water brake (WB), both in open and closed loop operation, i.e. with the water outlet valve operated manually and under electric command, was hunting, i.e. under constant command in water valve, oscillating behavior in speed was experienced. Figure B-3 presents the hunting behavior of the water brake, in open loop control. These speed oscillations rendered the further conduction of experiments impossible, for the safety of personnel and equipment. At this point it was decided that some measures had to be taken before the facility could work at its full potential.

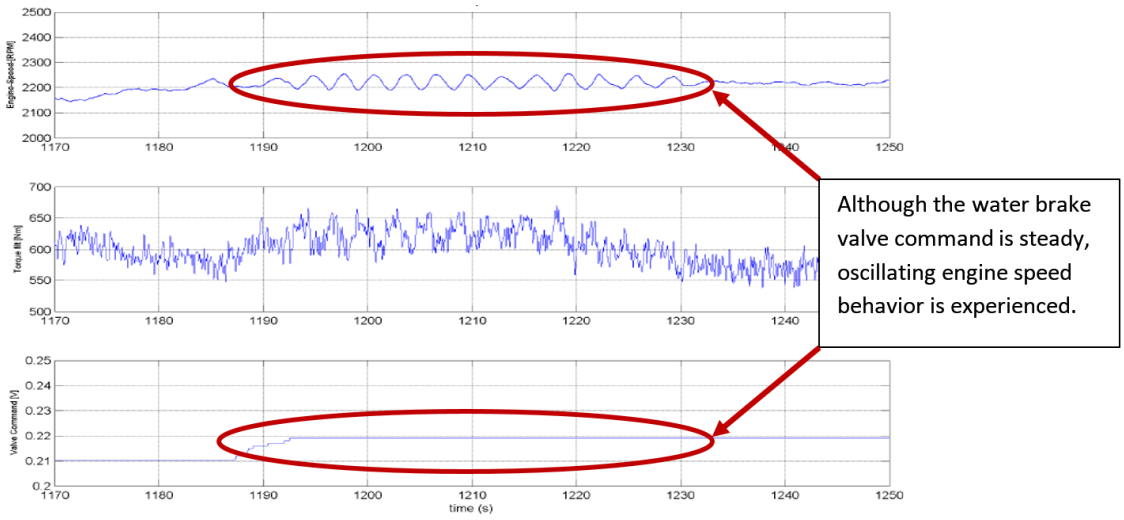

Figure -3: Tests performed for the commissioning of the WB, where the hunting behavior was recorded.

In order to determine what caused this behavior on the drivetrain, various sensors were installed as follows

- Diesel engine cooling water temperature sensor

- Diesel engine exhaust gas temperature sensor
- Turbocharger speed sensor
- Diesel engine fuel pressure
- WB water temperature sensor both on the inlet and the outlet
- Hydraulic dynamometer feed pump pressure sensor

Also, the Caterpillar DE built-in fault detection system was utilized, to make sure that the oscillations were not engine oriented. Some more tests were conducted with data being recorded from all the above sensors on the DAQ platform. It was noted that the WB inlet water pressure was lower than the value recommended by the manufacturer (Zoellner GmbH) for transient loads. With the above in mind, and after consulting with the dynamometer's manufacturer, it was decided to replace the water brake feed pump. A new water pump with the desired characteristics was chosen. The installation included design and manufacturing of new mount and piping and the addition of an inverter connected to the pump, so that the flow and pressure could be adjusted to meet various loading conditions.

With the new pump installed, the recorded water pressure was now within the recommended limits, but the oscillating speed behavior remained. At this point it was decided that a closed loop controller should act on the dynamometer's water regulating valve, so that it could maintain the load and consequently the speed at a fixed point. Various controllers were used including PIDs, but without noticeable improvement. Next, our attention was turned to the water brake itself. Being more than 30 years old and with many years of inactivity, all the visible caps were opened and inspected. This inspection showed that the water flowing from the stator to the rotor and vise versa, had caused significant accretion of inorganic materials on the sides of the water brake (Fig. B-4).

The next step was the disassembly of the drivetrain and removing the WB from the testbed in order for it to be sent to the manufacturer's headquarters for refurbishing. The water brake would there be dismantled and inspected, and any faulty

Figure -4: WB water outlet opened for inspection.

parts replaced. The part left the Laboratory's premises in March 2013 and returned September of the same year after a full rebuilt, when it was re-installed on HIPPO-1.

THIS PAGE INTENTIONALLY LEFT BLANK

Appendix C: λ Virtual Sensor Validation

In order to verify the accuracy of the λ virtual values, the output of the model was compared to actual (measured) λ values, as shown in Fig. C-5. A load demand profile was applied to the engine and the λ values from both sensors were recorded. When the torque output of the engine rises, the estimated λ values display almost identical behavior to the measured ones. When load is removed, the virtual sensor λ values display a small delay before meeting the measured values.

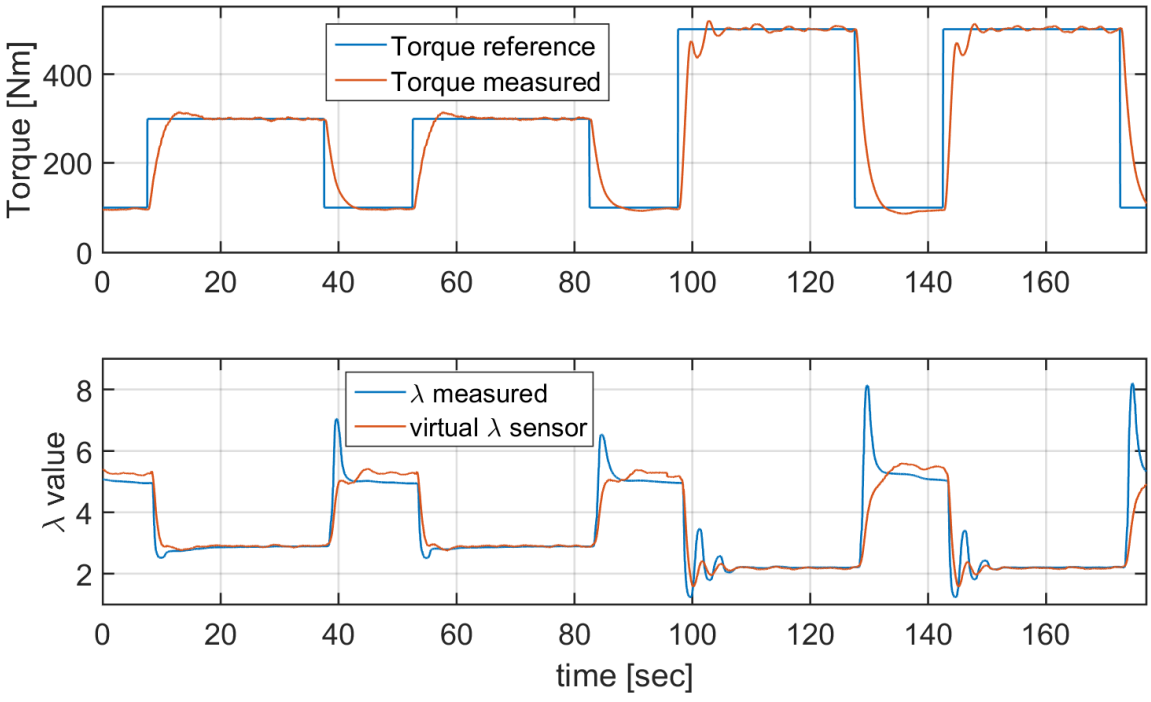

Figure -5: λ comparison between estimated and measured values. Top plot shows the applied load.

THIS PAGE INTENTIONALLY LEFT BLANK

Appendix D: Publications Related to this Thesis

The research performed within the framework of this Thesis has yielded the following scientific publications:

- S. Topaloglou, K. Bardis, G. Papalambrou, N. Kyrtatos, "Transient Load Share Management of a Diesel Electric Hybrid Powertrain for Ship Propulsion", International Journal of Powertrains, accepted (September 2016) for publication.

- S. Topaloglou, G. Papalambrou, N. Kyrtatos, "Robust Control of Diesel-Electric Hybrid Power Split for Marine Propulsion", submitted (July 2016) to IEEE Transactions on Control Systems Technology.

- S. Samokhin, S. Topaloglou, G. Papalambrou, K. Zenger, N. Kyrtatos, "Adaptive power-split control design for marine hybrid diesel powertrain", ASME Journal of Dynamic Systems, Measurement and Control, February 2017, Volume 139.

- S. Topaloglou, G. Papalambrou, N. Kyrtatos, "Energy management controller design for hybrid ship propulsion during transient operation", The 28^{th} CIMAC Congress, June 2016, Helsinki, Finland.

- S. Topaloglou, G. Papalambrou, N. Kyrtatos, "Controller Design for Hybrid Diesel Electric Ship Propulsion During Transient Operation", The 26^{th} International Ocean and Polar Engineering Conference, June 2016, Rhodes, Greece.

- G. Papalambrou, S. Samokhin, S. Topaloglou, N. Planakis, N. Kyrtatos, K. Zenger, "Model predictive Control for Hybrid Diesel-Electric Marine Propulsion", submitted (November 2016) to IFAC 2017 World Congress, Toulouse, France.

- N. Kyrtatos, G. Papalambrou, S. Topaloglou, A. Stamatellos, O. Zogou, "Design and Experimental Verification of a Variable Path Exhaust Gas Prototype Aftertreatment System for Marine Engines", International Marine Design Conference 2015 (IMDC 2015), Tokyo, Japan, May 2015.

- G. Papalambrou, S. Glaros, S. Topaloglou, and N. Kyrtatos "Model Reference Adaptive Control of a Marine Diesel Engine Combined with Electric PTI/PTO Motor", in Proceedings of Powertrain Modelling and Control (PMC) Conference, September 2012, Bradford, UK.

Transient Load Share Management of a Diesel Electric Hybrid Powertrain for Ship Propulsion

Sotiris K. Topaloglou

Laboratory of Marine Engineering (LME),
National Technical University of Athens,
Zografos, Greece
E-mail: akis@lme.ntua.gr

George Papalambrou

Laboratory of Marine Engineering (LME),
National Technical University of Athens,
Zografos, Greece
E-mail: george.papalambrou@lme.ntua.gr

Konstantinos Bardis

Laboratory of Marine Engineering (LME),
National Technical University of Athens,
Zografos, Greece
E-mail: kwstasbardis@gmail.com

Nikolaos Kyrtatos

Laboratory of Marine Engineering (LME),
National Technical University of Athens,
Zografos, Greece
E-mail: nkyrt@lme.ntua.gr

Abstract:

In this paper, a transient load share methodology for a hybrid diesel electric marine propulsion system is presented. Aim of the system is the performance enhancement and reduction of gaseous emissions during low-load transient operation. The controlled variable is λ while the manipulated variable is the torque from the electric motor regulated by a frequency inverter.

The model for the λ behavior is based on experimental identification while λ values in feedback loop come from an actual and a virtual sensor, the later based on first principles modeling. A nominal model is used for the synthesis of a robust H_∞ controller for the controlled variable regulation.

Robust Control of Diesel-Electric Hybrid Power Split for Marine Propulsion

Sotirios Topaloglou, Georgios Papalambrou, and Nikolaos Kyrtatos

***Abstract*—This paper presents a transient load share methodology for a hybrid diesel electric marine propulsion system. The target of the control system is the reduction of gaseous emissions and fuel consumption during low-load transient operation. The manipulated variable is lambda while the manipulated variable is the torque from the electric motor regulated by a frequency inverter.**

The model for the lambda behavior is based on experimental identification while lambda values in feedback loop come from an actual as well as a virtual sensor, based on engine modeling. A nominal model for the powertrain, derived through system identification, is used for the synthesis of a robust controller for the controlled variable regulation.

Successful hybridization was verified by experimental results in a full scale hybrid diesel electric powertrain under realistic loading scenarios.

***Index Terms*—Hybrid-Electric Propulsion, emissions control, diesel engines, robust control.**

I. Introduction

THE ever tightening emission requirements for port operations imposed by the legislation authorities on sea-going vessels justify the on-going research for novel technologies in the field of marine propulsion. Hybrid Diesel-electric propulsion is a promising technology for emission reduction and fuel efficiency enhancement.

Typically in the existing marine technology framework, ships are equipped with direct-driven propulsion machinery occasionally combined with a shaft generator system, known as Power Take Out (PTO), generating power for some of the electrical demands of ship. Current trends consider the usage of auxiliary power to assist the main engine in some load situations, such as high bollard pull, sailing in icy conditions, harbor maneuvering or "take-home" power, thus reverting the role to Power Take In (PTI) operation through powertrain *hybridization*. As a result, the size of main engine could be optimized to the propulsion power needed under normal conditions while additional power boost can be taken from auxiliary generators as required. More details can be seen in [1].

Depending on their architecture, Hybrid Electric Powertrains (HEP) fall mainly into one of the following two categories: a) parallel or b) series. In the parallel scheme, both the engine and the motor are connected to the transmission, and thus, they can power the vehicle either separately or in combination. In series hybrids, the electric motor is the only means of providing the demanded power.

The performance of a hybrid powertrain in terms of reducing both fuel consumption and exhaust emissions critically depends on the energy management strategy (EMS). An EMS is the supervising control algorithm that determines how the total power demand is shared between the power sources [2]. One main category of EMSs with limited, however, potential for marine power plants due to the requirement of the exact knowledge of the driving cycle include the optimization techniques found in [3], [4], [5] and [6]. Moreover, heuristic methods such as fuzzy logic and neural networks have been adopted in [7], [8] and [9] but neither achieve an optimal solution nor robustness with respect to performance.

The previous control strategies considered mainly fuel economy without a particular emphasis in reduction of emissions. The subject of emission reduction in a quasi-static framework is discussed in [10], [2], [11] and [12]. However the incorporated quasi-static models for emission formation disregard the substantial rise of pollutant emissions during transient operation of diesel engines (DE) due to the presence of thermodynamic delays mainly associated with turbocharger [13].

The formulation of transient emission reduction is presented in [14], where the optimal EMS for a diesel hybrid electric powertrain is calculated, considering the transient pollutant particulate matter emissions. In the same direction, [15], an EMS is considered using a frequency-domain power distribution (FDPD) strategy, which requires a priori knowledge of the loading profile.

The reduction of NOx emission in both steady state and transient operating conditions has been examined in [16]. The optimal power split in steady state is provided by an EMS while the reduction of transient NOx emissions is achieved through the smoothing of the DE torque demand by utilizing the EM torque as torque compensator. However, the dynamic control law is not robust with respect to exogenous disturbance and unmodeled dynamics that inevitably exist in real-world hybrid electric powertrains.

The rationale behind our approach is to reduce the intensity of the transient loading phenomenon in the DE with assistance from the EM. It takes advantage of the rapid conversion between electrical and mechanical energy in EM to assist the DE that has a limited torque delivery due to its thermodynamic nature. The concept of the above methodology is presented schematically in Fig. 1. The electric motor assists the diesel engine at low-load operation, where the internal combustion engine produces low torque, so as to meet up with the torque

The authors are with the Laboratory of Marine Engineering (LME), National Technical University of Athens, Zografos, Greece (e-mail: akis@lme.ntua.gr; george.papalambrou@lme.ntua.gr; nkyrt@lme.ntua.gr).

Manuscript received June xx, 2016; revised June xx, 2016 .

Sergey Samokhin[1]
School of Electrical Engineering,
Aalto University,
Otaniementie 17,
Espoo 02150, Finland
e-mail: sergey.samokhin@aalto.fi

Sotiris Topaloglou
School of Naval Architecture
and Marine Engineering,
National Technical University of Athens,
Zografou Campus,
Athens 15780, Greece
e-mail: akis@lme.ntua.gr

George Papalambrou
Assistant Professor
School of Naval Architecture
and Marine Engineering,
National Technical University of Athens,
Zografou Campus,
Athens 15780, Greece
e-mail: george.papalambrou@lme.ntua.gr

Kai Zenger
School of Electrical Engineering,
Aalto University,
Otaniementie 17,
Espoo 02150, Finland
e-mail: kai.zenger@aalto.fi

Nikolaos Kyrtatos
Professor
School of Naval Architecture
and Marine Engineering,
National Technical University of Athens,
Zografou Campus,
Athens 15780, Greece
e-mail: nkyrt@lme.ntua.gr

Adaptive Power-Split Control Design for Marine Hybrid Diesel Powertrain

It is known that mechanical wear and tear of components of large marine engines throughout their lifetime can cause the engine dynamics to alter. Since traditional control systems with fixed parameters cannot deal with this issue, the engine performance may degrade. In this work, we introduce adaptive control algorithms capable of adapting the control system in order to preserve the engine performance once its dynamics deviate from the nominal ones. Particularly, the direct and indirect model reference adaptation mechanisms are studied. In this work, the case of degraded oxygen sensor is investigated as an example of engine components deterioration throughout its lifetime. The controllers are implemented in Simulink, and their performance is evaluated under both nominal and degraded sensor conditions. Specifically, the sensor degradation is imitated by altering its time-delay. In such conditions, adaptive controllers demonstrate a notable improvement in tracking performance compared to the fixed parameters proportional-integral (PI) controller. Finally, the designed controllers are validated on the hybrid marine engine testbed using dSpace rapid prototyping system. [DOI: 10.1115/1.4034804]

1 Introduction

During the last decades, marine diesel engine emission regulations have become increasingly stringent due to stricter environmental requirements imposed by the International Maritime Organization (IMO) [1]. As a result, achievement of near-zero emissions has recently become one of the key targets for marine engine manufacturers [2,3].

Recently, the combination of an internal combustion engine with an electric motor has emerged as a powerful approach for reducing the emissions within the automotive industry [4]. A large number of research papers have been devoted to evaluating various aspects of hybrid electric vehicles (HEVs), including components sizing, control systems design, and topologies investigations. The control of HEVs is usually categorized into rule- and optimization-based algorithms [5]. Various optimization-based algorithms have been proposed for HEVs control, including model-predictive control [6], optimal control based on Pontryagin's minimum principle [7,8], and genetic algorithms [9]. Typically, these algorithms solve a constrained optimal control problem aimed at minimizing the engine fuel consumption, resulting in a globally optimal controller [4].

However, such optimization-based control algorithms rely on fixed parameters and therefore provide a global optimum only in the nominal case, i.e., the case for which they were designed [5]. Moreover, mechanical wear and tear of power-train components throughout the vehicle lifetime may cause its dynamics to change, leading to the nonoptimized use of power, since the optimal tuning of control systems differs for new and worn-out engines [10,11].

This problem becomes more critical in the marine industry, as large-scale marine diesel engines are typically customized for each individual customer and are therefore produced in very limited quantities. Together with high running costs, this prevents thorough tuning and testing which is, for example, available in the automotive industry, where engines are mass-produced [12]. Moreover, since engines mounted on large vessels are more difficult to maintain, the control systems must be designed sufficiently robust to deal with engine dynamics variation. Such variation can occur, for example, due to severe operating conditions or aggressive load transients (e.g., sailing through rough seas).

Many papers have addressed the problem of control system adaptation to varying engine dynamics in the automotive industry. These include classical adaptive controllers [13], adaptive model predictive controllers (MPC) [14], and controllers based on neural

[1]Corresponding author.
Contributed by the Dynamic Systems Division of ASME for publication in the Journal of Dynamic Systems, Measurement, and Control. Manuscript received February 12, 2016; final manuscript received September 19, 2016; published online November 14, 2016. Assoc. Editor: Ardalan Vahidi.

2016 | 050

Energy Management Controller Design for Hybrid Ship Propulsion During Transient Operation

06 Controls & Automation

Sotiris Topaloglou, Laboratory of Marine Engineering/National Technical University of Athens

George Papalambrou, Laboratory of Marine Engineering/National Technical University of Athens
Nikolaos Kyrtatos, Laboratory of Marine Engineering/National Technical University of Athens

This paper has been presented and published on the occasion of the 28th CIMAC World Congress 2016 in Helsinki. The CIMAC Congress is held every three years, each time in a different member country.
The Congress programme centres around the presentation of Technical papers on engine research and development, application engineering on the original equipment side and engine operation and maintenance on the end-user side. The topics of the 2016 event covered Product Development of gas and diesel engines, Fuel Injection, Turbochargers, Components & Tribology, Controls & Automation, Exhaust Gas Aftertreatment, Basic Research & Advanced Engineering, System Integration & Optimization, Fuels & Lubricants, as well as Users' Aspects for marine and land-based applications.

Proceedings of the Twenty-sixth (2016) International Ocean and Polar Engineering Conference **www.isope.org**
Rhodes, Greece, June 26-July 1, 2016

ISBN 978-1-880653-88-3; ISSN 1098-6189

Controller Design for Hybrid Diesel Electric Ship Propulsion during Transient Operation

Sotirios K. Topaloglou
George I. Papalambrou
Nikolaos P. Kyrtatos
National Technical University of Athens, Laboratory of Marine Engineering.
Athens, Greece

ABSTRACT

This work investigates the improvement in performance of a combustion engine with the assistance of an electric motor, with appropriate control systems, for transient load uptake, smoke emission reduction, reduced pollutant emissions and lower fuel consumption.
For the hybrid diesel electric powertrain, an energy control management strategy dictates the required torque from the electric motor so as to track a reference air-to-fuel ratio/stoichiometric (λ-value) in the diesel engine.
The feasibility and validity of the proposed control strategy was tested experimentally. A comparison between the hybrid powertrain and the standard engine setup (without the assistance from the electric motor), shows the benefits of a hybrid setup during transient loading conditions.

KEY WORDS: Hybrid diesel electric; hybrid ship; H-infinity control; AFR closed loop; ship exhaust emission reduction.

INTRODUCTION

One promising technology for reduction of gaseous emissions and fuel consumption of ships is the diesel-electric hybrid propulsion, i.e. a diesel engine assisted by an electric motor, with both machines coupled onto a common drive shaft. Various topologies of hybridized power trains have been exhaustively studied from various perspectives in heavy trucks and automotive applications.

A considerable number of publications in this field has been devoted to the development of energy management strategies (EMS) (Fekri and Assadian, 2012). EMS is the supervisory control algorithm which specifies the energy split among the various power sources which make up the propulsion system, (Lin; Peng; Grizzle and Kang, 2003). One main category of EMS consists of optimization techniques, with diverse approaches as found in (Sciaretta and Guzzella, 2003; Ramsbottom and Assadian, 2006; Lin; Kang; Grizzle and Peng, 2001).

This method is not directly applicable in marine power plants due to the requirement of the exact knowledge of the driving cycle by the optimization routine. Another broad category comprises heuristic methods such as fuzzy logic, as adopted in (Salman; Schouten and Kheir, 2000; Baumann; Washigton; Glenn and Rizzonni, 2000). The advantages are the easiness to implement and the simplicity to conceive; the drawback is that they neither achieve an optimal solution nor robustness with respect to performance.

The above control strategies have dealt mainly with fuel economy without a particular emphasis on emission reduction. The subject of emission reductions in a quasi-static framework is discussed in (Lin; Peng; Grizzle and Kang, 2003; Lin; Peng and Grizzle, 2004; Tate; Grizzle and Peng, 2010; Johnson; Wipke and Rausen, 2000). However the incorporated quasi-static models for emission formation disregard the substantial rise of pollutant emissions during transient operation of Diesel engines (DE) due to the presence of thermodynamic delays mainly associated with turbocharger (Rakopoulos and Giakoumis, 2006).

A method to calculate the optimal EMS for a diesel hybrid electric power train taking into account the transient pollutant particulate matter emissions is presented in (Nuesch; Wang; Isenegger; Onder; Steiner and Guzzella, 2014).

The reduction of NOx emission in both steady state and transient operating conditions has been examined in (Grondin and Qurel, 2012). Here, the optimal power split in steady state is provided by an EMS while the reduction of transient NOx emissions is achieved through the smoothing of the DE torque demand by utilizing the EM torque as torque compensator. The dynamic control law is not robust with respect to exogenous disturbances and un-modeled dynamics that inevitably exist in real- world hybrid electric powertrains.

The main purpose of the present paper is to examine the feasibility of emission reduction along with fuel consumption reduction, during the transient loading of a diesel hybrid-electric marine propulsion plant, under closed loop control.

Model Predictive Control for Hybrid Diesel-Electric Marine Propulsion ⋆

Georgios Papalambrou * **Sergey Samokhin** ** **Sotirios Topaloglou** *
Nikolaos Planakis * **Nikolaos Kyrtatos** * **Kai Zenger** **

* *National Technical University of Athens, Laboratory of Marine Engineering, Zografou, 15773, Greece (e-mail: george.papalambrou@lme.ntua.gr).*
** *Aalto University, Department of Electrical Engineering and Automation, 02150 Espoo, Finland (e-mail: sergey.samokhin@aalto.fi, kai.zenger@aalto.fi).*

Abstract: In this work, the problem of energy management strategies in hybrid diesel-electric marine propulsion systems is investigated with the implementation of two types of Model Predictive Controllers. The system behavior is described by models based on system identification as well as on first-principles. These models were used for the design of linear and adaptive predictive controllers respectively. The controllers were successfully tested at HIPPO-1 testbed, at the Laboratory of Marine Engineering, evaluating diverse strategies for disturbance rejection, system stability, and operation of the plant within desirable limits.

Keywords: hybrid marine engine, predictive control, λ control, transient operation

1. INTRODUCTION

Strict emission regulations imposed by legislation authorities (e.g. International Maritime Organization-IMO) make marine engine manufacturers to look for new opportunities for emissions reduction. One promising technology for emissions reduction and fuel efficiency enhancement is hybridization, i.e. usage and coordination of more than one energy sources used for propulsion.

This research work tackles the problem of energy management strategies (EMS) in hybrid diesel-electric marine propulsion systems, without any battery storage capacity. Such a system decides in real time the amount of power delivered at each time constant by the energy sources present in the experimental marine power train. Objectives are to investigate a) the interaction between the power sources and b) the feasibility of the hybrid configuration to achieve reduced exhaust emissions and improved fuel consumption during transient loading operation. This could lead to diesel engine downsizing as is the case in the "modern" point of view in marine propulsion.

Usually, the engine control units contain a certain amount of single closed-loops, with many look up tables in order to achieve closed-loop control of the multi-parametric and strongly non-linear engine behavior, Ripaccioli et al. [2009]. Today, a more sophisticated and complicated control method is needed: one that continuously decides the operation point of the plant, while enforcing the operating constraints and optimizing the energy consumption, in terms of fuel and electric energy consumption.

Several strategies for power management have been applied so far, including dynamic programming, stochastic dynamic programming, equivalent fuel consumption minimization (ECMS) and model predictive control (MPC). Of the many advanced control design methodologies, MPC seems to be the most capable to handle multivariable processes, satisfy constraints, deal with long time delays and utilize plant response to measured and unmeasured disturbances knowledge, Taghavipour et al. [2015]. MPC has been used in a broad range of applications, such as diesel engine control, del Re et al. [2009], Ortner and del Re [2007], Adachi et al. [2009], catalyst control, Majecki et al. [2015], Trimboli et al. [2009], Hybrid Electric Vehicles (HEV), Ripaccioli et al. [2009], Borhan et al. [2009], Plug-in Hybrid Electric Vehicles (PHEV), Taghavipour et al. [2015], etc.

Usually the objective of the EMS is to minimize fuel consumption. In the work presented here, the control problem is recast in an alternate way so as to track λ reference while ensuring that certain constraints, like NOx and fuel consumption are met.

2. SYSTEM DESCRIPTION AND MODELING

2.1 Experimental Facility

The hybrid propulsion powertrain HIPPO-1 test bed at Laboratory of Marine Engineering, NTUA (LME) (seen

⋆ Authors GP, ST, NK gratefully acknowledge the support of EC/DG RTD H2020/HERCULES-2 project, as well as the support of Lloyds Register Foundation, within the LRF NTUA Centre of Excellence in Ship Total Energy-Emissions-Economy, for the development and extension work on the hybrid integrated propulsion powertrain and related HIPPO-1 diesel electric test bed.
Authors SS and KZ gratefully acknowledge the funding from the HERCULES-2 project, funded by the European Commission, DG Research, under Contract SCP1-GA-2011-284354.

Design and Experimental Verification of a Variable Path Exhaust Gas Prototype Aftertreatment System for Marine Engines

Nikolaos P. Kyrtatos[1], Georgios Papalambrou[1], Sotirios Topaloglou[1], Anastasios Stamatellos[2] and Olympia Zogou[2]

ABSTRACT

The installation of exhaust gas aftertreatment units (ATU) both as retrofits and in new buildings, often faces size and cost issues. In applications of soot filters to reduce black smoke emissions, one other issue is the regeneration cycle needed to avoid filter blocking and increased back pressure on the upstream engines. However if the soot filter is only used during part of the engine operation e.g. during load up, then not only a smaller size filter can be used, but also the regeneration needs are greatly reduced.

A variable path exhaust arrangement was designed where the exhaust pipe splits in two parallel branches (ATU and bypass) where portions of the gas flow can be directed either through the ATU or the bypass section and then mixed again. Controllable butterfly valves in the two branches are regulated in real –time, based on measurements of the composition of the exhaust stream blend in the downstream stack. The gas flow control unit also connects to the engine control to optimize performance during load changes.

A full scale experimental prototype of the variable path exhaust system was built and a dedicated control system was designed. Results from the operation of the variable path system to reduce black smoke emissions during engine load increases, are presented.

KEY WORDS

Exhaust gas aftertreatment unit; soot filter; marine diesel engines; engine control

INTRODUCTION

The problem of smoke emissions during acceleration in a marine diesel engine under load occurs due to temporary inability of the charge air system (turbocharger lag) to supply a sufficient amount of air to burn completely the fuel quantity required to meet the increasing load on the engine, as the ship accelerates.

For the reasons explained above, high speed ferries on tight schedules will inevitably emit visible smoke during maneuvers and acceleration. Visible smoke emissions are not yet regulated by international legislation but are expected to be so in the near future. Ferry operators are sensitive to passenger perception of smoke emissions and perceived smoke emissions is more prominent in Greek island ports during the bright summer.

One possible solution for Particulate Matter (PM) abatement is the use of aftertreatment devices (ATU) in the form of Particulate Filters (DPF). In this type of filter, the exhaust flow is forced through very small channels (μm openings) where solid PM is collected, with a trapping efficiency close to 90%. The method is well-established in practical applications as no modifications affecting engine performance are required as long as the back pressure on the engine remains moderate.

The biggest challenge that DPF systems face is their early-clogging due to accumulation of the collected PM inside the filter. The reduction of the exhaust flow through the filter is directly translated to an increase of the engine backpressure. In turn, increased exhaust backpressure has a number of side-effects on the diesel engine, mainly causing increase in fuel

[1] Laboratory of Marine Engineering (LME/NTUA), National Technical University of Athens, Athens, Greece
[2] Thermodynamics and Thermal Engines Laboratory, University of Thessaly, Volos, Greece

Model Reference Adaptive Control of a Marine Diesel Engine Combined with Electric PTI/PTO Motor

G. Papalambrou [1], S. Glaros [1], S. Topaloglou [1], and N. Kyrtatos [1]

[1] Laboratory of Marine Engineering, National Technical University of Athens, Athens, Greece

Abstract: This paper investigates the applicability of robust Model Reference Adaptive Control (MRAC) for the control of speed in a marine diesel engine combined with an electric Power-Take-In/Power-Take-Out (PTI/PTO) motor. Results of numerical simulations with a mean-value engine model (MVEM) are given where realistic loading is applied. These showed good performance of the engine control system: a satisfactory adaptive control system could be designed without necessarily having accurate information about the engine parameters, and consequently, configuration changes could be easily accounted.

Keywords—model reference adaptive control, marine diesel engines.

1-Introduction

The aim of this work is to investigate the applicability of Model Reference Adaptive Control (MRAC) for the control of speed and load in marine diesel engines. Of particular interest is the use of low-order models that will represent the plant, preferably of first order, while keeping the control algorithm as simple as possible. There is continuous interest in speed engine control problem, through the use of model based control approach, in order a) to eliminate the requirement for precise engine model, as in classical or optimization algorithms and b) to reduce the conservatism inherent to robust control algorithms. The speed control problem is to ensure that the engine rotational speed ω, tracks the desired reference speed, within the frame of operation of a marine engine, which includes the application of sudden external loads. The present work was carried out in two directions: a) the derivation of suitable engine models for adaptive control and b) the selection of appropriate MRAC methodologies. The brief literature review which follows focuses on these two areas.

In [1], a mathematical model of a turbocharged diesel engine was developed which was further linearized and provided transfer functions for use in control studies. The transfer functions varied over the operating range from low load and low speed to high load and high speed. Their type was second order with zero and delay. With a similar aim, in [2] a model of a large turbocharged 2-stroke marine diesel engine is presented, providing relations for engine speed and turbocharger speed in the form of transfer functions, based on first principles. In [3, p. 282-295] the application of self-tuning to a turbocharged diesel engine for the regulation of engine speed is presented. The diesel engine was modelled by a first order model relating the fuel rack position to engine speed. Experimental results verified the control methodology, considering various parameters like pole placement polynomials, forgetting factors, sample rates, controller order. In [4] a pole assignment and a PI self-tuning algorithm were applied for the control of engine speed and smoke in a diesel engine during transients. Experimental results showed that objectives were met. Two self-tuning algorithms were compared in [5], as were applied for the idle speed regulation in a heavy-duty diesel engine. Recursive least squares were used for parameter identification while minimum variance and pole placement were developed and tested on a nonlinear engine model. Both self-tuners were able to converge quickly in controller parameters, the first type achieved faster settling times with slightly higher overshoot. Not many publications exist for work relating MRAC and internal combustion engines. An early work can be found in [6], where the application of MRAC with identification for the control of speed in a diesel engine is presented. The algorithm was similar to self-tuning, it was implemented in discrete form and stability was based in hyperstability concepts. Recently [7], presented a successful extension of the standard MRAC method, for systems with time delay, called posicast, which was applied to the idle speed control problem in a spark ignition engine. Simulation and experimental results demonstrated the improvement by employing such an adaptive controller. Finally, in [8], the work of the authors in model-based engine control system design is presented, with the aim to reduce smoke from marine diesel engine exhaust emissions, during transient operation, by injecting compressed air in intake manifold, with compressor surge avoidance at the same time. Model Predictive Control was employed in experiments with a marine diesel engine, while models for exhaust smoke opacity and intake pressure were derived with system identification, in a multivariable formulation.